Photovoltaic and Nano

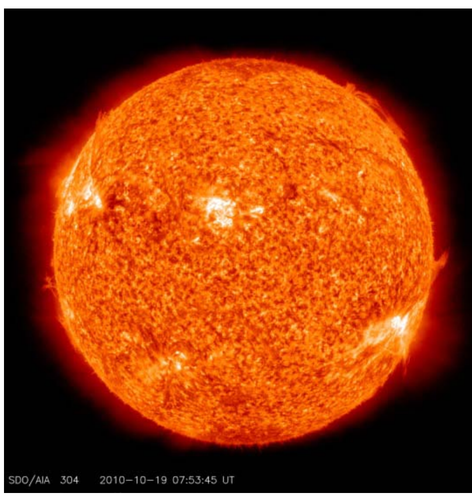

Outline

- Introduction
  - What is solar energy
  - Evolution of solar cells
  - Solar cell development
  - Principle & analysis
- Si solar cell
- CIGS/CZTS solar cell
- Organic solar cell
  - Small-molecule solar cell
  - BHJ solar cell
- Why “nano” can help in solar cell

What Is Solar Energy?

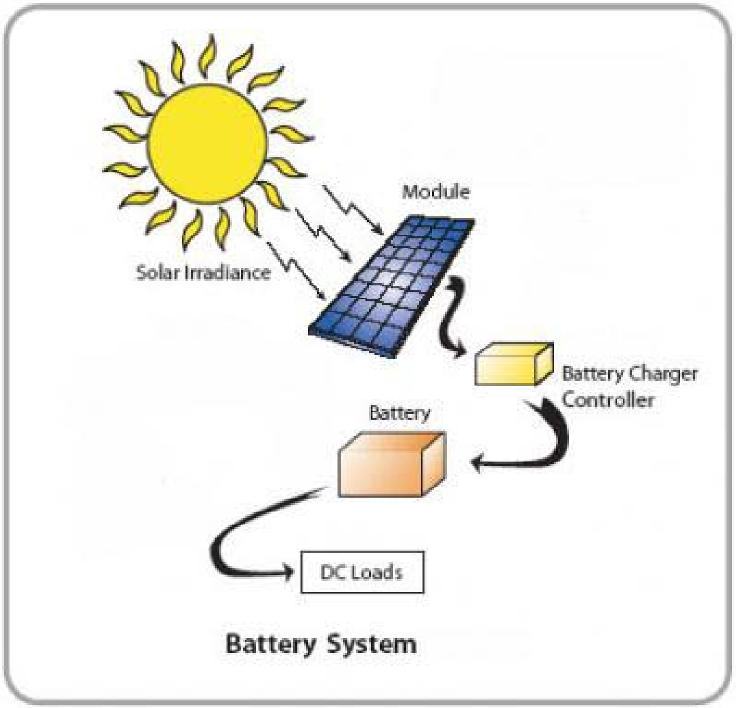

Solar Energy

The radiant solar Energy is from nuclear energy and the temperature of the Sun is ~6000K

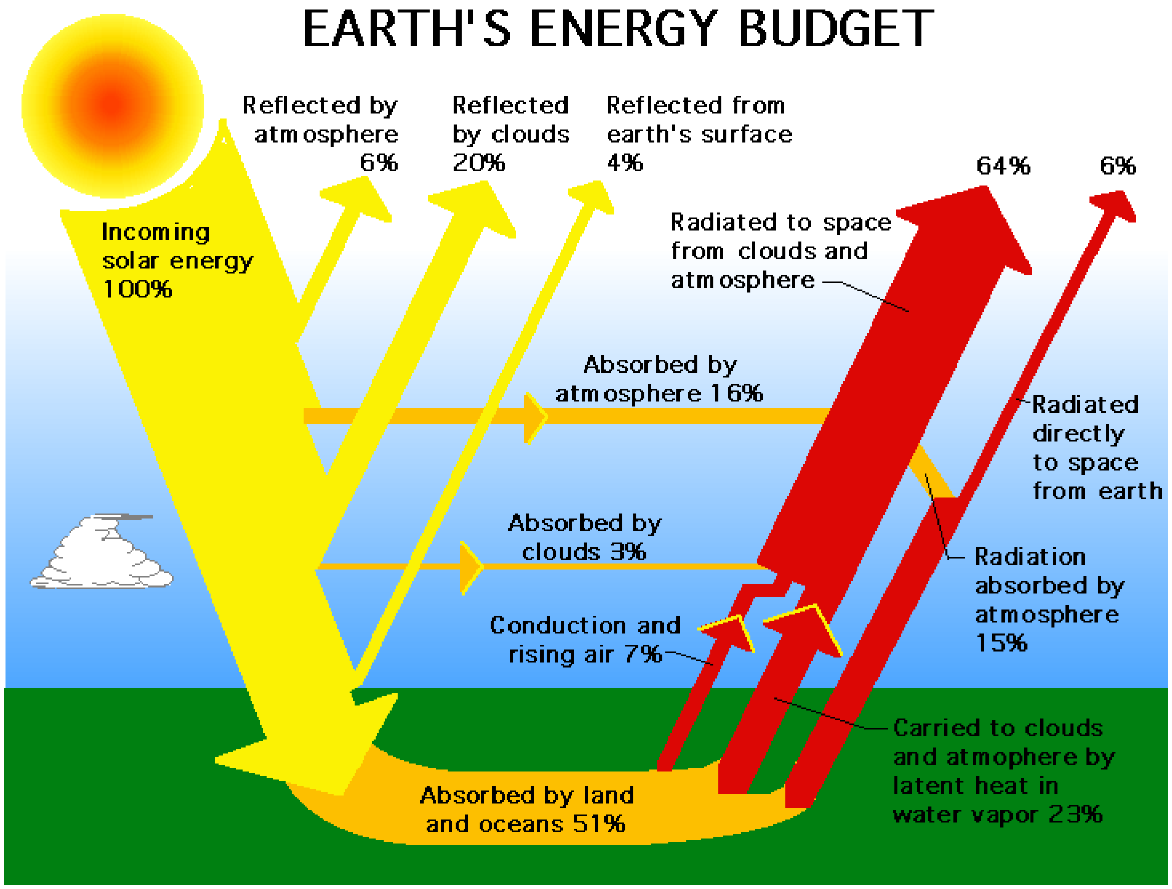

Source: NASA

Solar Radiation

❶UV (<400 nm) ❷Visible (400-800 nm) ❸Infrared (>800 nm)

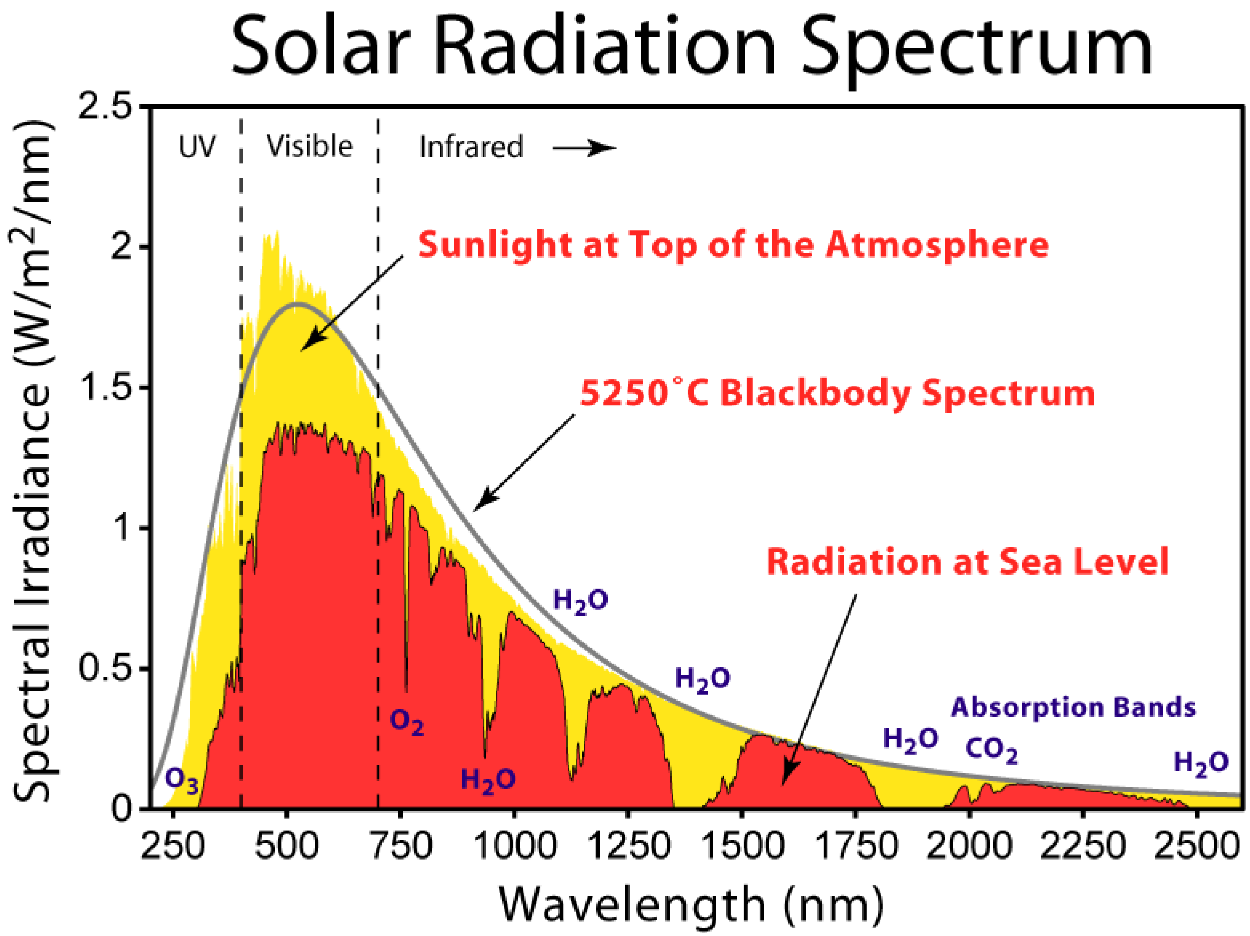

Air Mass

L/L_0 = air-mass coefficient

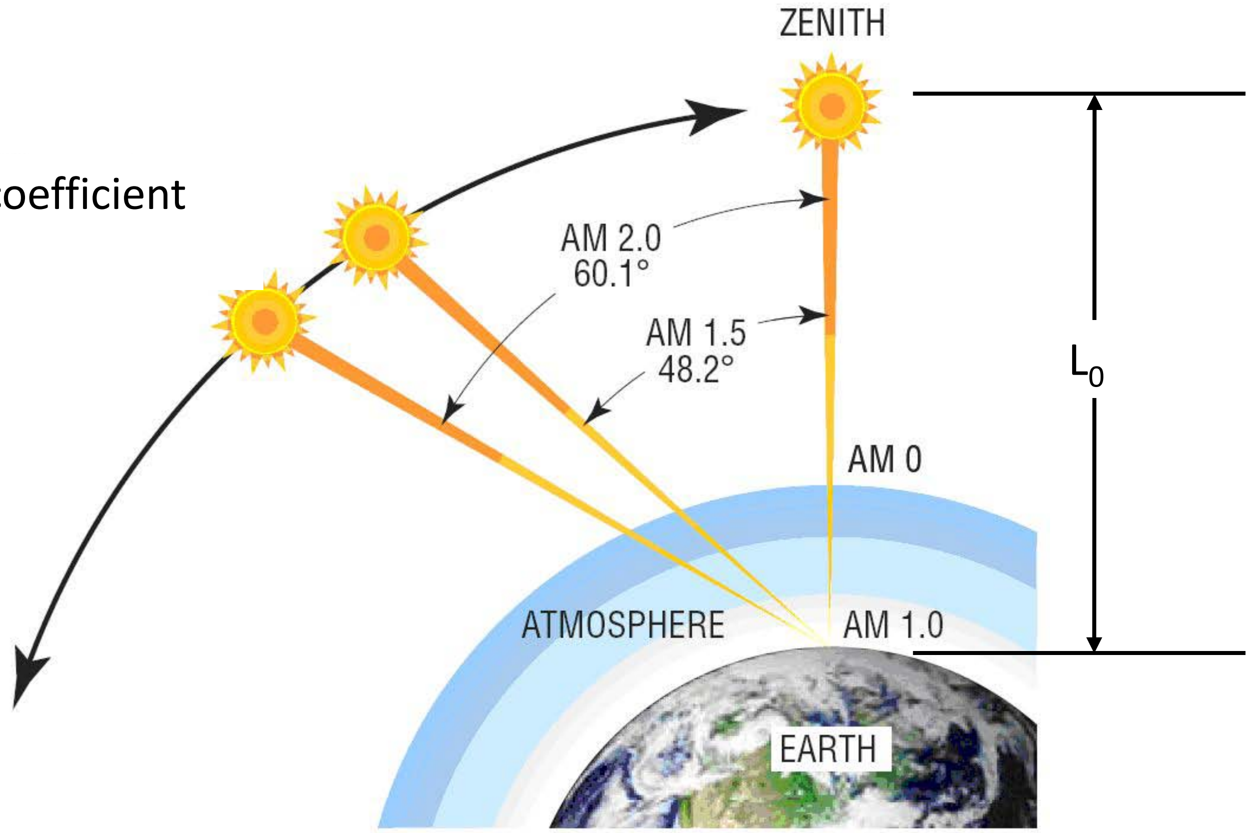

Source: Newport company

The energy spectrum AM 1.5 ➡ standard spectrum for measuring the efficiency of solar cells

Applications


Hubble Space Telescope


Solar hat fan


Solar array


Solar car


Solar street light


Solar water heater


Solar charger

Evolution of Solar Cells

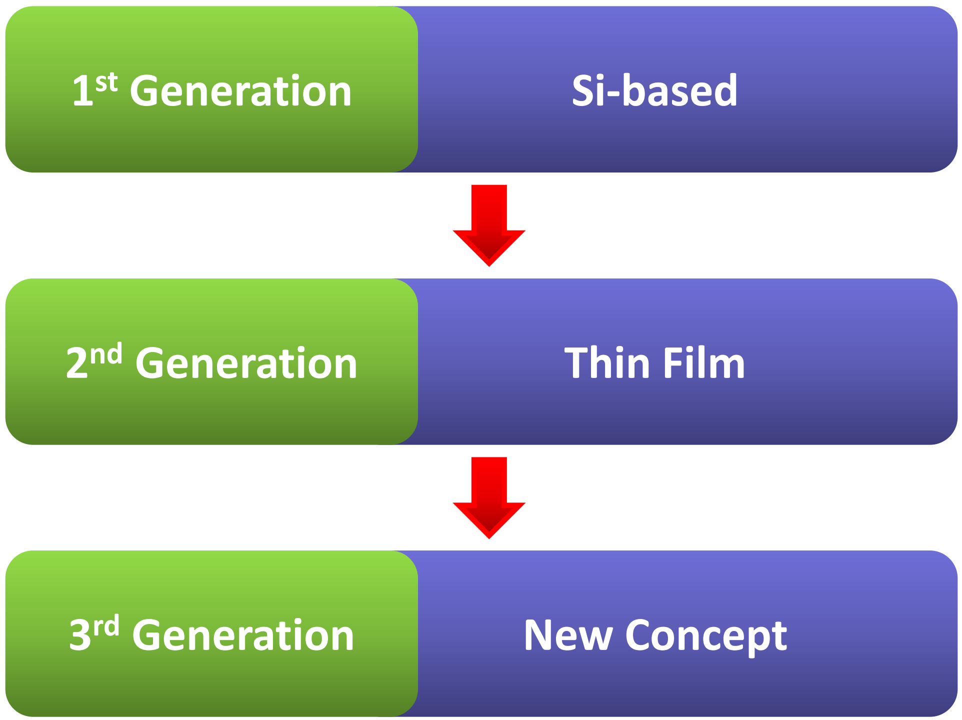

Categories & Efficiency

Categories of solar cells			Efficiency
Si-based	Crystalline	Single crystalline	12-20%
		Poly crystalline	10-18%
	Amorphous	Si, SiGe, SiC	6-9%
Thin Film	Single crystalline	GaAs, InP	18-30%
	Poly crystalline	CdS, CdTe, Cu(In, Ga)Se_2	10-20%
New Concept	Nano & Organic	P3HT:PCBM, CuPC/C60, ZnO, TiO_2	≤7%

Solar Cells Developments

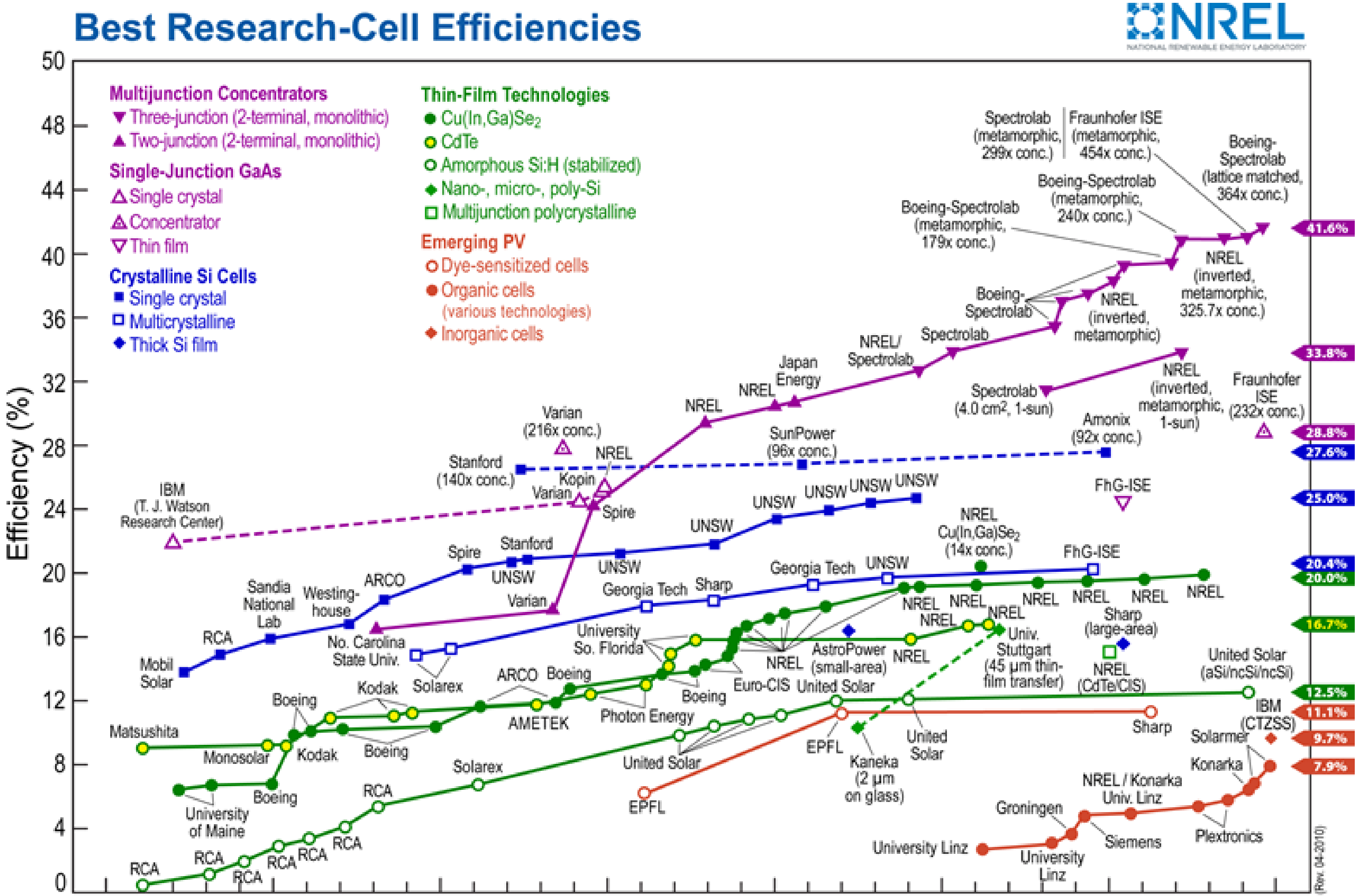

How Does a Photovoltaic Solar Cell Work?

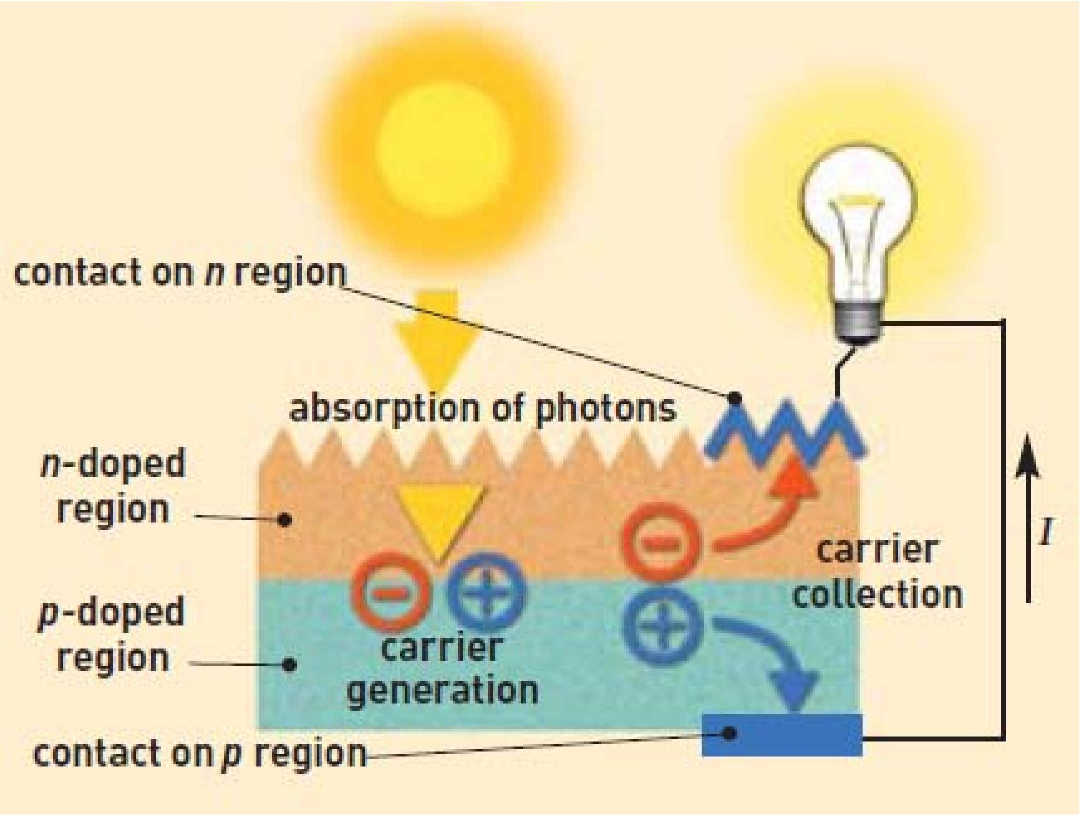

Basic Principle of Photovoltaic Device

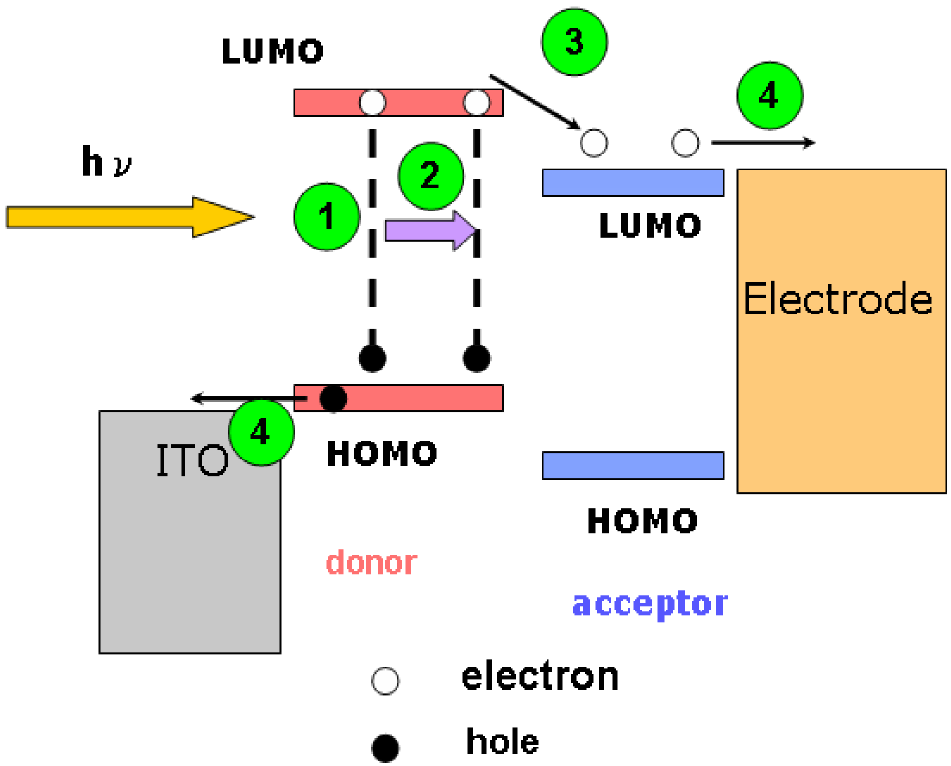

① Absorption of a photon leading to the formation of an excited state, the electron-hole pair (exciton).

② Exciton diffusion to a region (organic/organic interface or organic/metal interface).

③ The charge separation occurs.

④ Charge transport to the anode (hole) and the cathode (electron), to supply a direct current for the consumer load.

η_A: absorption efficeincy
η_{ED} : exciton diffusion efficeincy
η_{CT} : charge transfer efficeincy
η_{CC} : carrier collection efficeincy

External Quantum Efficiency(EQE): $\eta_{ext}=\eta_A \times \eta_{ED} \times \eta_{CT} \times \eta_{CC}$

H. Hoppe and S. Sariciftci, J. Mater. Res. **19**, 1924 (2004).

Basic Principle of Photovoltaic Device

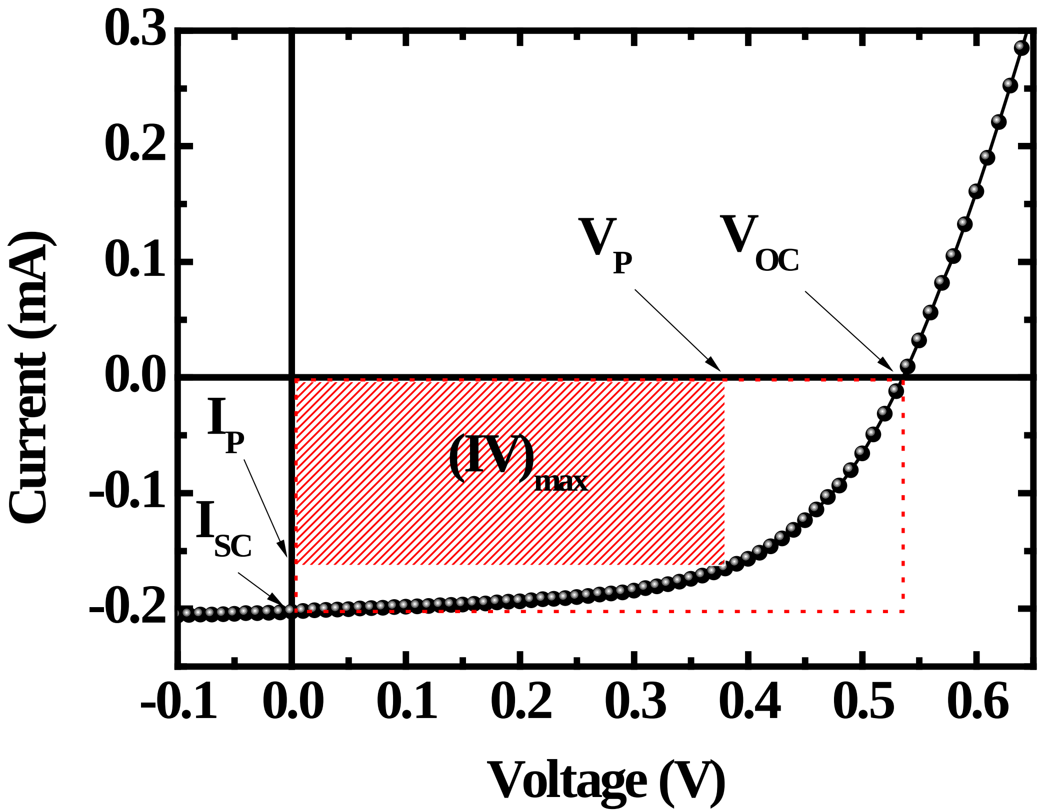

$$FF \equiv \frac{(IV)_{max}}{I_{SC}V_{OC}}$$

$$P_{max} = (IV)_{max} = V_{OC} \cdot I_{SC} \cdot FF$$

$$\eta(\lambda) \equiv \frac{I_{SC}(\lambda) \cdot V_{OC}(\lambda) \cdot FF(\lambda)}{P_{light}}$$

Basic Principle of Photovoltaic Device

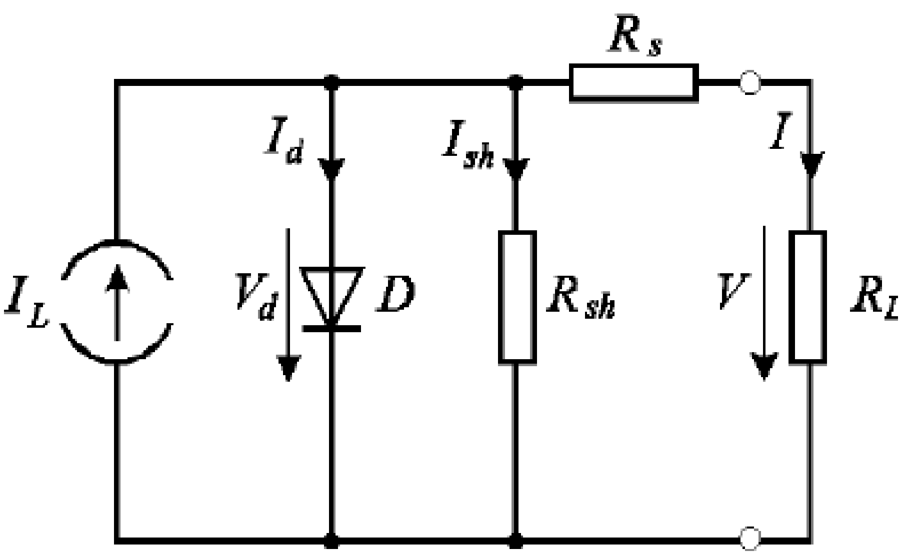

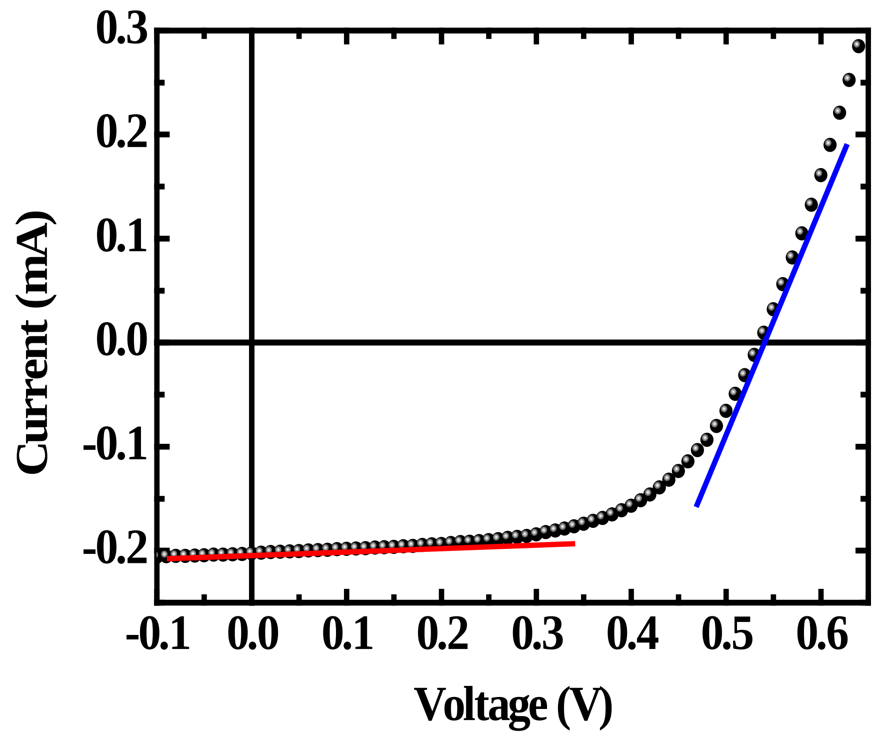

R_s (series resistance): mobility of the specific charge carriers in the respective transport medium
R_{sh} (shunt resistance): recombination of charge carriers near the interface

D. I. K. Petritsch, *Organic solar cell architectures*, PhD thesis, 2000

Analytical Technique

- Measurement of power conversion efficiency (PCE)
  - J-V characteristics (Voc, J_{sc}, Fill factor, R_s, R_{sh})
  - Incident Photo Conversion Efficiency
- Time of flight measurement
- Conductive Atomic Force Microscopy
- Time-resolved Photoluminescence
- Transmission Electron Microscopy

Analytical Technique

Measurement of power conversion efficiency (PCE)

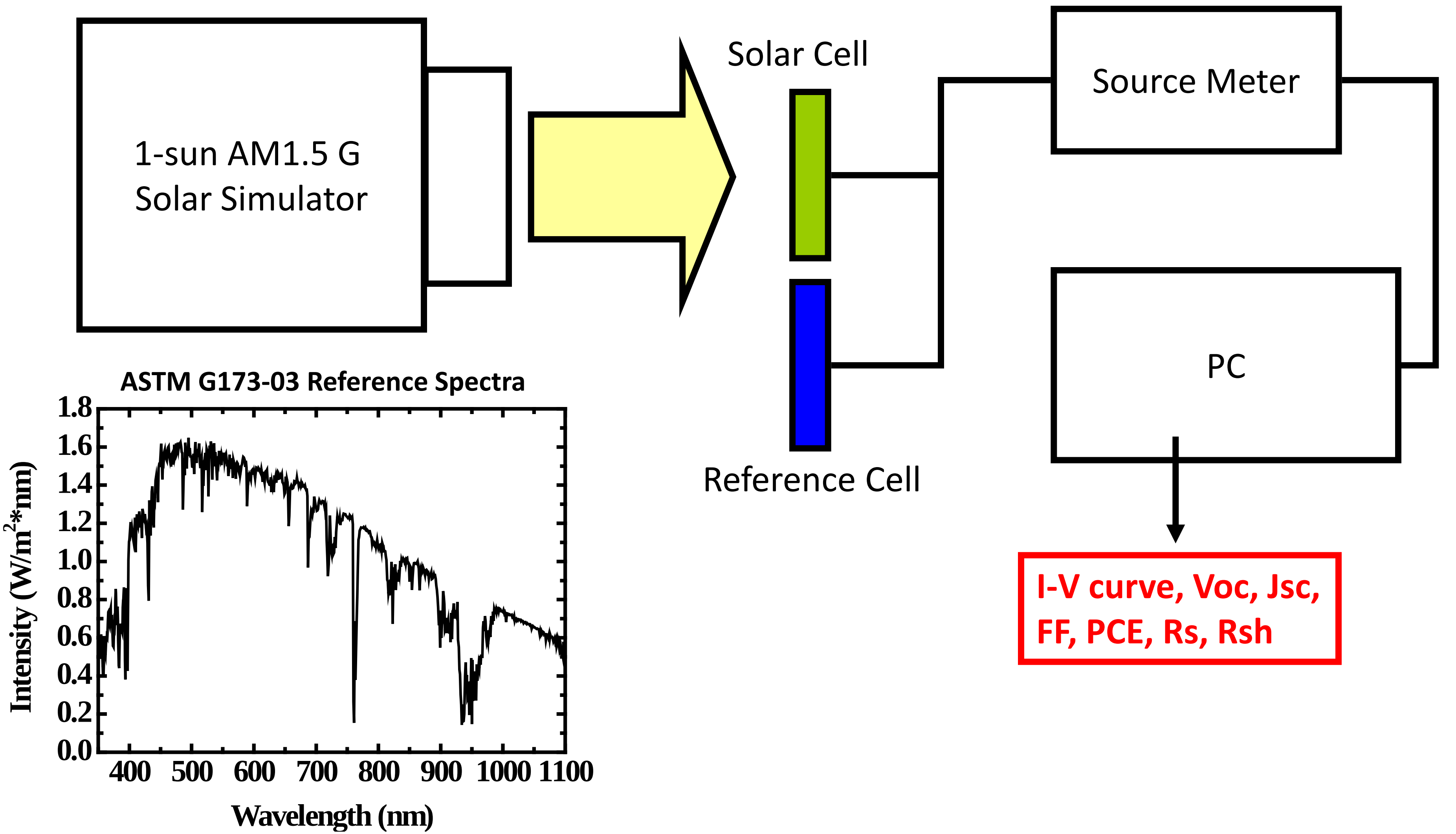

Standard ASTM G173-03, Standard Tables for Reference Solar Spectral Irradiances: Direct Normal and Hemispherical on 37 ° Tilted Surface, American Society for Testing and Materials, West Conshocken, PA, USA.

Analytical Technique

Measurement of power conversion efficiency (PCE)

- Standard J-V measurement system

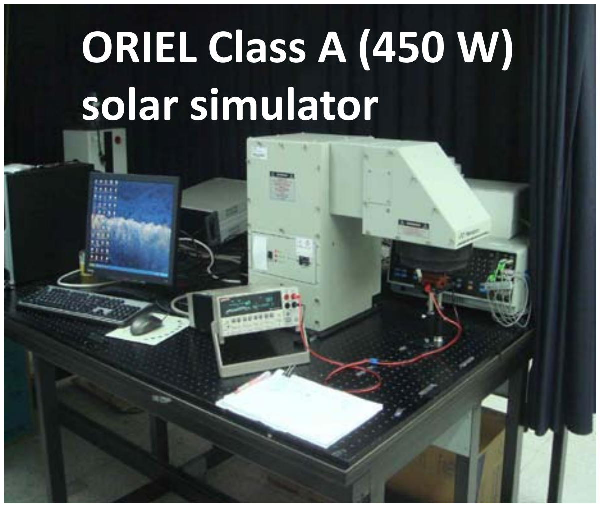

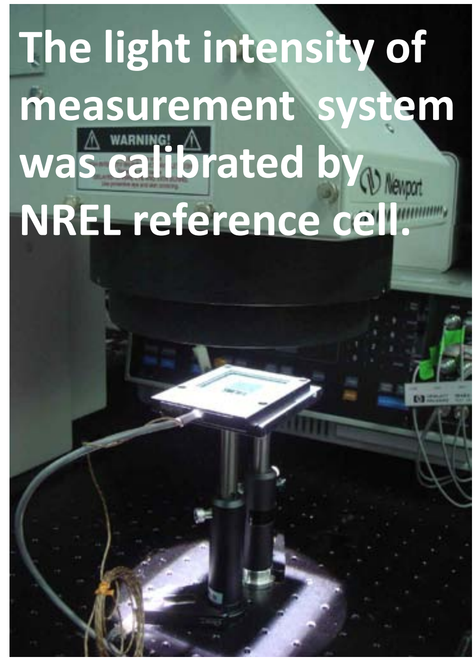

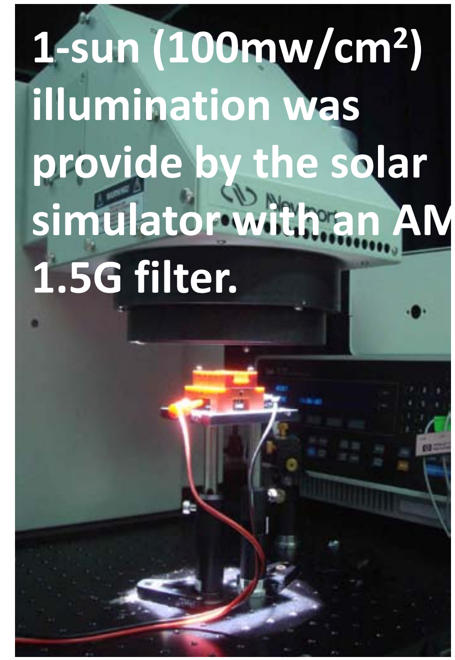

Device was illuminated under AM 1.5G, 1-sun illumination, which was provide by an ORIEL class A solar simulator.

(Si-testing cell: active area of 10*10 cm^2 < 1 % error)

Analytical Technique

Measurement of carrier mobility

- *Time-of-Flight (TOF) Measurement*

The sample of TOF is a single layer device with a semi-transparent metal electrode

ITO (100 nm) / Organic material (~ 1 μm) / Al (10 nm)

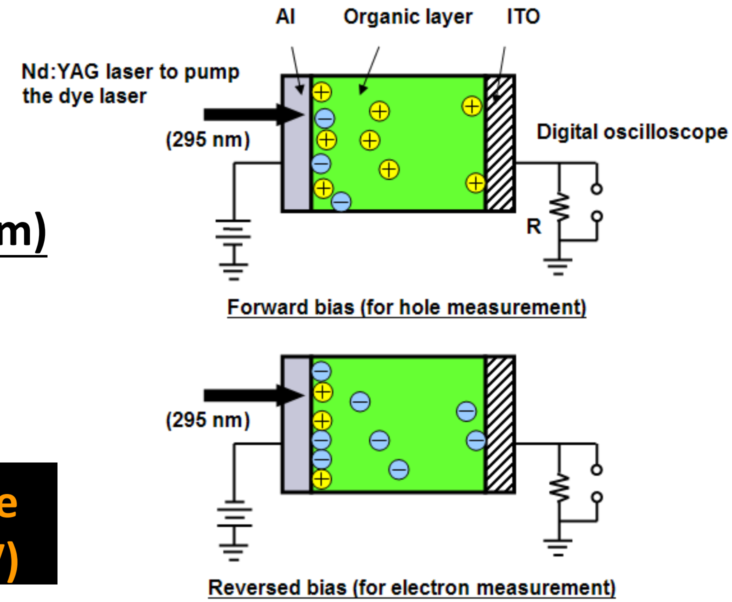

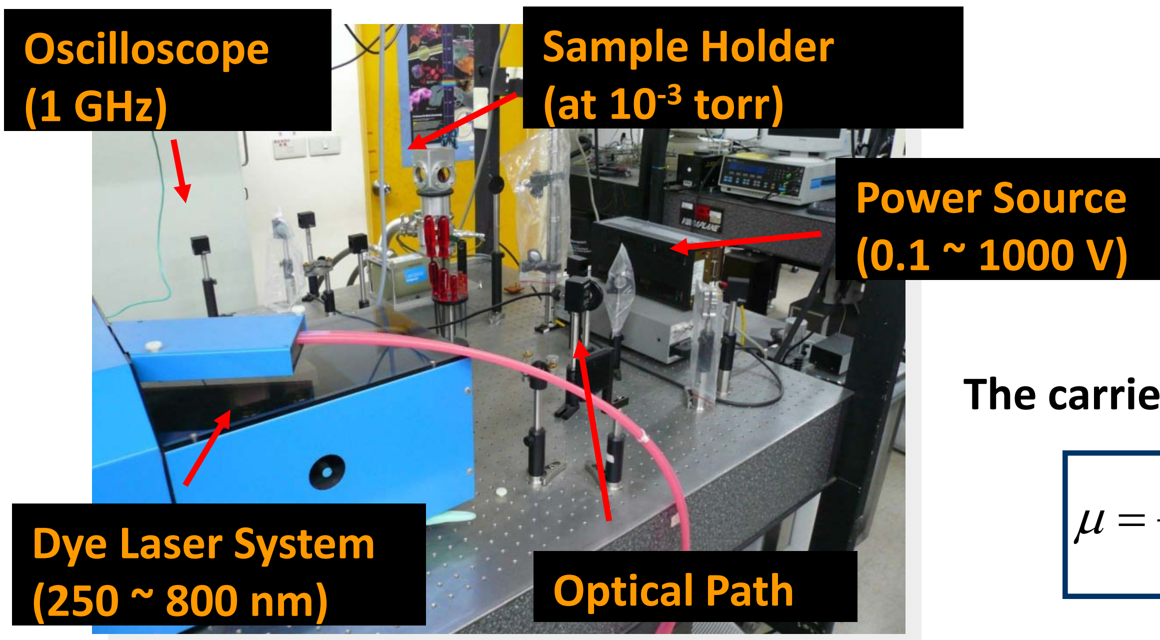

M. F. *Wu et. Al., Adv. Funct. Mater*. **17**, 1887 (2007).

The carrier mobility (m) is given by

$$\mu = \frac{D}{t_T E}$$

Where *D* is the thickness of organic layer, t_T is the transit time, and *E* is the applied electric field.

Analytical Technique

Conductive Atomic Force Microscopy

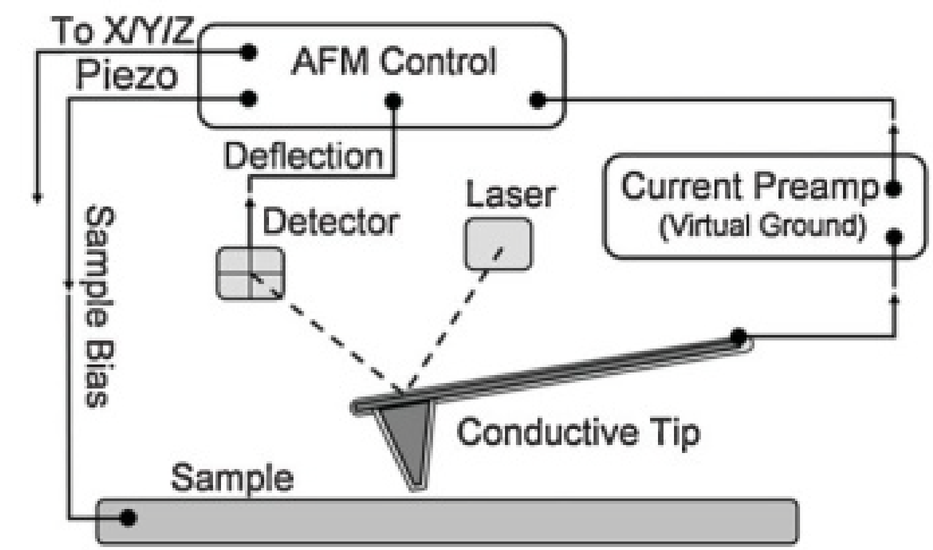

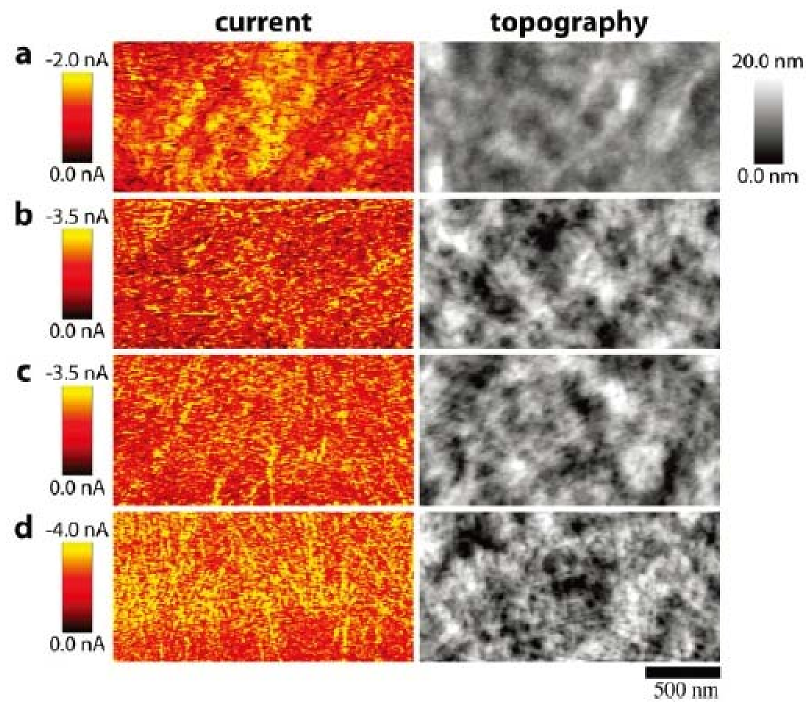

Conductive AFM images of pure P3BT-nw films

- Localized area analysis
- Bias voltage is applied between the conductive tip and the surface.
- The current flowing through the tip is detected with a current preamplifier and recorded as a function of position.

Analytical Technique

Time-resolved Photoluminescence

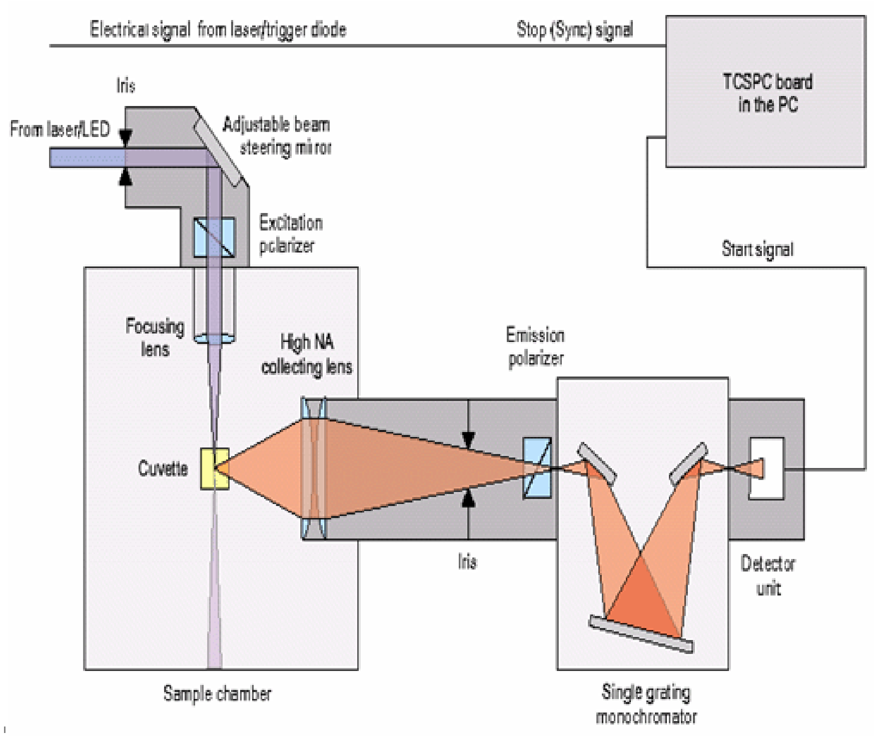

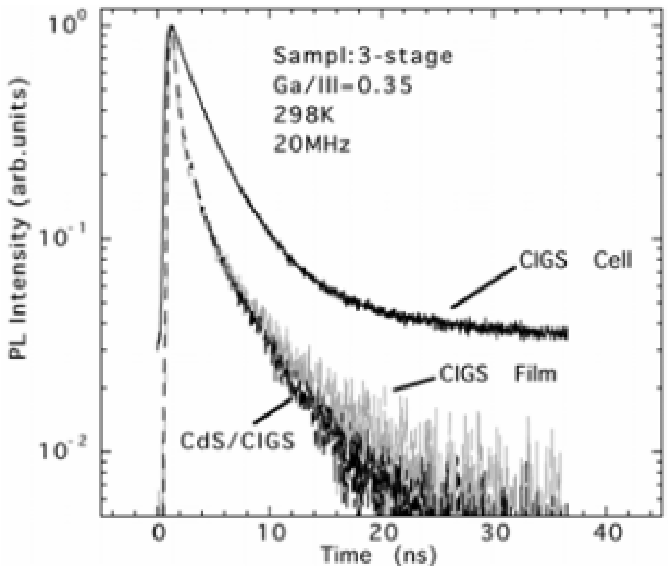

Typical PL decay curves of NBE-PL of CIGS thin film, CdS/CIGS and CIGS solar cell.

S. Shirakata *et al.*, physica status solidi (c) **6**, 1059 (2009).

TRPL is measured by exciting luminescence from a sample with a pulsed light source, and then measuring the subsequent decay in photoluminescence (PL) as a function of time.

➡ To measure the carrier lifetime

Analytical Technique
Transmission Electron Microscopy

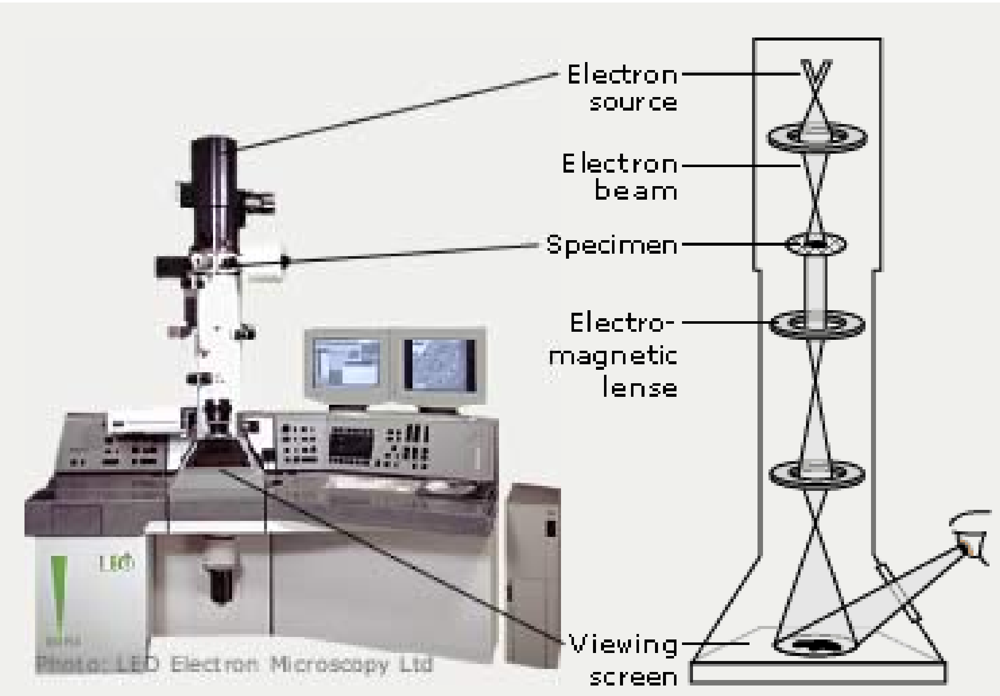

http://nobelprize.org/educational/physics/microscopes/tem/index.html

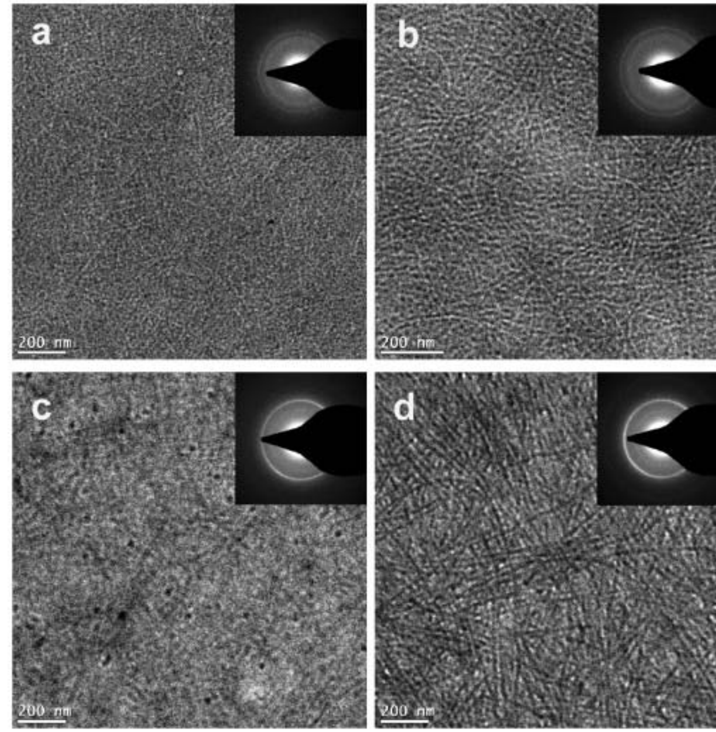

Bright-field TEM images of P3BT-nw/PC71BM (1:1) blend thin films (a,b) and pure P3BT-nw films (c, d) under condition A (a, c) and condition D (b, d).
The films were spin-casted on top of ITO/PEDOT substrates and peeled off by putting the samples in water. The insets are the electron diffraction of the corresponding film

H. Xin *et al*., ACS Nano **4**, 1861 (2010).

Facilities for Device Fabrication

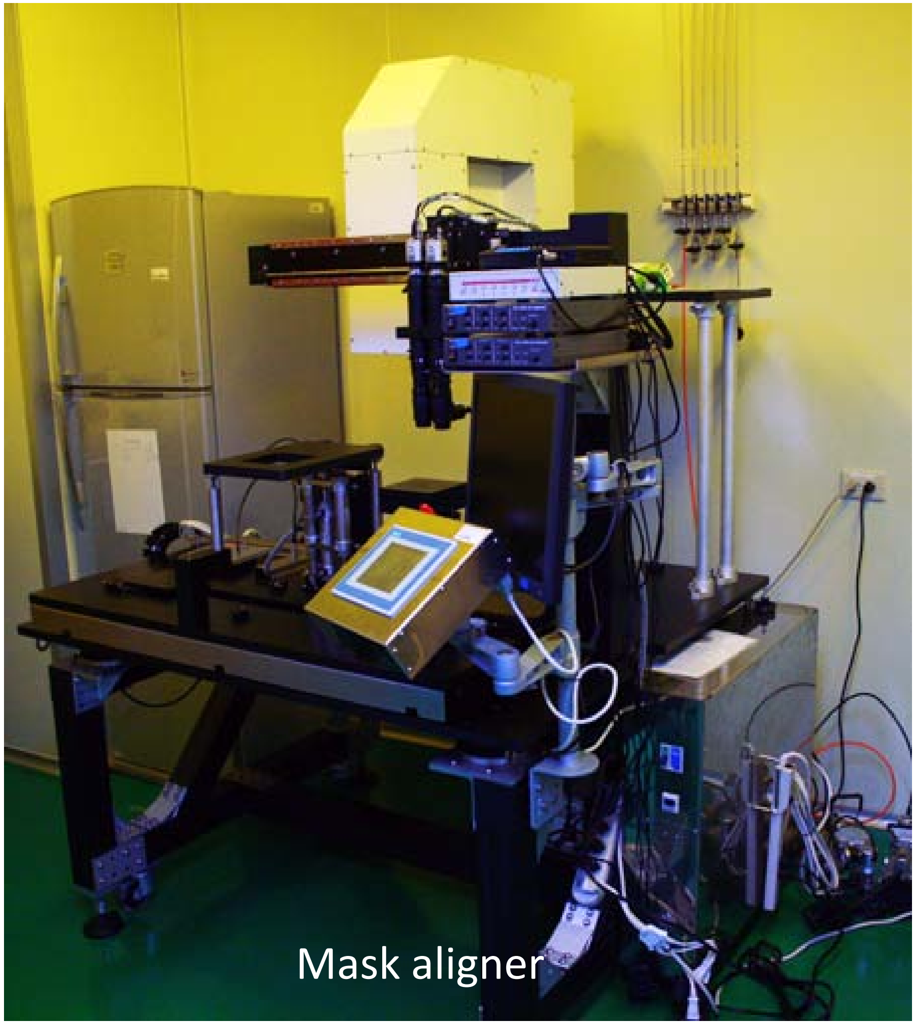

Mask aligner

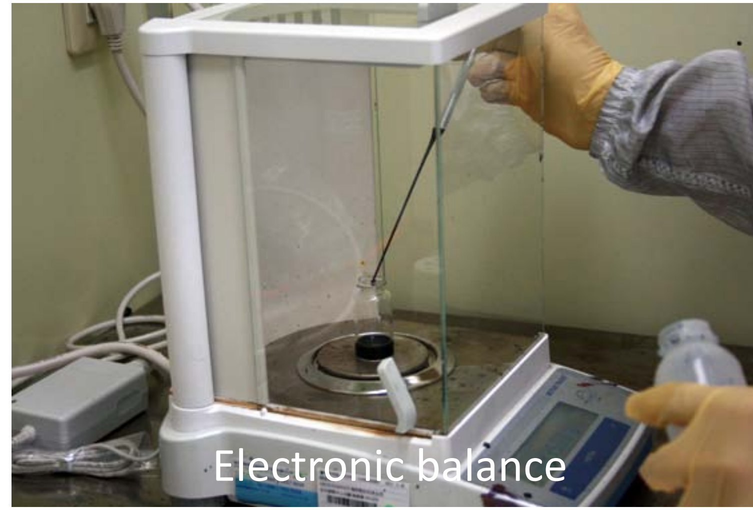

Electronic balance

Spin coater & hot plate

Facilities for Device Fabrication

Si Solar Cells

Wafer-based Si solar cells

- Single crystalline Si solar cell (c-Si)
  - ➡ Highest efficiency, most expensive
- Poly-crystalline Si solar cell
- Ribbon Si solar cell

Thin film Si solar cells

- Amorphous Si solar cell (a-Si)
- macro-crystalline Si solar cell (mc-Si)

◆ **Thin-film technologies**

Advantage ➡the amount of material required ↓ ➡ material cost ↓
➡flexibility, lighter weight, ease of integration.

Disadvantage ➡energy conversion efficiency ↓

Technology Development

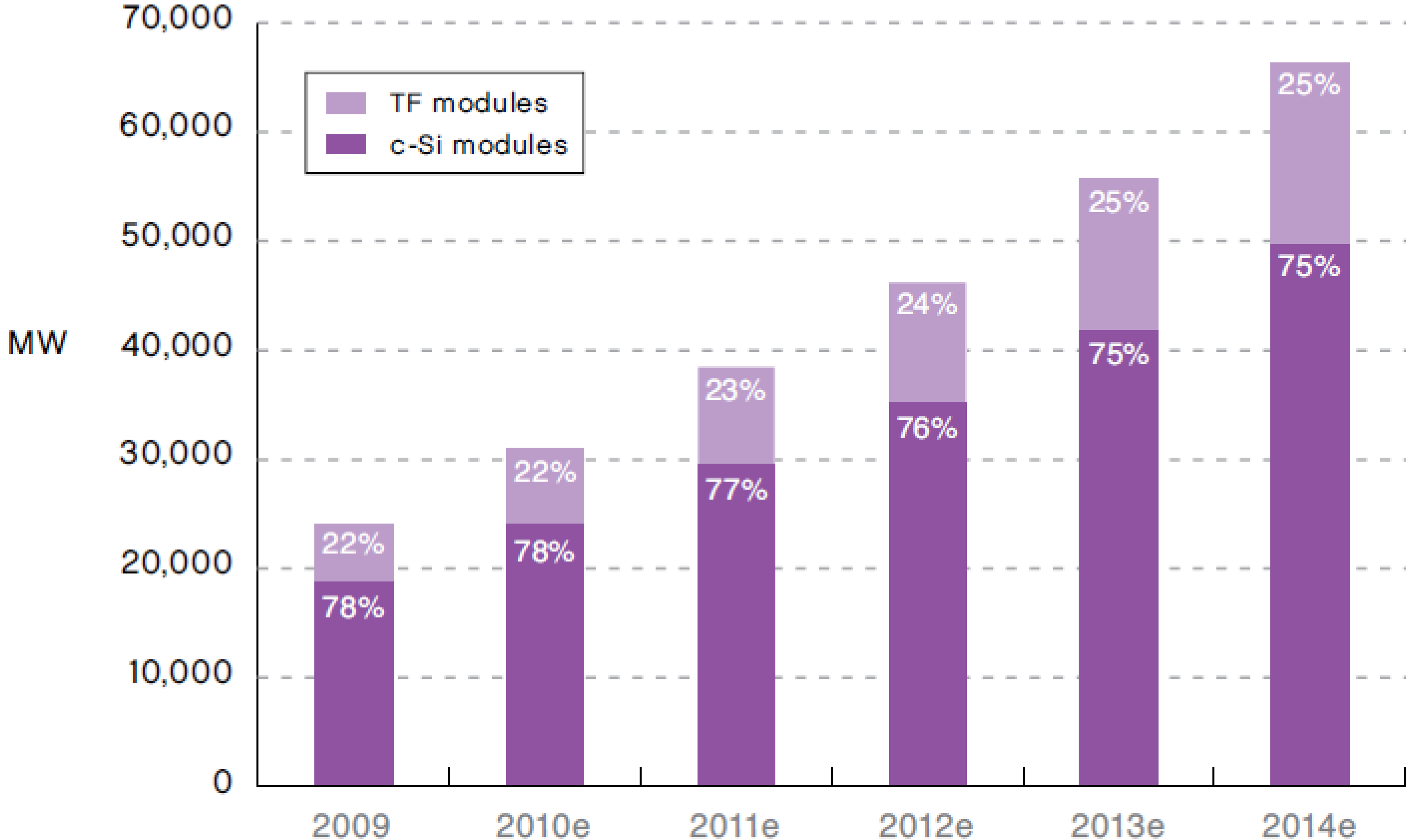

Production Capacity Outlook – Crystalline and Thin Film technologies

Source: EPIA 2009

Structures of Si-based Thin Film Solar Cells

Superstrate

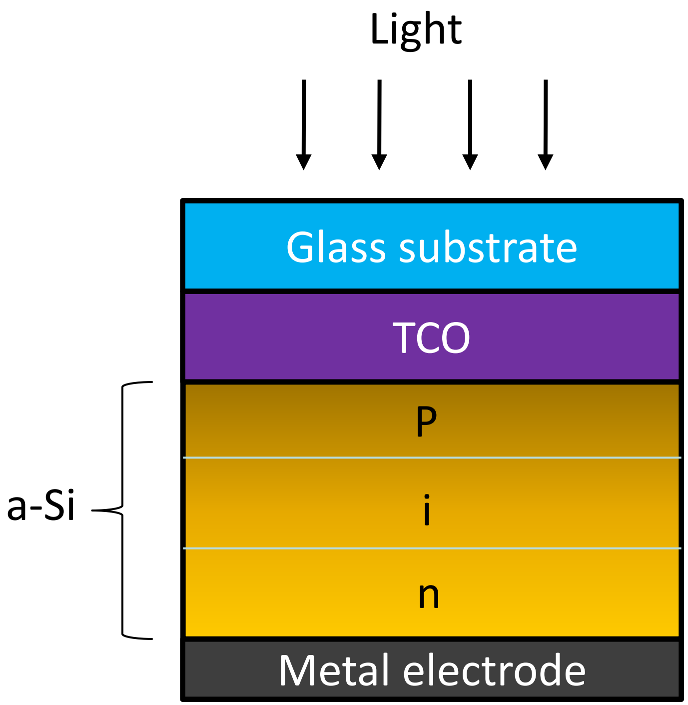

Substrate

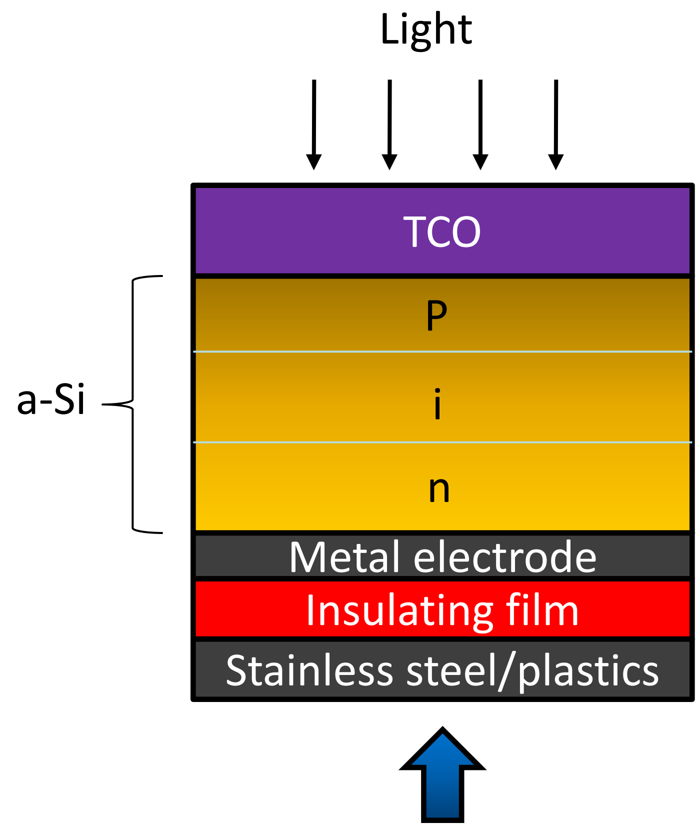

Roll-to-Roll process for flexible photovoltaic device

Fabrication process of a-Si solar cell

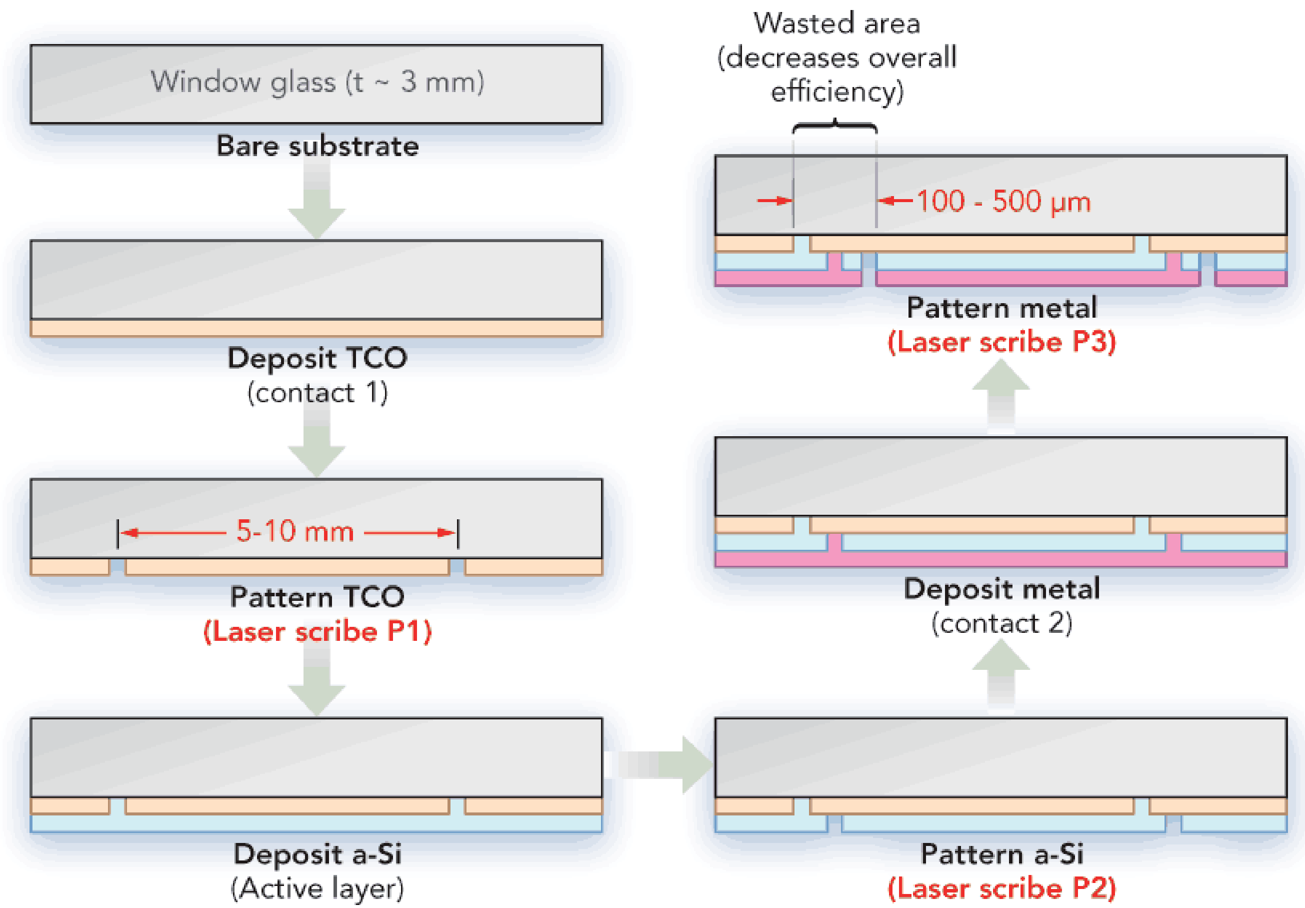

CIGS/CZTS Solar Cell

CIGS solar cell

$CuIn_xGa_{1-x}Se_2$

What is CZTS solar cell?

$Cu_2ZnSn(S_xSe_{1-x})_4$

●Copper Indium Gallium Diselenide (CIGS) Solar Cells

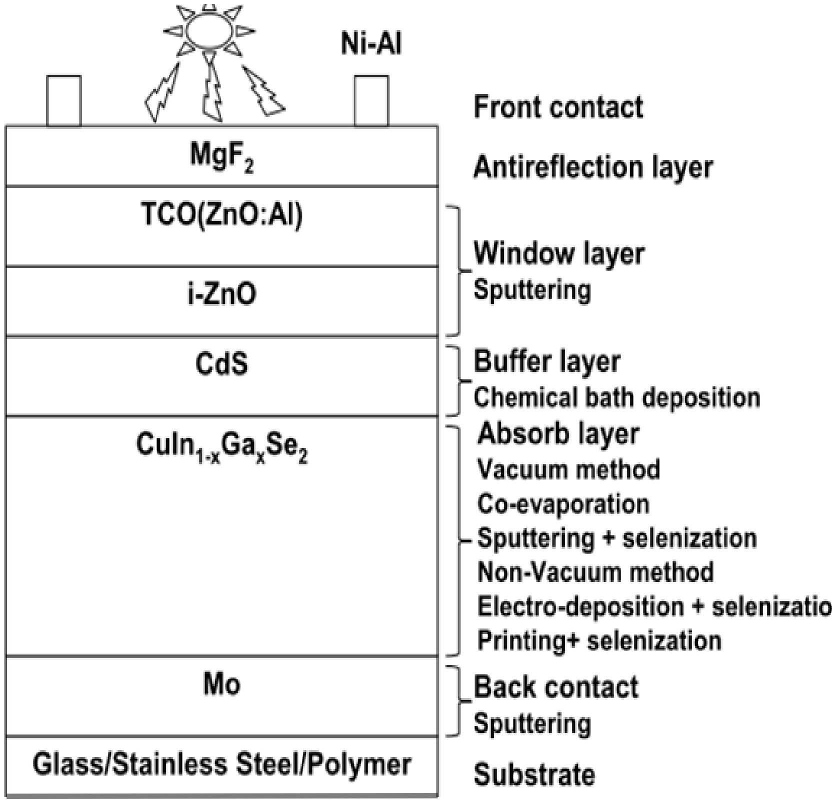

Device structure

Advantages

- High cell efficiency (19.2%) and module efficiency (13.4%).
- The band-gap can be determined by the In/Ga ratio
- Can be deposited on flexible substrates
- Comparatively long lifetime

Disadvantages

- Limited availability of indium
- Toxicity of CdS n-type buffer layer

Crystallographic Properties of CIGS/CZTS

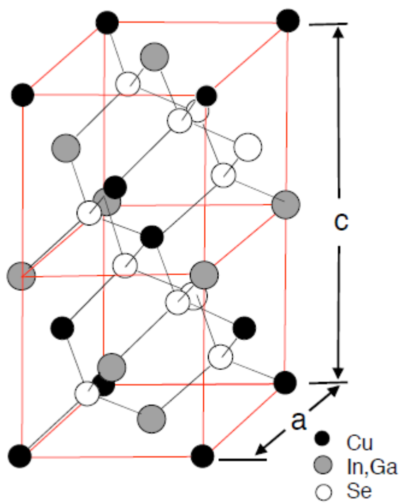

CIGS
(Chalcopyrite)

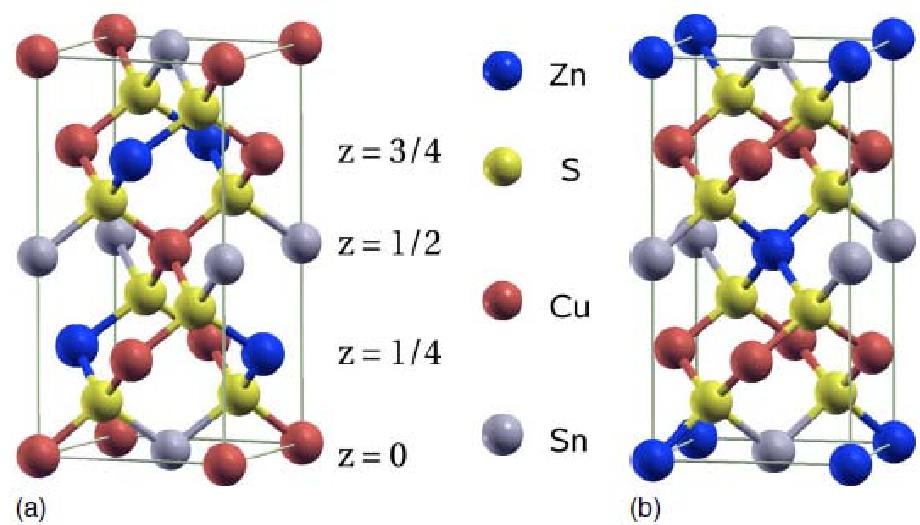

Schematic representations of the (a) kesterite and (b) stannite structures

J. Paier *et al.*, *Phys. Rev.* **B 79**, 115126 (2009).

CIGS solar cell manufacture

Vacuum method			
Co-evaporation		Sputtering + selenization	
👍	👎	👍	👎
Best cell:19.9% Best module: 14%	● Process control ● Modest material utilization	● Process control ● Sputtering is mature technology ● Moderate conversion efficiency ● Two steps can be combined	● Reaction kinetics can be slow ● Targets costly ● Adhesion ● H_2Se hazardous, attacks metal foils
Non-vacuum method			
Electro-deposition + selenization		Printing + selenization	
👍	👎	👍	👎
● Process control ● High production rates ● High materials utilization	● Low conversion efficiency ● Uniformity ● Adhesion ● H_2Se hazardous	Best cell:16.4% Best module: 11%	● Low conversion efficiency ● Reaction kinetics can be slow ● H_2Se hazardous

Global CIGS Manufacturer

Manufacturer		Substrate	Process	Module Efficiency (%)
Japan	Showa Shell	glass	Sputter/Selenization	14
	Honda	glass	Selenization	13.9
U.S.A.	Global Solar	steel	Co-evaporation/R2R	10
	Ascent Solar	polymer	Co-evaporation	-
	Nanosolar	flexible	Print/RTP	11
	Daystar	glass	Sputter	10
	ISET	glass/flex	Ink/Selenization	13.6/glass
	Miasole	glass	Sputter	-
	SoloPower	steel	ED/RTP	-
Europe	Avancis	glass	Sputter/RTP	-
	Würth Solar	glass	Co-evaporation	13

CZTS Solar Cell Device

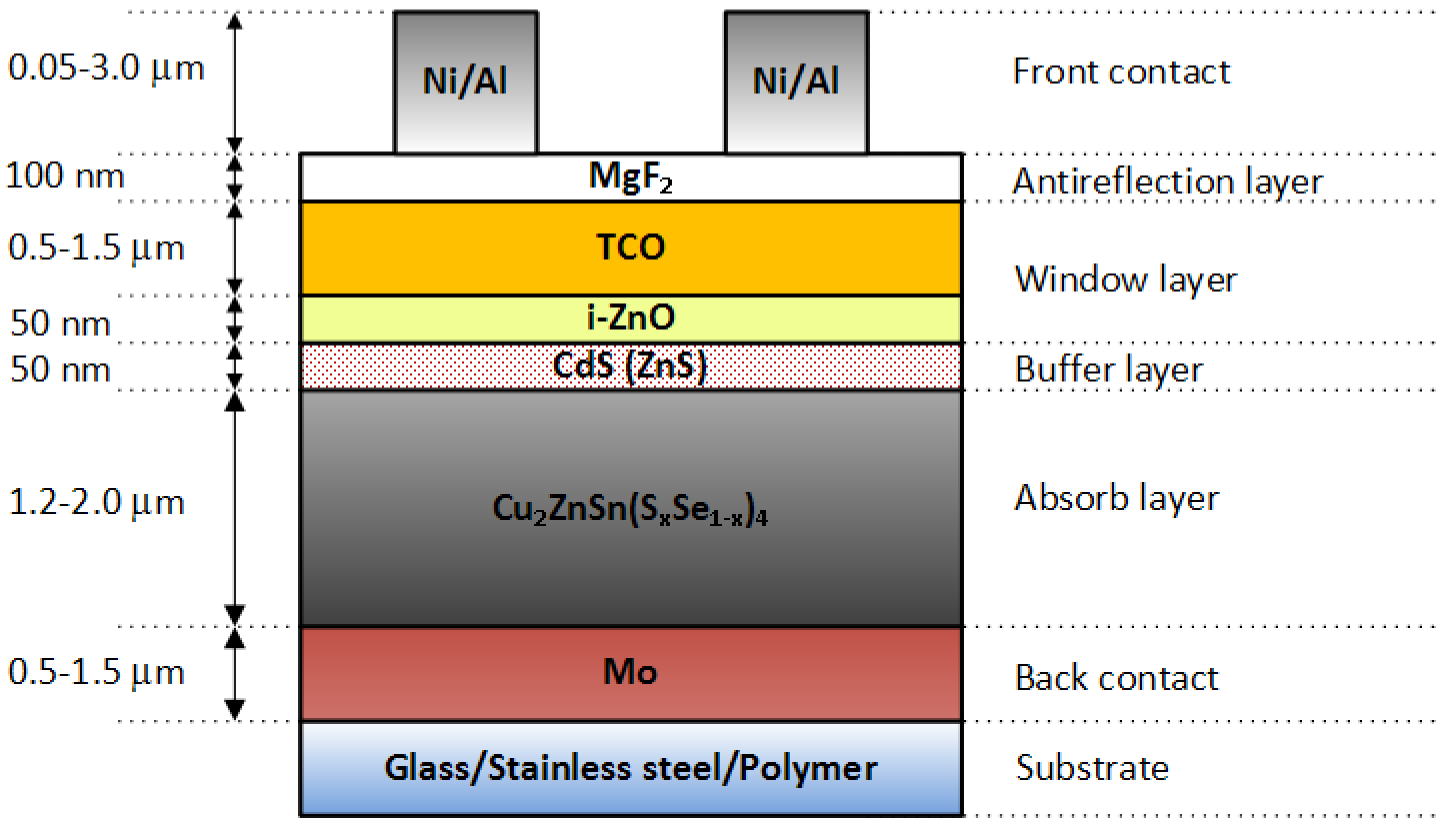

Approaches for the Preparation of CZTS Thin Film

	Best efficiency	
Physical vapor method		
Sputtering	6.77%	K. Jimbo *et al.*, *Thin Solid Films* **515**, 5997 (2007). H. Katagira *et al.*, *Appl. Phys. Express* **1**,041201 (2008). T. Tanaka *et al.*, *J. Phys. Chem. Solids* **66**, 1978 (2005).
Evaporation	1.79%	H. Araki et al., *Thin Solid Films* **517**, 1457 (2008). H. Katagiri et al., *Sol. Energy Mater. Sol. Cells* **49**, 407 (1997). T. Tanaka *et al.*, *Phys. Status Solidi C* **3**, 2844 (2006).
Chemical deposition method		
Electro-deposition	3.4%	M. Kurihara *et al.*, *Physica Status Solidi* C **6**, 1241 (2009). A. Ennaoui *et al.*, *Thin Solid Films* **517**, 2511 (2009). H. Araki *et al.*, *Sol. Energy Mater. Sol. Cells* **93**, 996 (2009).
Photochemical deposotion	-	K. Moriya *et al.*, *Phys. Status Solidi* C **3**, 2848 (2006).
Sol-gel	1.01%	M. Y. Yeh *et al.*, *J. Sol-Gel Sci. Technol.* **52**, 65 (2009). K. Tanaka *et al.*, *Sol. Energy Mater. Sol. Cells* **93**, 583 (2009). K. Tanaka *et al.*, *Sol. Energy Mater. Sol. Cells* **91**, 1199 (2007).
Spray pyrolysis	-	N. Nakayama *et al.*, *Appl. Surf. Sci*. **92**, 171 (1996). J. Madarasz *et al.*, Solid State Ionics, 439 (2001). N. Kamoun *et al.*, *Thin Solid Films* **515**, 5949 (2007).
Solution-based synthesis	9.66%	T. K. Todorov *et al.*, *Adv. Mater.* **22**, E156 (2010). S. C. Riha *et al.*, *J. Am. Chem. Soc.* **131**, 12054 (2009). Q. Guo *et al.*, J. Am. Chem. Soc. **131**, 11672 (2009). C. Steinhagen et al., *J. Am. Chem. Soc.* **131**, 12554 (2009).

Vacuum Method for CZTS Solar Cell

Nagaoka National College of Technology

Cu,Zn,Sn, S deposition

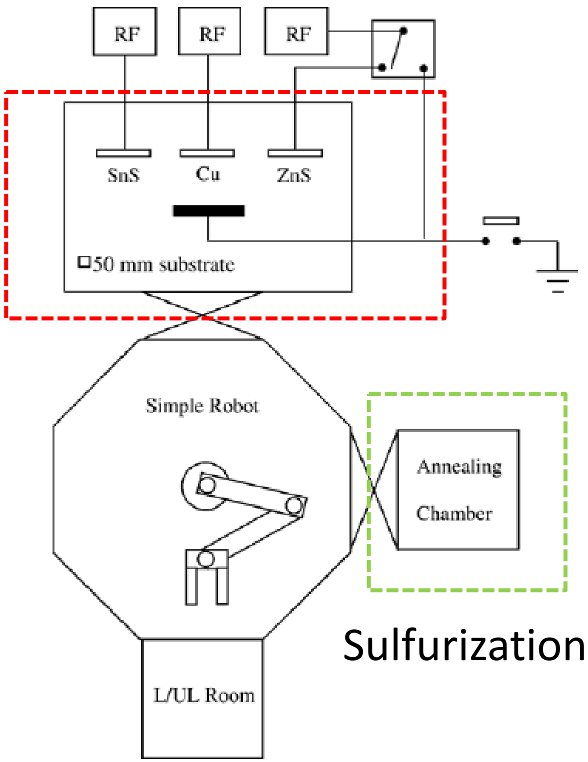

Sulfurization

Inline-type vacuum apparatus

Co-sputtering

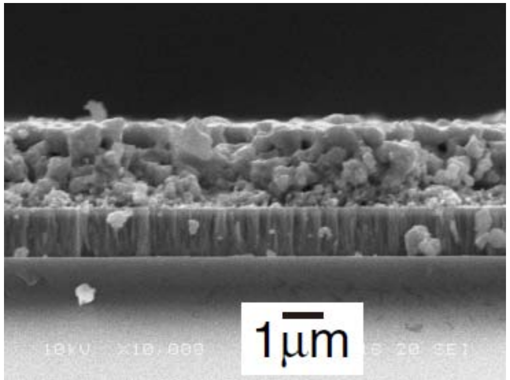

SEM image of the cross-sectional view of the CZTS absorber layer on the Mo electrode layer.
Many voids in the CZTS absorber layer were confirmed

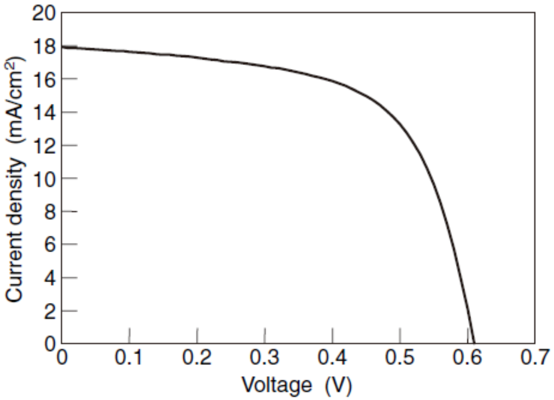

η = 6.77%
V_{oc} = 610 mV
J_{sc} = 17.9 mA/cm^2
FF = 0.62

K. Jimbo *et al.*, *Thin Solid Films* **515**, 5997 (2007).
H. Katagira *et al.*, *Appl. Phys. Express* **1**,041201 (2008).

Vacuum method

Stacking Sequence of Precursors (1)

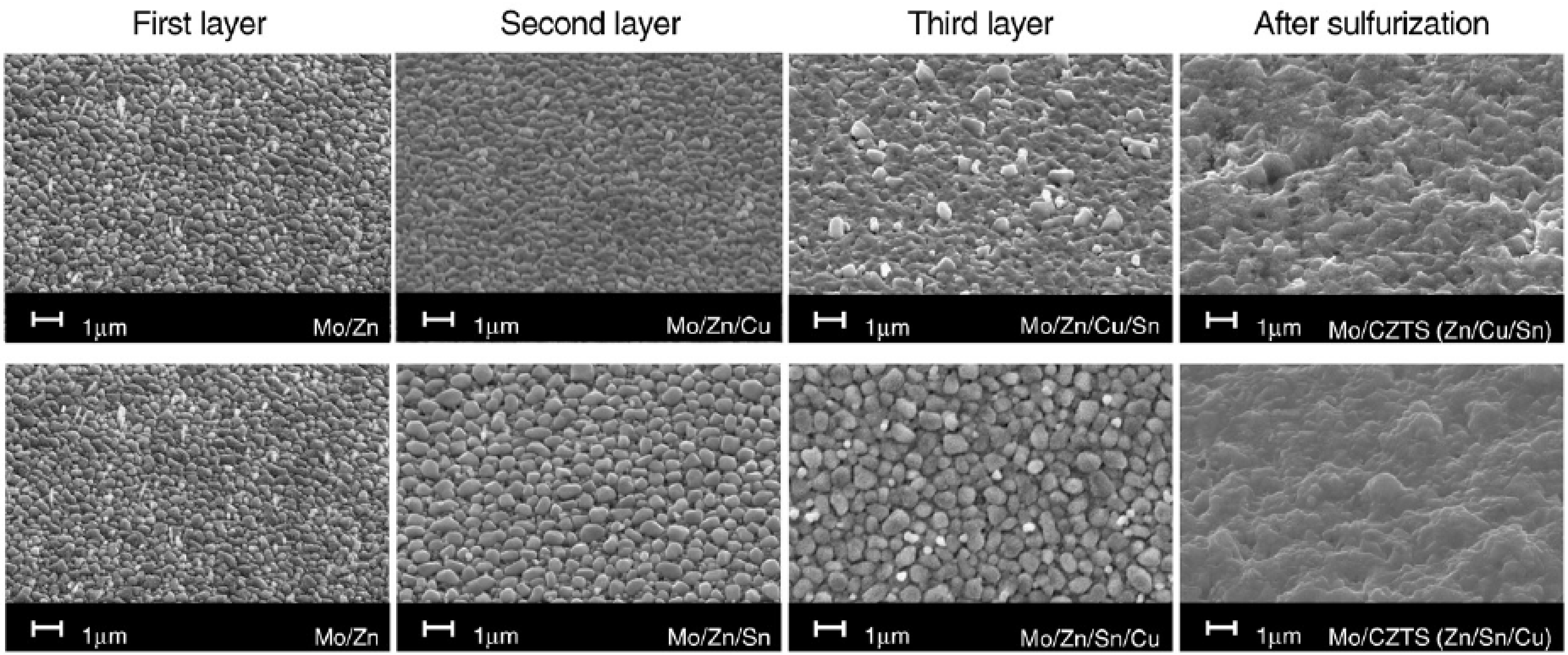

SEM micrographs of the precursors and sulfurized films

e-beam evaporation

H. Araki *et al.*, *Thin Solid Films* **517**, 1457 (2008).

Stacking Sequence of Precursors (2)

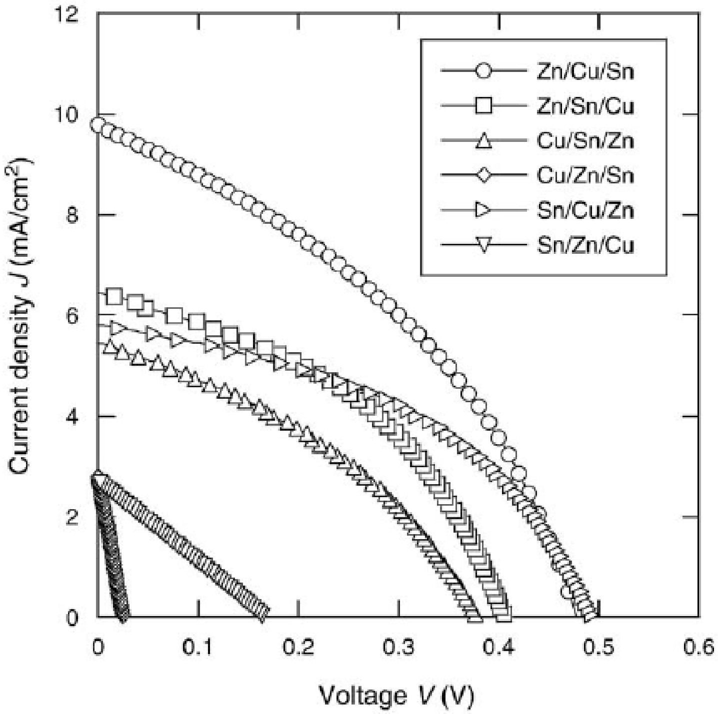

Comparison of the I–V characteristics of cells used six stacking orders of the precursors.

Photovoltaic properties of the solar cells

Stacking order	Group	Photovoltaic properties of cells				
		Area (cm^2)	V_{oc} (mV)	J_{sc} (mA/cm^2)	Fill factor	Efficiency (%)
Mo/Zn/Cu/Sn	A	0.132	478	9.78	0.38	1.79
Mo/Zn/Sn/Cu	A	0.135	406	6.44	0.43	1.12
Mo/Cu/Sn/Zn	A	0.120	377	5.43	0.38	0.77
Mo/Cu/Zn/Sn	B	0.166	24	2.60	0.27	0.01
Mo/Sn/Cu/Zn	B	0.126	495	5.81	0.45	1.29
Mo/Sn/Zn/Cu	C	0.150	166	2.54	0.25	0.11

A large conversion efficiency was observed in the cells with stacking order where Cu and Sn were adjacent.

H. Araki *et al.*, *Thin Solid Films* **517**, 1457 (2008).

Compositions of CZTS Thin Film

Chemical composition and compositional ratio of CZTS thin films with several composition

Sample No.	Chemical composition				Compositional ratio		
	Cu (at%)	Zn (at%)	Sn (at%)	S (at%)	Cu/(Zn+Sn)	Zn/Sn	S/Metal
CZTS-0.49	16.0	16.2	16.7	51.1	0.49	0.97	1.05
CZTS-0.69	20.0	14.1	15.1	50.8	0.69	0.93	1.03
CZTS-0.80	22.1	13.7	14.0	50.3	0.80	0.98	1.01
CZTS-0.91	23.5	12.7	13.1	50.7	0.91	0.98	1.02
CZTS-0.99	25.0	12.6	12.8	49.6	0.99	0.98	0.98
CZTS-1.01	26.1	11.8	12.2	49.9	1.09	0.97	1.00
CZTS-1.18	27.4	11.4	11.9	49.4	1.18	0.96	0.98

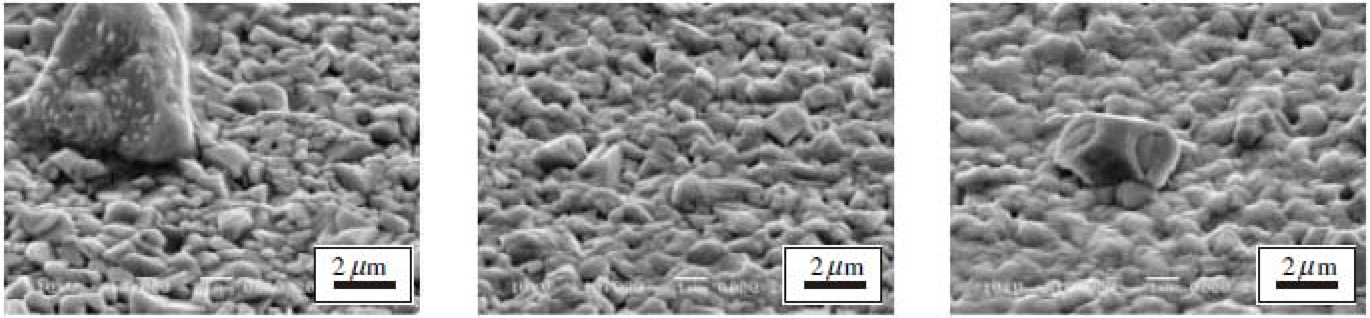

(a) (b) (c)

SEM micrographs of the surface of CZTS films with various compositions. These numbers correspond to their Cu/(Zn+Sn) ratio. (a) CZTS-0.49 (b) CZTS-0.83 (c) CZTS-1.18.

Zn-rich, Cu-poor compositions are desirable for the CZTS
Cu/(Zn+Sn) = 0.8-0.9 suitable for absorber

H. Katagiri, *Thin Solid Films* **480–481**, 426 (2005); K. Jimbo *et al.*, *Thin Solid Films* **515**, 5997 (2007);
T. Kobayashi *et al.*, *Jpn. J. Appl. Phys.* **44**, 783 (2005); K. Moriya *et al.*, *Jpn. J. Appl. Phys.* **47**, 602 (2008).

Organic Solar Cells

- **Why Organic Solar Cells**
  - low cost, roll-to-roll process
  - light weight, flexibility
  - selectivity of materials
- **Drawback of Organic Solar Cells**
  - poor efficiency
  - stability, life time issue

R. F. Service, Science. **309**, 548(2005)

Device Structure

- **Planer Heterojunction OSC**
  - Formed between a homogeneous donor layer and a homogenous acceptor layer
  - Charge collection efficiency(η_{CC}) will be relatively large
  - The exciton diffusion efficiency(η_{ED}) might be a bottleneck

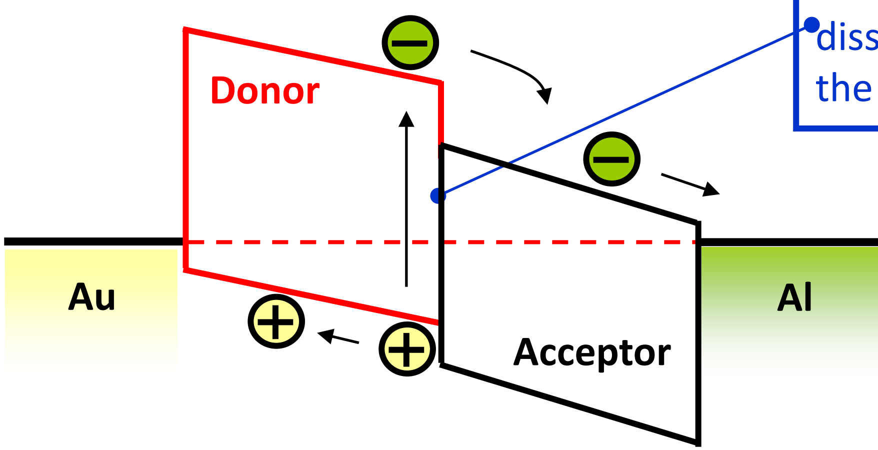

Bilayer device

Photogenerated excitons can only be dissociated at the D-A interface and thus the device is exciton diffusion limited.

The bilayer structure usually use in the small molecular OSC system with the thermal evaporation fabrications.

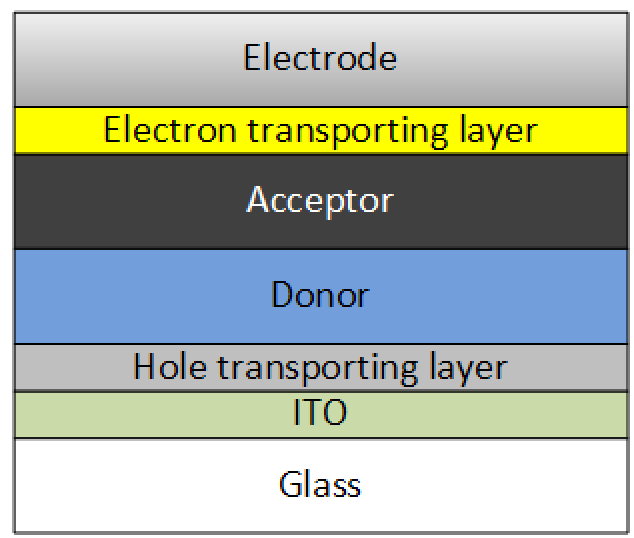

Device Structure

- **Mixed HJ(Blending, BHJ) OSC**
  - Usually used in polymer based organic solar cell employs the solution process
  - The η_{ED} approaches to unity in the mixed HJ generally
  - Charge collection efficiency(η_{CC}) in mixed HJ OSC often plays the role of the bottleneck

The donor is blended with the acceptor. Thus, photogenerated excitons can be dissociated into charges immediately.

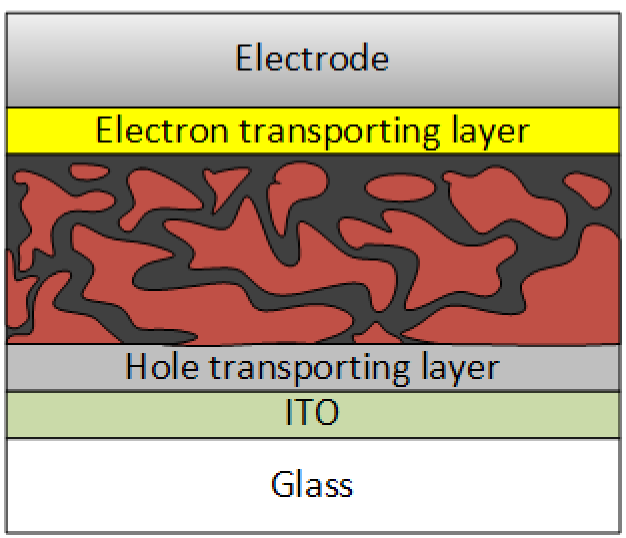

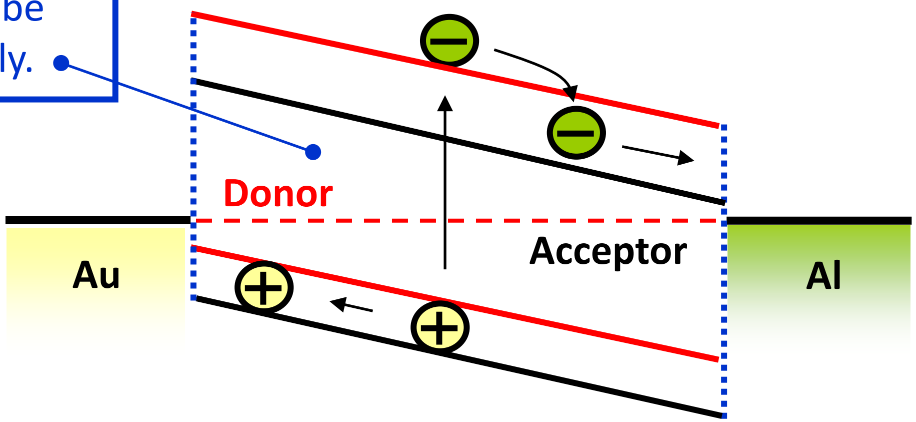

Bulk heterojunction

The polymer OSC systems usually use the BHJ structure with the spin coating process.

Fabrication Process of Organic Photovoltaic Device

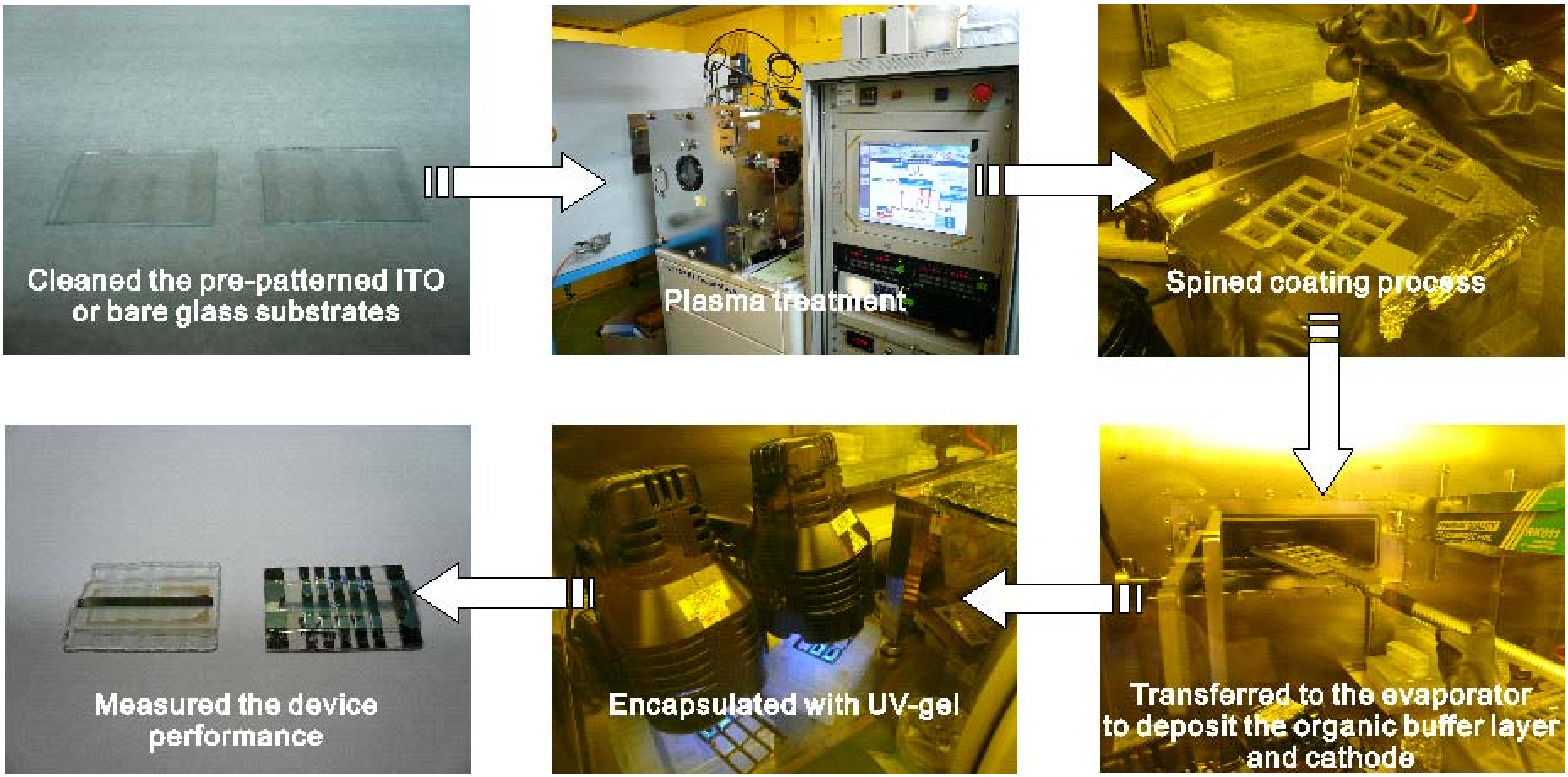

Active Materials

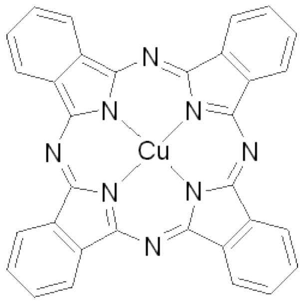

copper phthalocyanine
(CuPc)

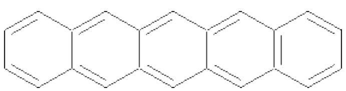

pentacene

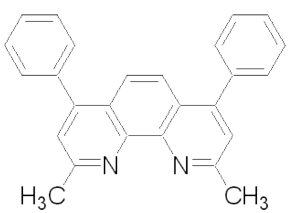

bathocuproine
(BCP)

small molecular materials

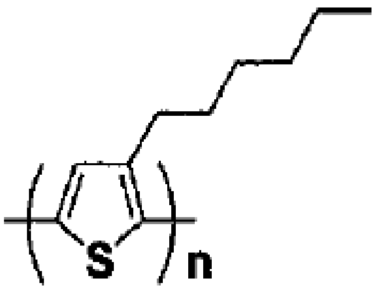

P3HT

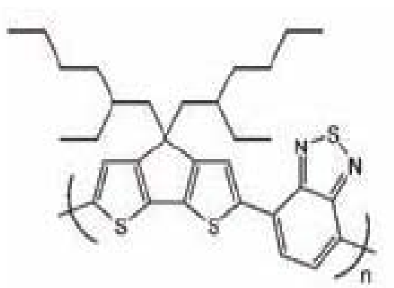

PCPDTBT

polymer materials

C_{60}

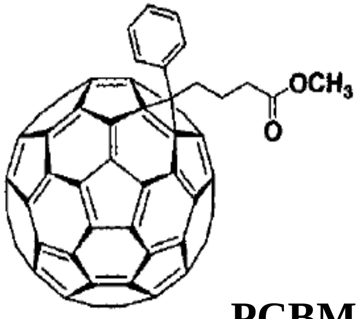

PCBM

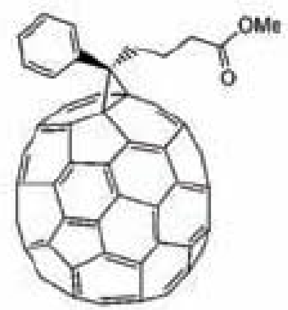

$PC_{70}BM$

fullerene system

Evolution of OSC

The first breakthrough of organic based solar cell

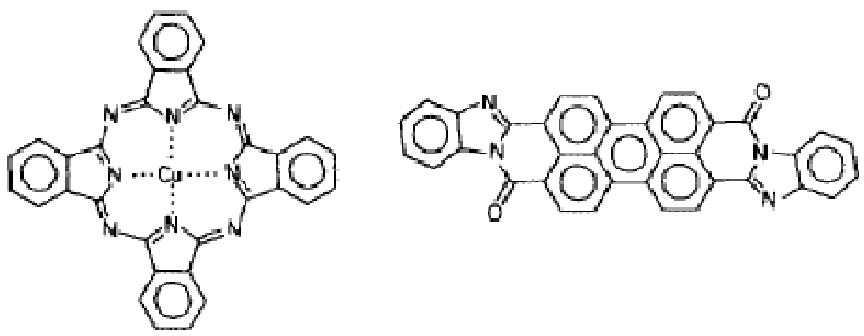

CuPc PV

Tang's group in 1986.
Deposit CuPc and PV thin film in sequence by thermal evaporation under high vacuum. The power conversion efficiency reaches 1%

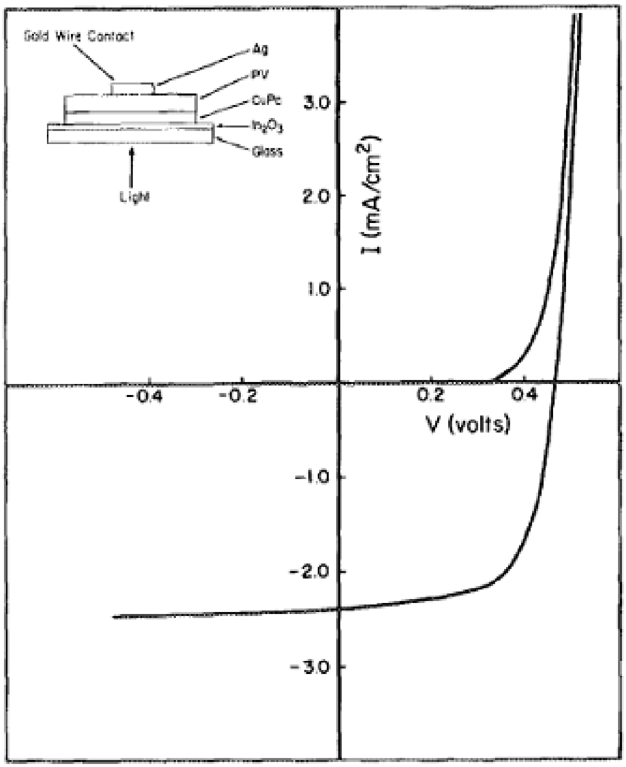

Under 75 mW/cm^2 illumination
Active area: 0.1 cm^2

C. W. Tang, Appl. Phys. Lett. **48**, 183 (1986)

Evolution of OSC

Using BCP as the exciton blocking layer

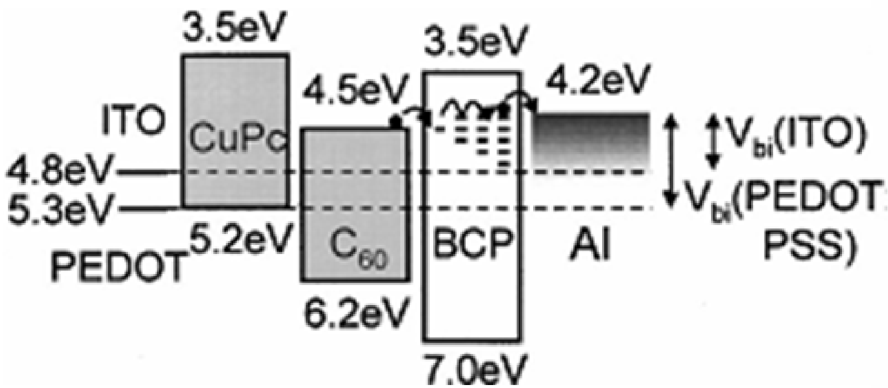

Introducing of C60 and BCP as the acceptor and exciton blocking layer respectively. The power conversion efficiency reaches 3%

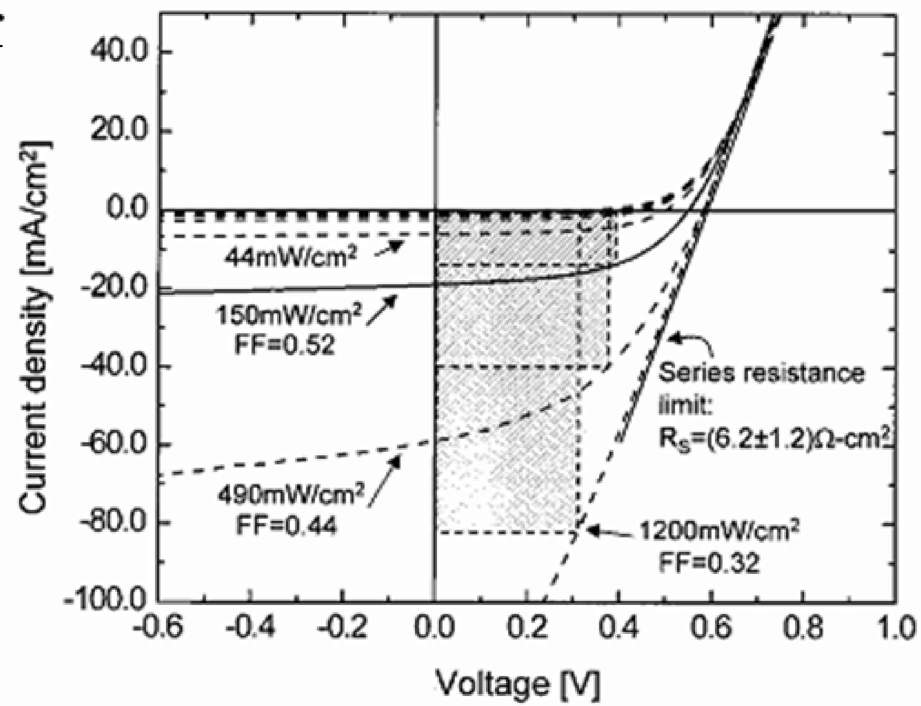

Under 150 mW/cm^2 illumination
Active area: 0.0079 cm^2

P. Peumans and S. R. Forrest, Appl. Phys. Lett. **79**, 126 (2001)

Evolution of OSC

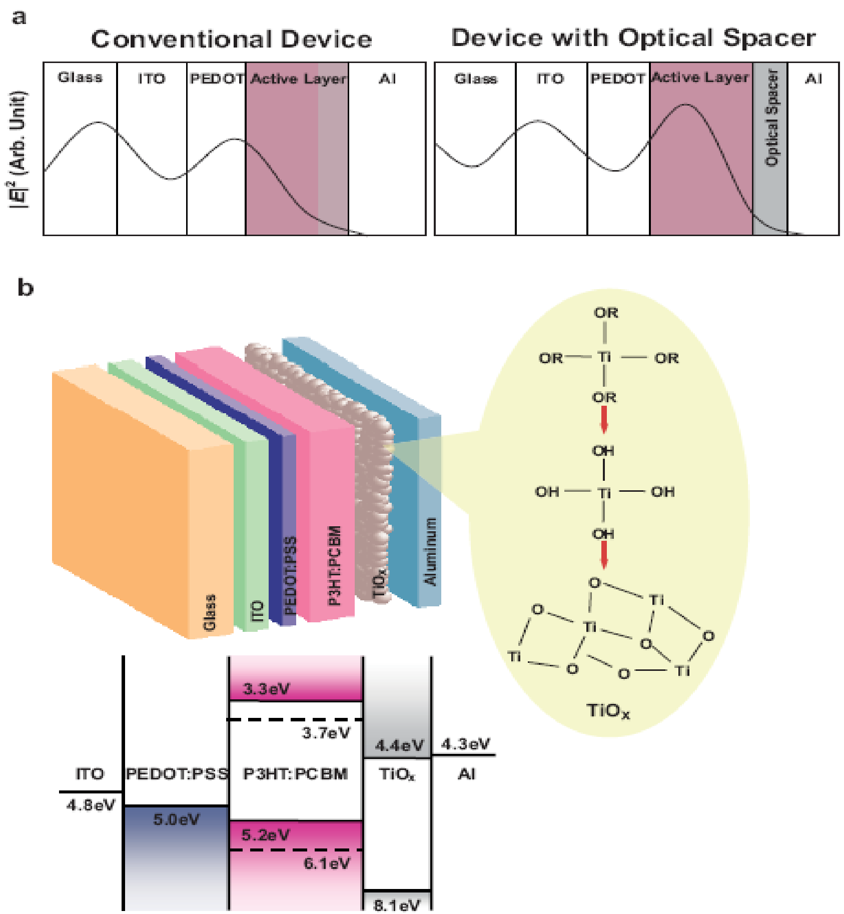

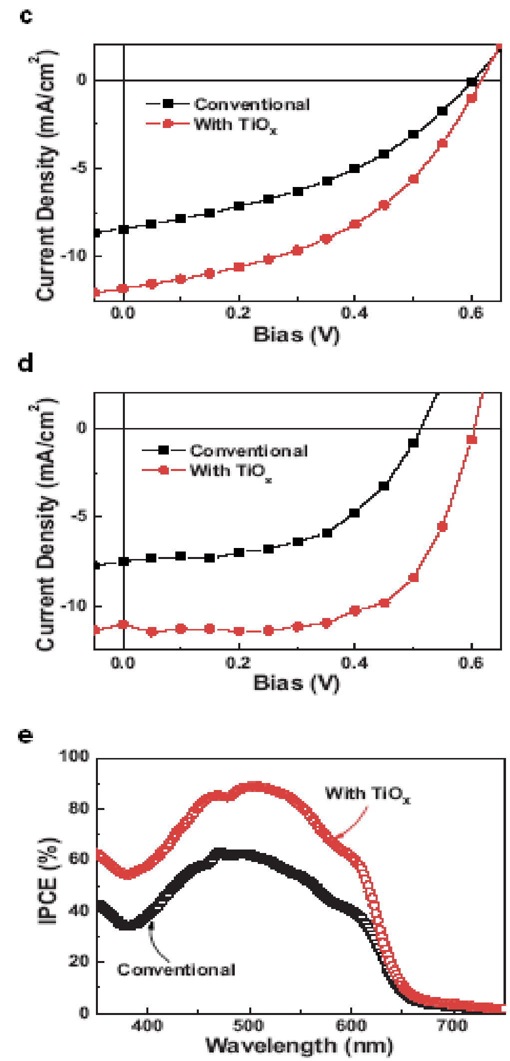

TiOx with high electron mobility acts as the hole blocking layer and the optical spacer.
The power conversion reaches 5 %

J. Y. Kim, S. H. Kim, H. H. Lee, K. Lee, W. Ma, X. Gong, and A. J. Heeger, Adv. Mater. **18**, 572 (2006)

Evolution of OSC

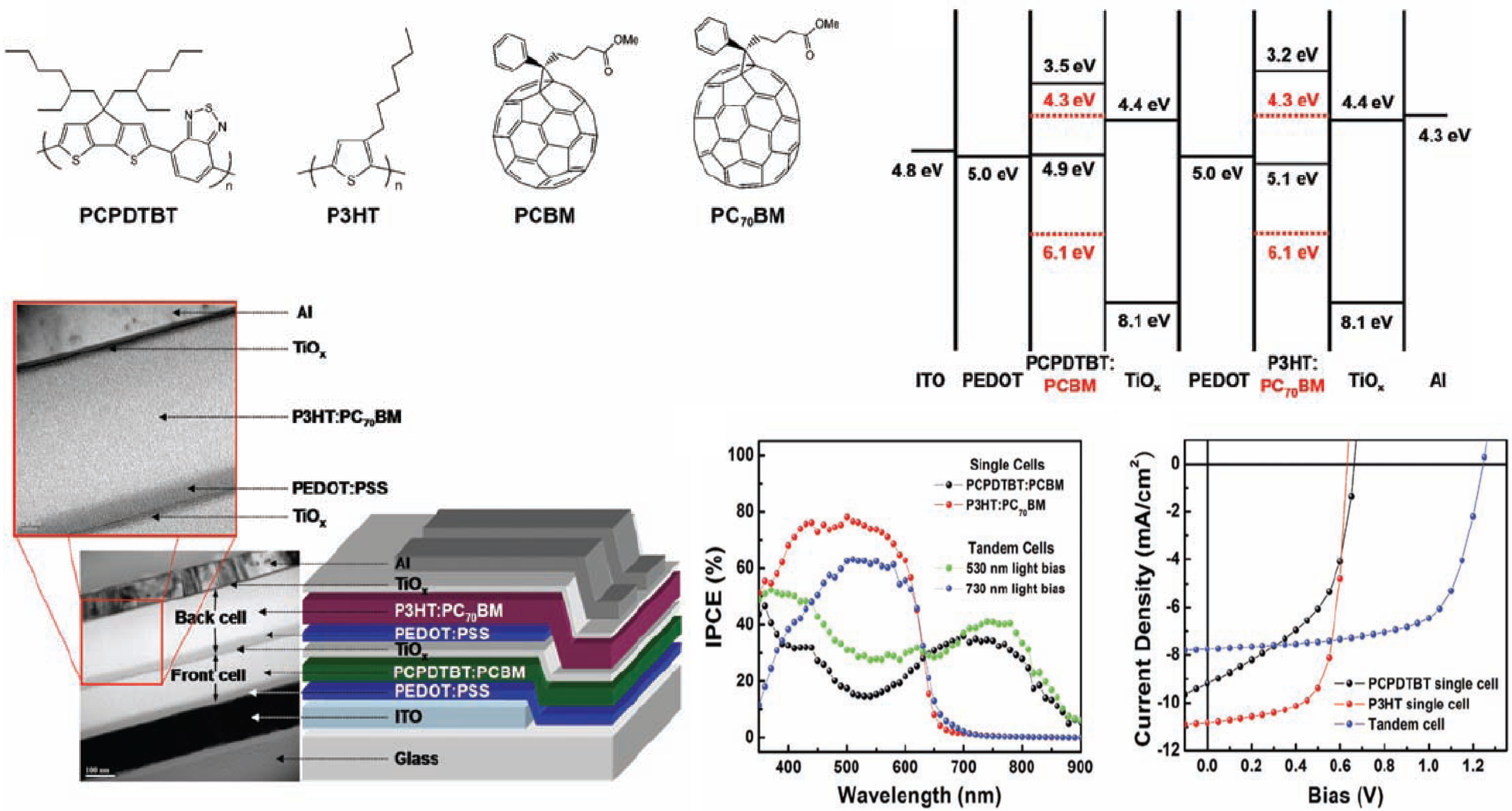

The tandem device introduces the optical spacer and the low band gap material. The power conversion efficiency reaches 7%, which is one of the highest value of the record of efficiency in OSC.

J. Y. Kim. K. Lee, N. E. Coates, D. Moses, T. Q. Nguyen, M. Dante, and A. J. Heeger, Science 317, 222 (2007)

BHJ Solar Cell

First Bulk heterojunction photovoltaics

➡ Composite films of MEH-PPV and fullerenes exhibit η_c of about 29 percent of electrons and η_e of about 2.9 percent.

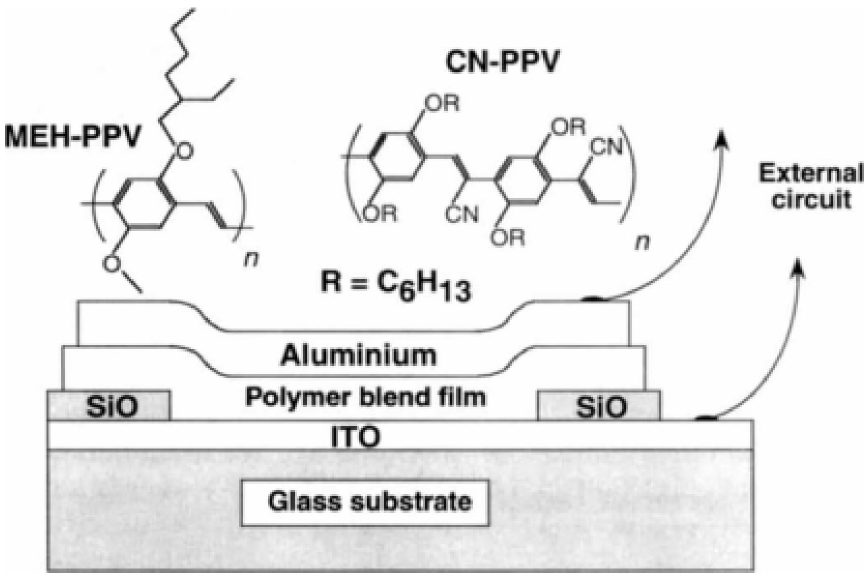

Schematics of MEH-PPV/C60 solar cells

J. J. M. Halls *et al.*, *NATURE.* **376**, 498-500 (1995)

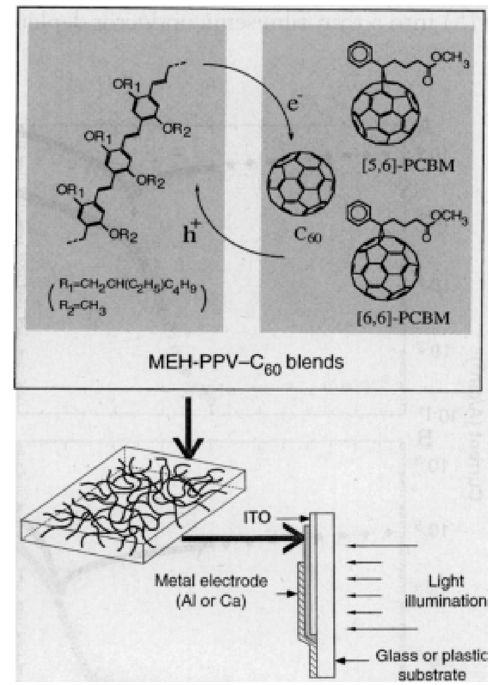

Photo-induced electron transfer from the excited state of a conducting polymer onto buckminsterfullerene, C60, is reported

G. Yu. *et al.*, *SCIENCE.* **270**, 1789-1791 (1995)

P3HT:PCBM Solar Cell

Bulk heterojunction solar cells using P3HT as the electron donor and PCBM as the acceptor were fabricated in the following simple structure: **ITO/PEDOT/P3HT:PCBM/Metal**

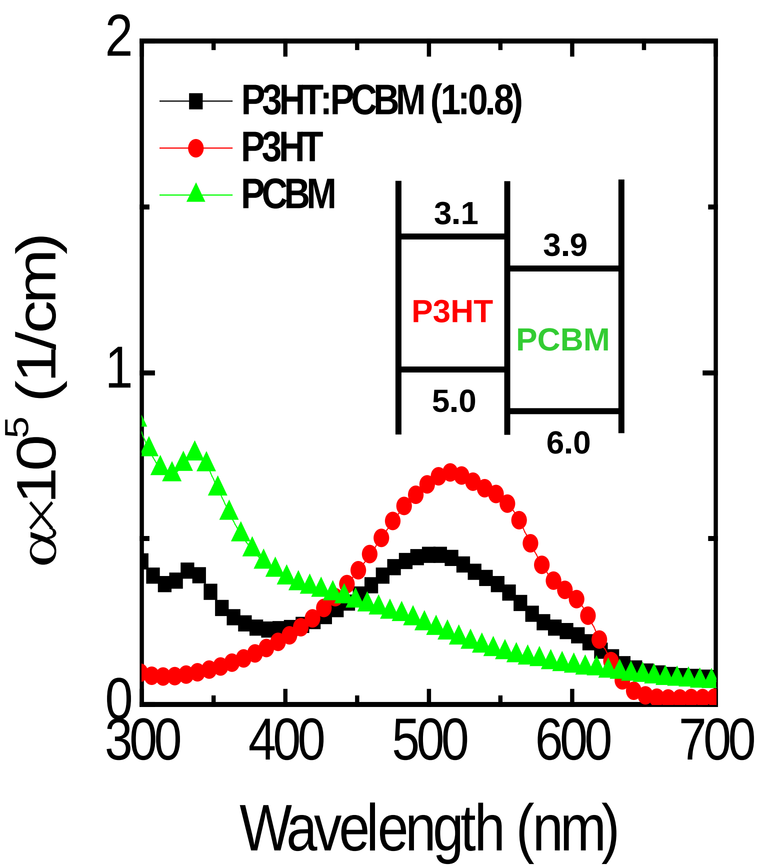

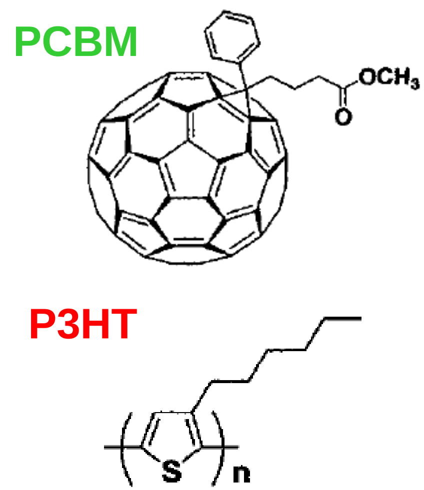

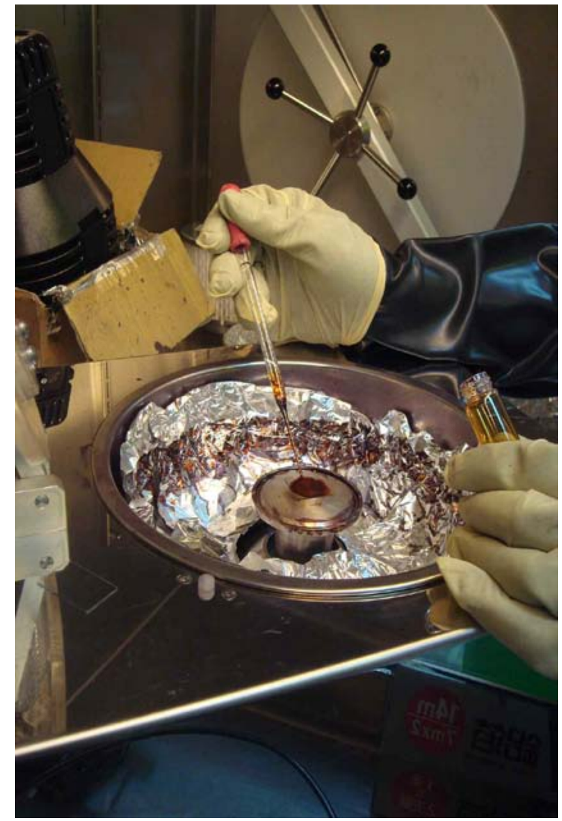

P3HT:PCBM Solar Cell

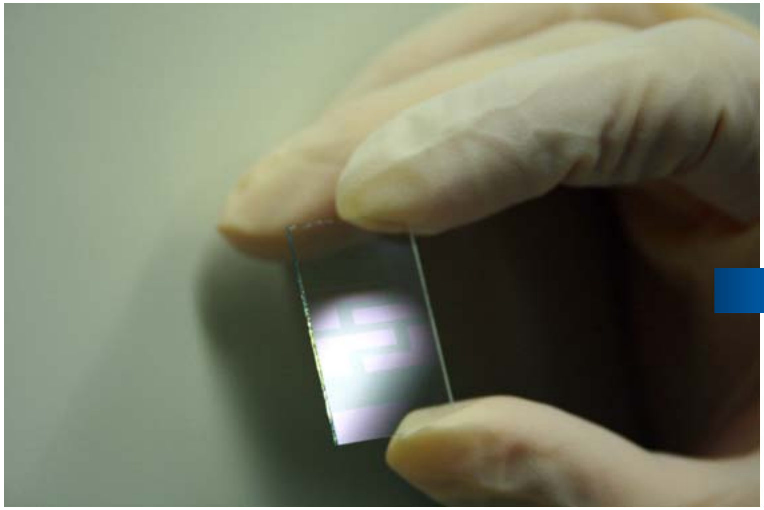

Patterned ITO substrate

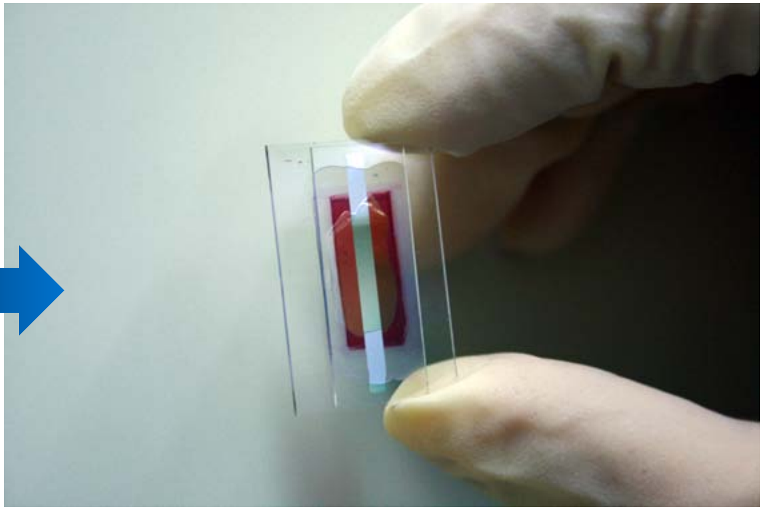

Completed P3HT:PCBM solar cell

The Determining Factors of Fabricating Organic Photovoltaic Devices

	Resulting influence		
	Absorption	Morphology	Mobility
Solvent	✓	✓	-
Composition	✓	✓	-
Molecular weight	-	-	✓
Thermal annealing	✓	✓	✓
Solvent annealing	✓	✓	-
Additives	✓	✓	-
Buffer layer	-	-	-
Metal contact	-	-	-

Absorption

P3HT:PCBM films casted from chlorobenzene (CB) solution absorb more red light than the films casted from chloroform (CF) solution.

Absorption Maximum - 460 nm (CF)

Absorption Maximum - 510 nm (CB)

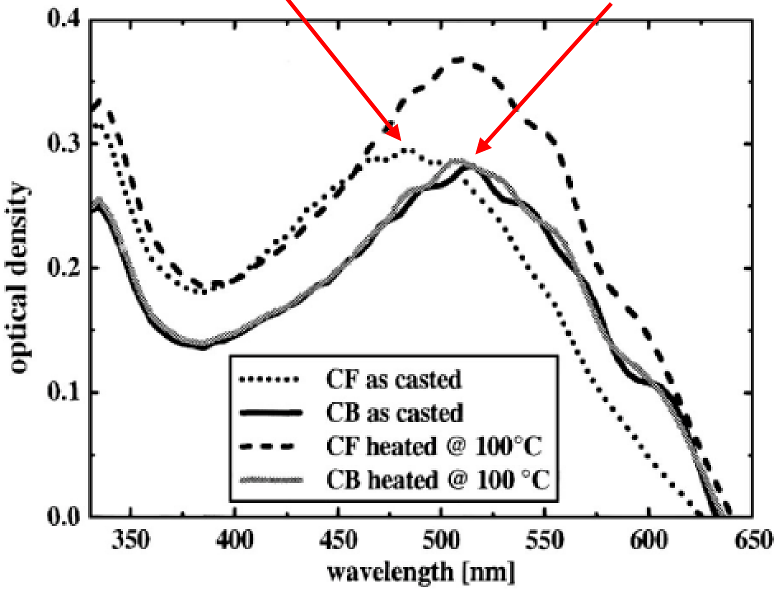

M. Al-Ibrahim *et al.*, *Appl.Phys.Lett.* **376**,201120 (2005)

Crystallinity

The slow evaporation rate of high boiling point solvent and the slow film growth rate may assist P3HT film in forming high degree of crystalline structure.

Boiling point	
Chloroform (CF)	61.2 °C
Chlorobenzene (CB)	131.0 °C
Dichlorobenzene (DCB)	180.5 °C

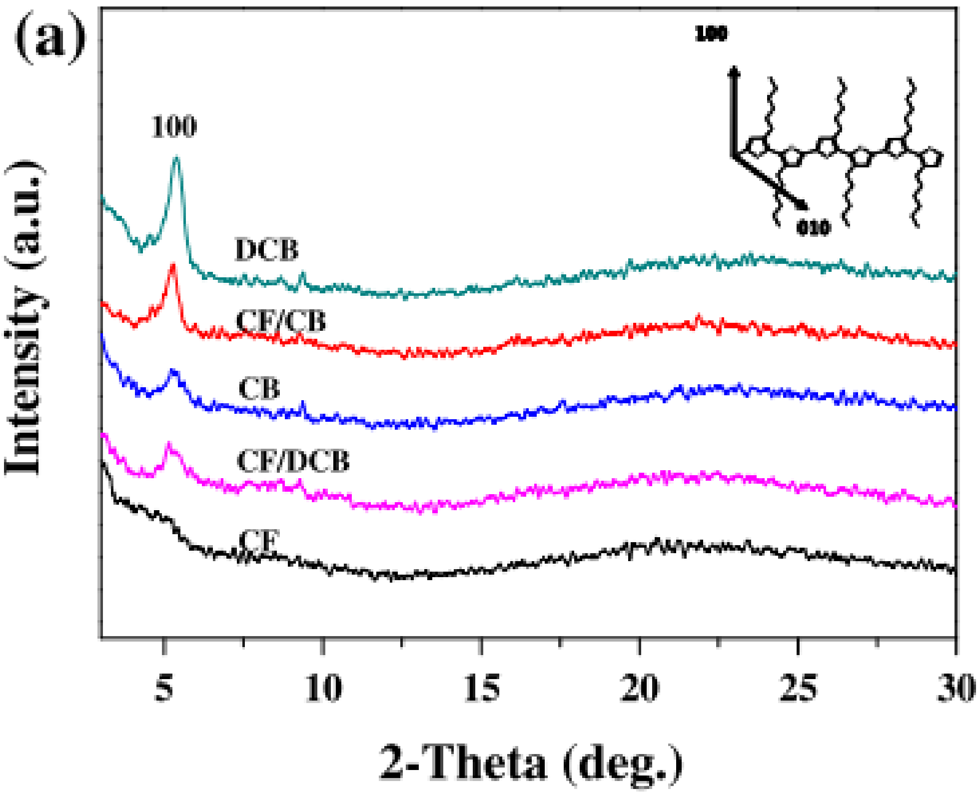

Y. S. Kim *et al.*, *Current Applied Physics.* **10**,985 (2010).

Morphology

Low boiling point solvents (CF and CB) ➡ smoother surface
High boiling point solvents (DCB) ➡ Rougher surface

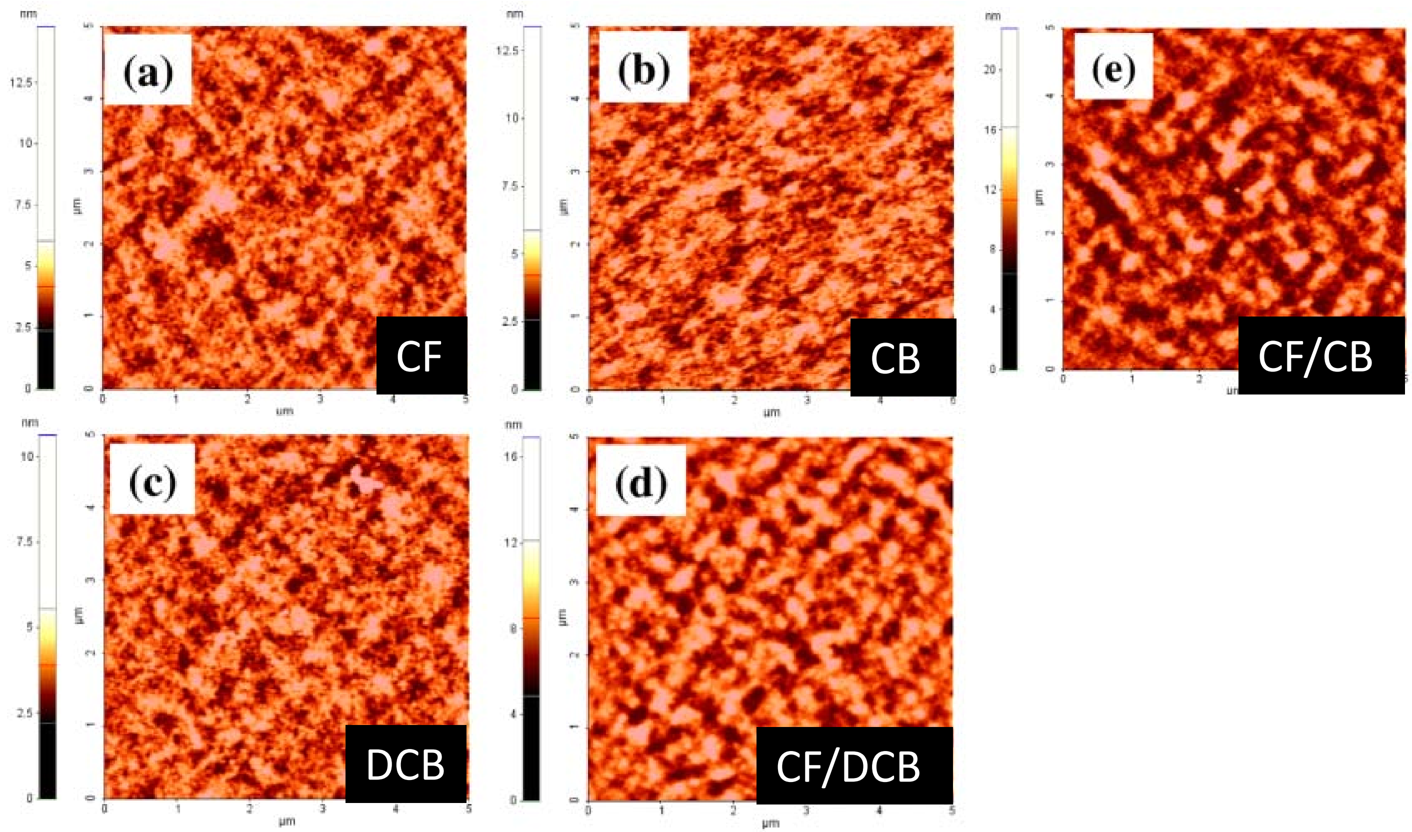

Y. S. Kim *et al.*, *Current Applied Physics.* **10**,985 (2010).

Absorption

The content of P3HT ↑, the absorption spectra of P3HT
➡Absorption ↑ (450 ~ 650 nm)
➡become broader
➡red-shifted

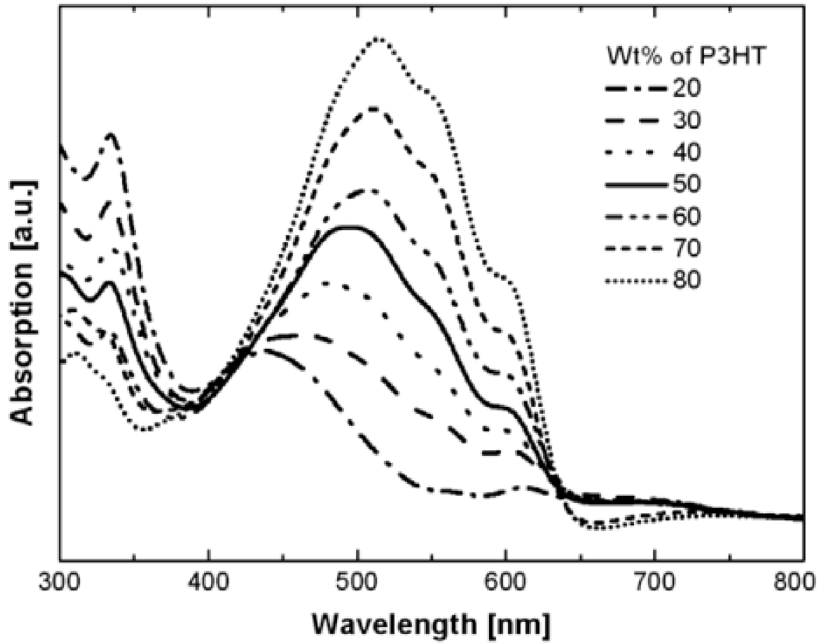

Wt% of P3HT [%]	20	30	40	50	60	70	80
P3HT λ_{max} (nm)	437	461	482	495	507	512	515

W. H. Baek *et al., Organic Electronics* **11**, 933 (2010).

Phase Segregation

Photoluminescence (PL) quenching decreasing after thermal annealing
➡Phase segregation of both P3HT and PCBM increases upon annealing
➡less efficient photoinduced electron transfer between P3HT and PCBM

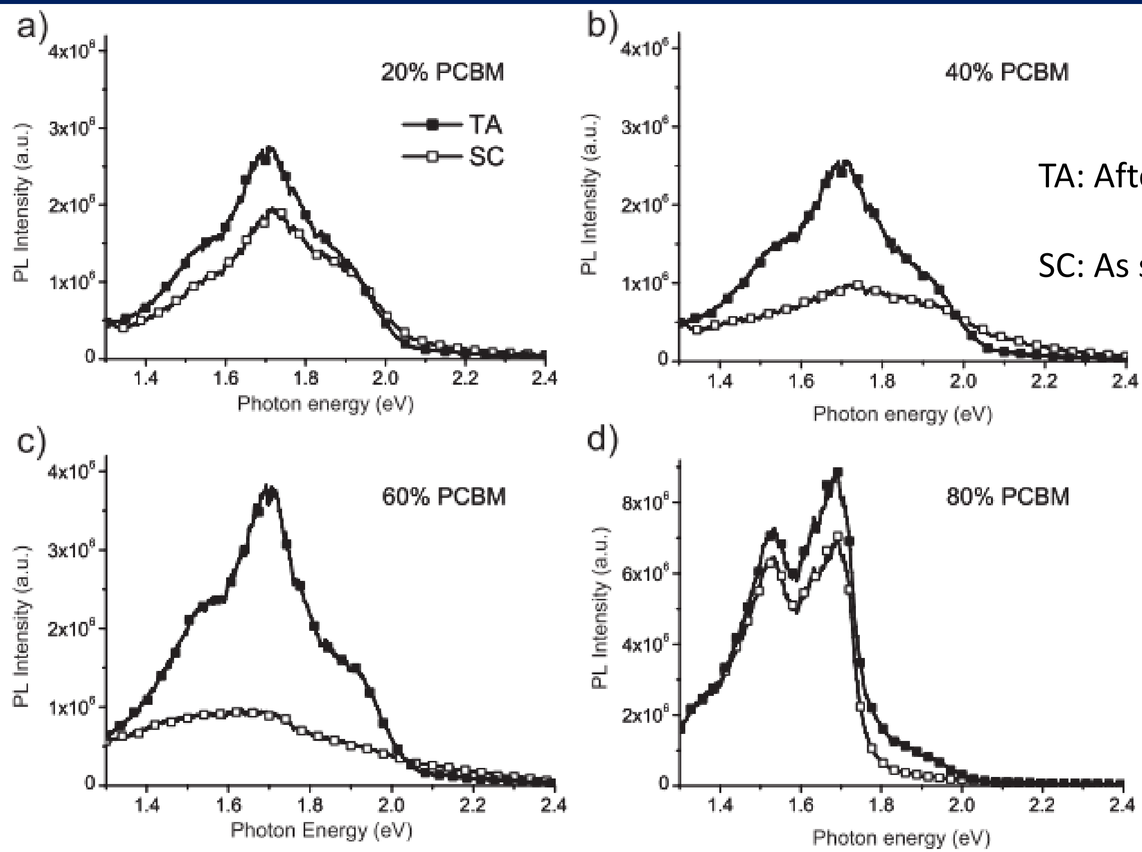

TA: After thermal annealing

SC: As spin-coated

➡PL quenching will change obviously before and after annealing as P3HT/PCBM ratio ~ 1

S. S. van Bavel *et al.*, *Adv. Funct. Mater*. **20**, 1458 (2010).

Morphology

The fraction of the highly ordered fiber structure of P3HT increased as the P3HT composition increased up to 50 wt.% and decreased as the composition increased further.

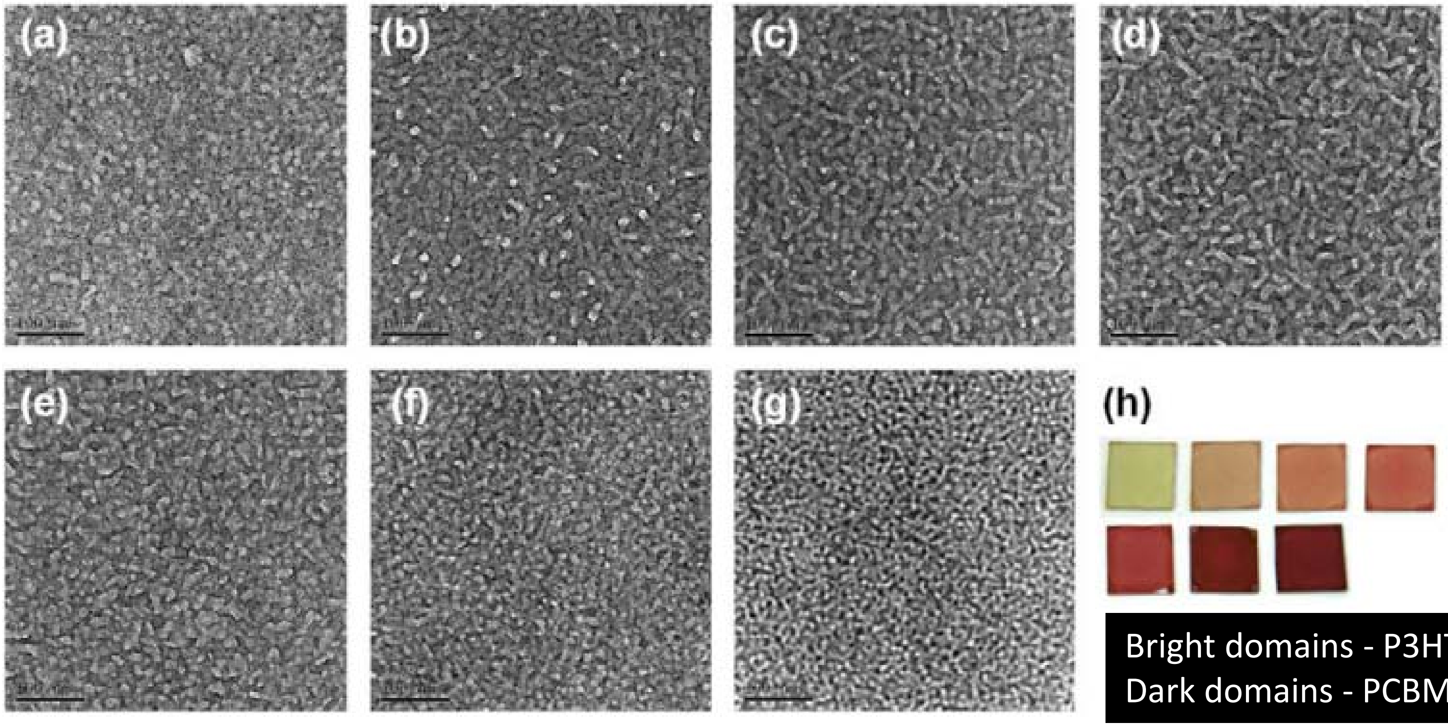

Bright domains - P3HT-rich areas
Dark domains - PCBM-rich areas

(a) 20% (b) 30% (c) 40% (d) 50% (e) 60% (f) 70% (g) 80% of P3HT

W. H. Baek *et al., Organic Electronics* **11,** 933 (2010).

Mobility

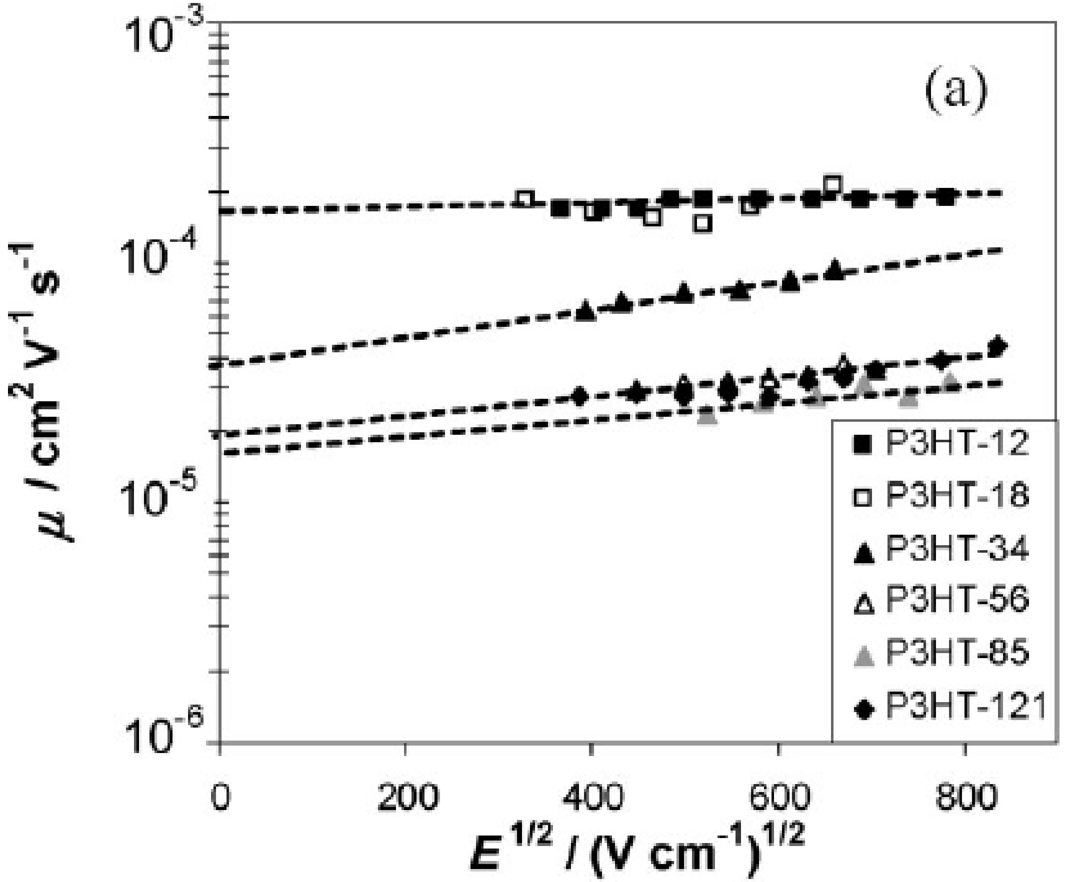

Molecular weight ↑
➡mobility ↓

	P3HT-13	P3HT-18	P3HT-34	P3HT-56	P3HT-85	P3HT-121
M_n	13.0 kDa	17.6 kDa	34.4 kDa	55.6 kDa	85 kDa	121 kDa
M_w/M_n	2.0	1.8	2.1	2.8	2.6	3.7

A. M. Ballantyne *et al., Adv. Funct. Mater.* **18**, 2373 (2008).

Device Performance

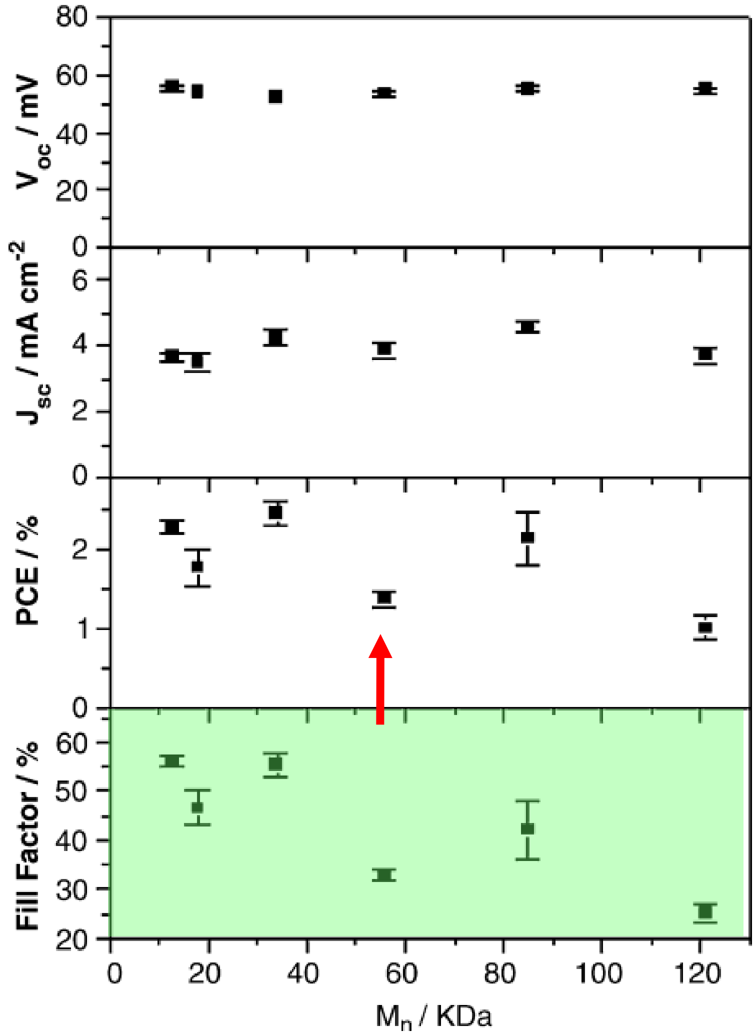

➡ decrease in PCE

Obvious decrease in FF

A. M. Ballantyne *et al., Adv. Funct. Mater.* **18**, 2373 (2008).

The Mechanism of Thermal Annealing
- Redistribution of active materials

At elevated temperature
➡ isolated molecules of PCBM diffuse into larger aggregates
➡ in those PCBM-free regions - P3HT aggregates can be converted into P3HT crystallites.

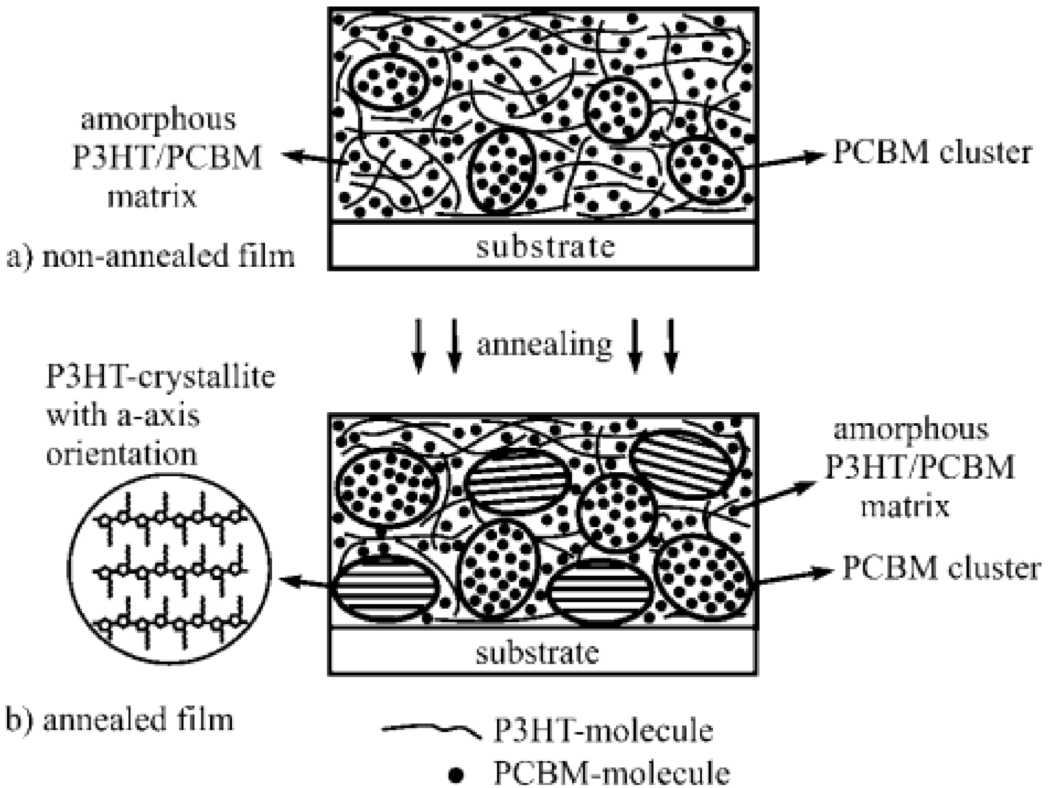

T. Erb *et al., Adv. Funct. Mater.* **15**, 1193 (2005).

Optical Absorption

The annealed sample showed stronger optical absorption (high crystallinity).

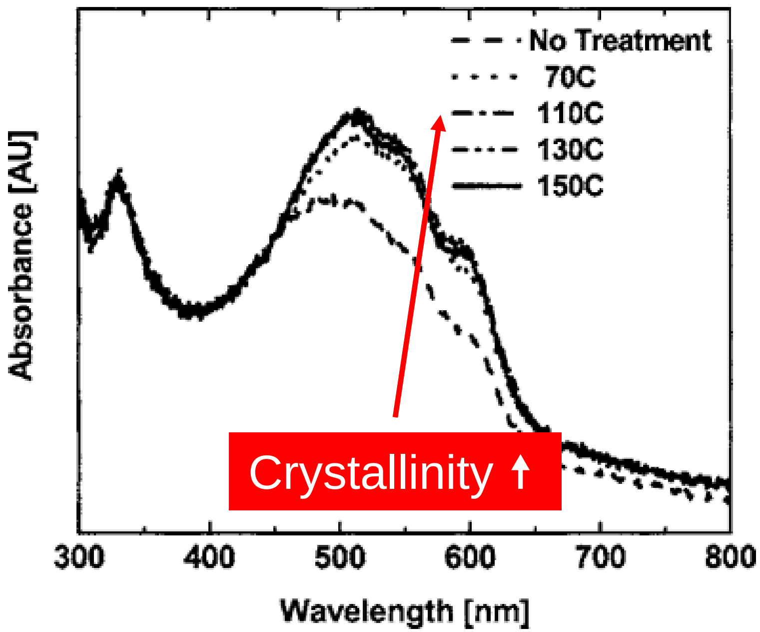

G. Li *et al., J. Appl. Phys.* **98**, 043704 (2005).

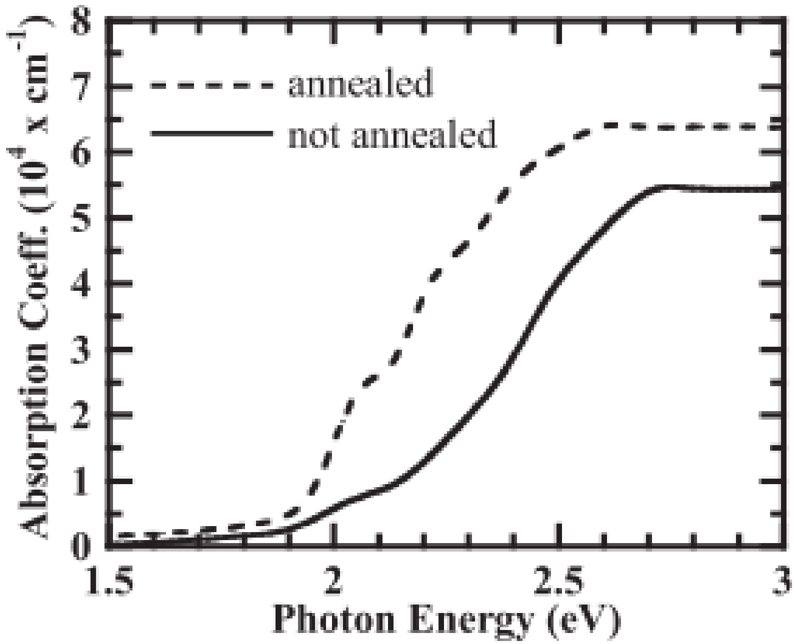

T. Erb *et al., Adv. Funct. Mater.* **15**, 1193 (2005).

Crystallinity

(investigated by XRD)

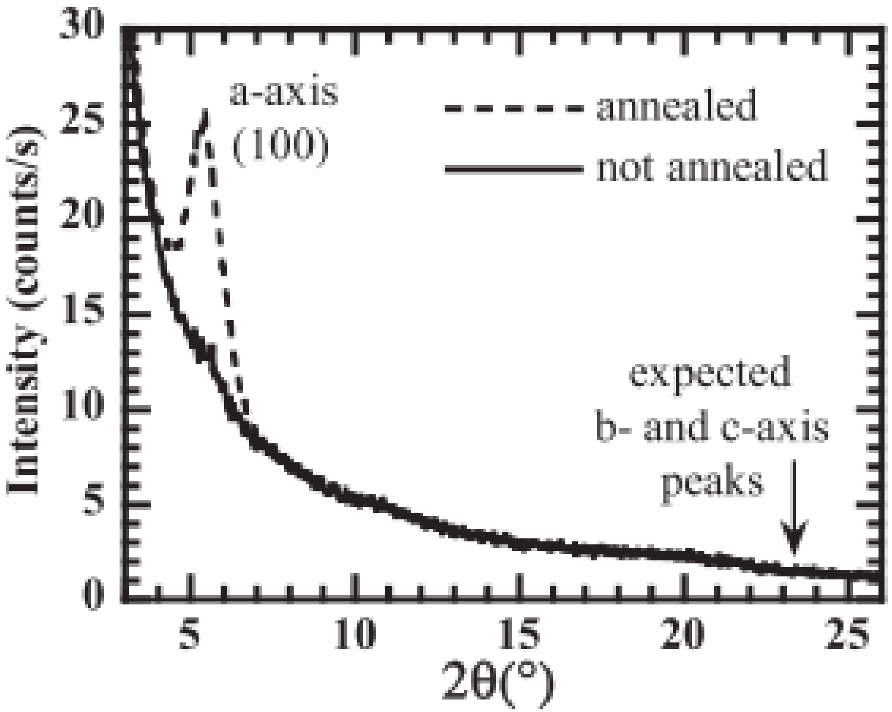

T. Erb *et al., Adv. Funct. Mater.* **15**, 1193 (2005).

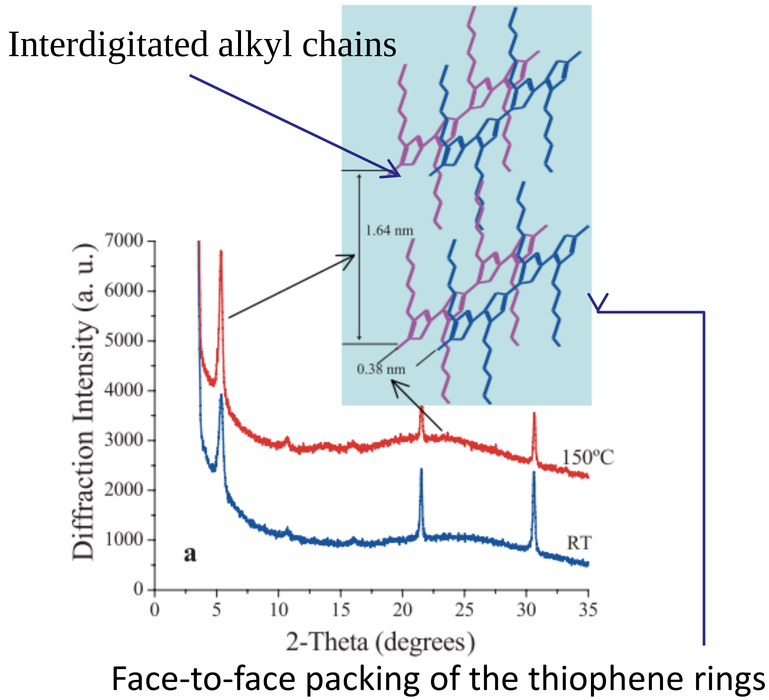

W. Ma *et al., Adv. Funct. Mater.* **15**, 1617 (2005).

Morphology control

The interpenetrating networks are not well developed.

The morphology of interpenetrating networks becomes clearer and easily visible.

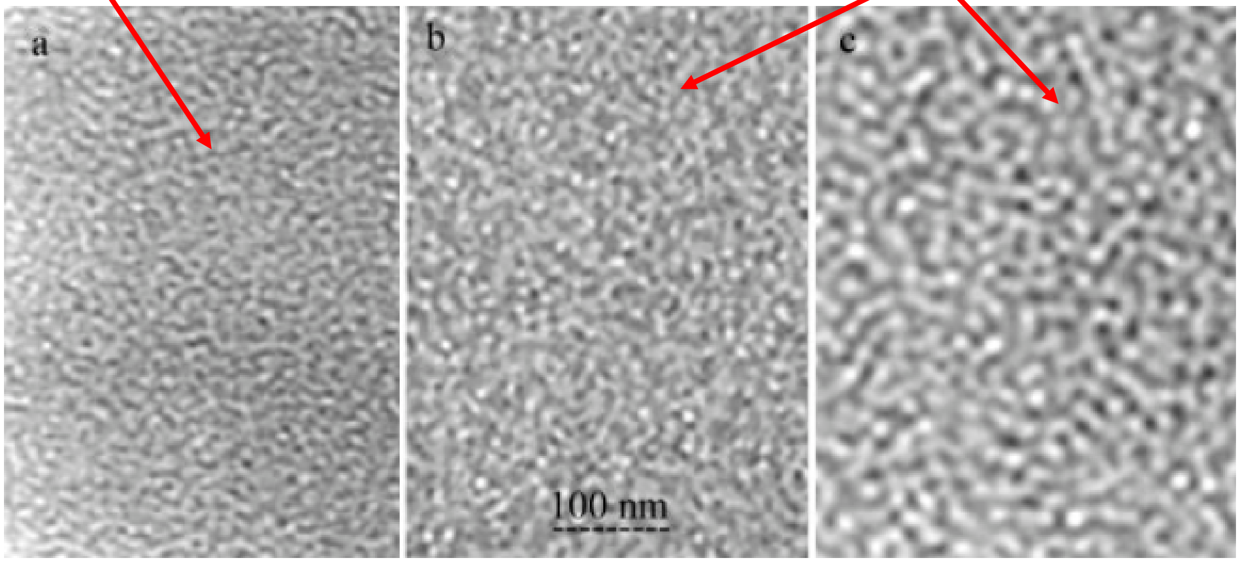

TEM images of P3HT:PCBM film bulk morphology before thermal annealing(a), after thermal annealing at 150 ^{o}C for 30 min(b), and after thermal annealing at 150 ^{o}C for 2 h(c).

W. Ma *et al.*, *Adv. Funct. Mater.* **15**, 1617 (2005).

Mobility

With increasing annealing time

➡Mobility ↑ (improved charge separation and transport due to the phase separation between P3HT and PCBM).

However, a large extent of phase separation

➡ reduces the bicontinuous phases ⇨ mobility↓ again

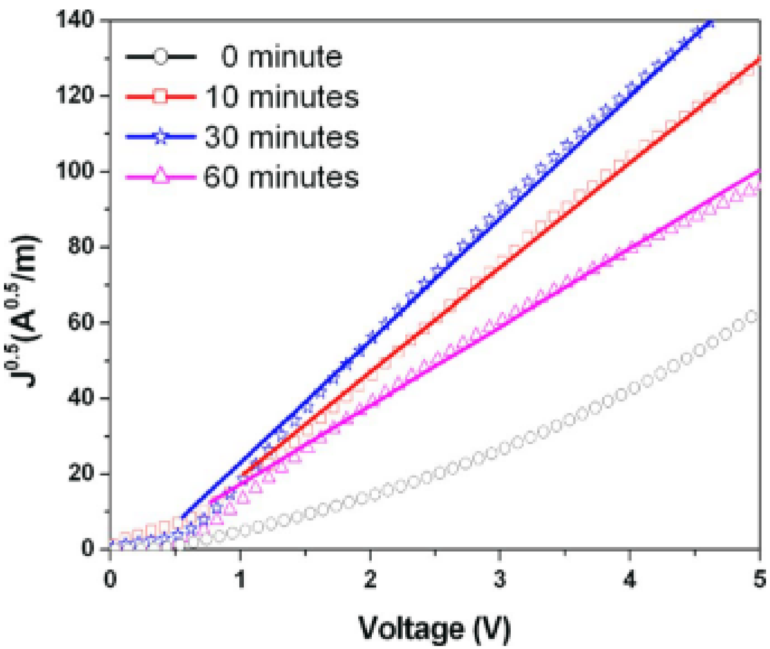

TABLE I. Mobility and performance of the P3HT/PCBM solar cells under A.M. 1.5 illumination (100 mW/cm^2) annealed at 140 °C for different times.

increase

Annealing time (min)	V_{oc} (V)	J_{sc} (mA/cm^2)	FF (%)	η (%)	Mobility (cm^2/V s)
0	0.58	6.72	27.14	1.06	2.51×10^{-05}
10	0.62	10.02	42.32	2.61	2.01×10^{-03}
30	0.64	11.15	54.27	3.85	2.64×10^{-03}
60	0.59	5.06	44.90	1.35	1.02×10^{-03}

decrease

Y. C. Huang *et al.*, J. Appl. Phys. **106**, 034506 (2009)

The Concept of Solvent Annealing

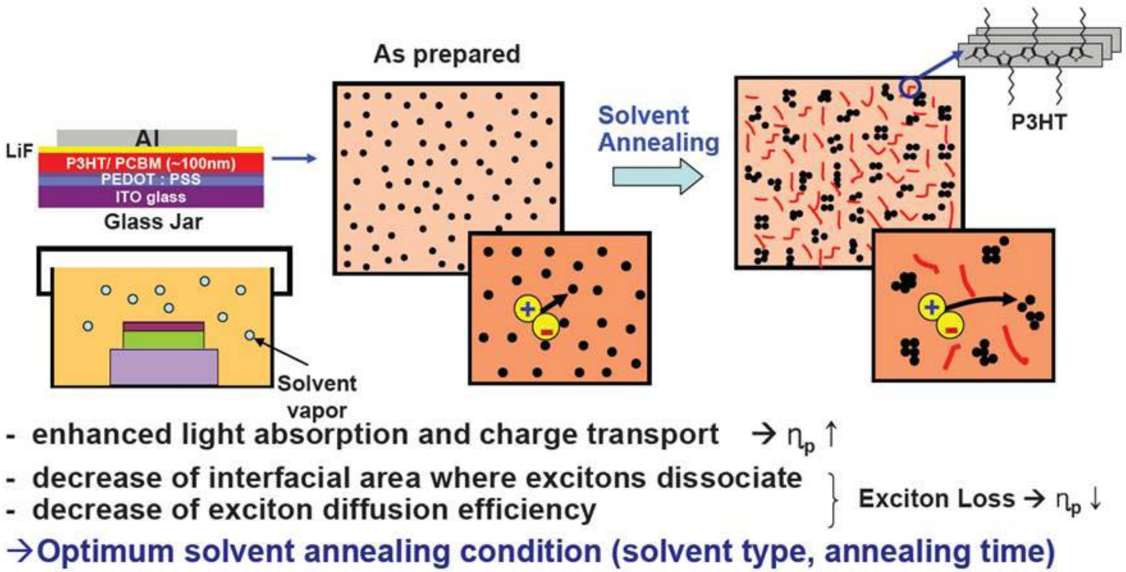

The solubility and volatility of annealing solvent have a substantial effect on the degree of nanoscale phase separation of photoactive organic films. By controlling solubility and vapor pressure of annealing solvent, we can optimize morphology and molecular ordering of solar cells

Absorption

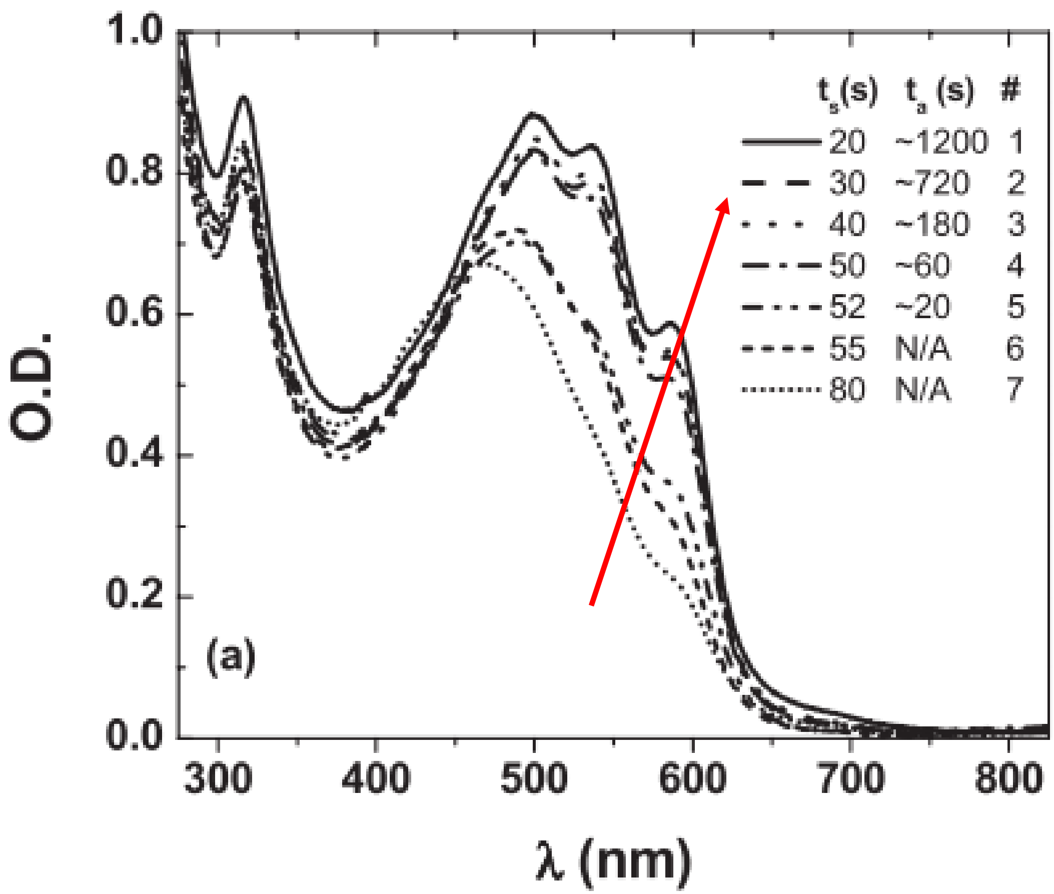

Solvent annealing time ↑

Vibronic shoulder ↑

t_s : spin-coating time
t_a : solvent annealing time

G. Li *et al.*, *Adv. Funct. Mater.* **17**, 1636 (2007).

Morphology Controlled by Solvent Properties

(investigated by TEM)

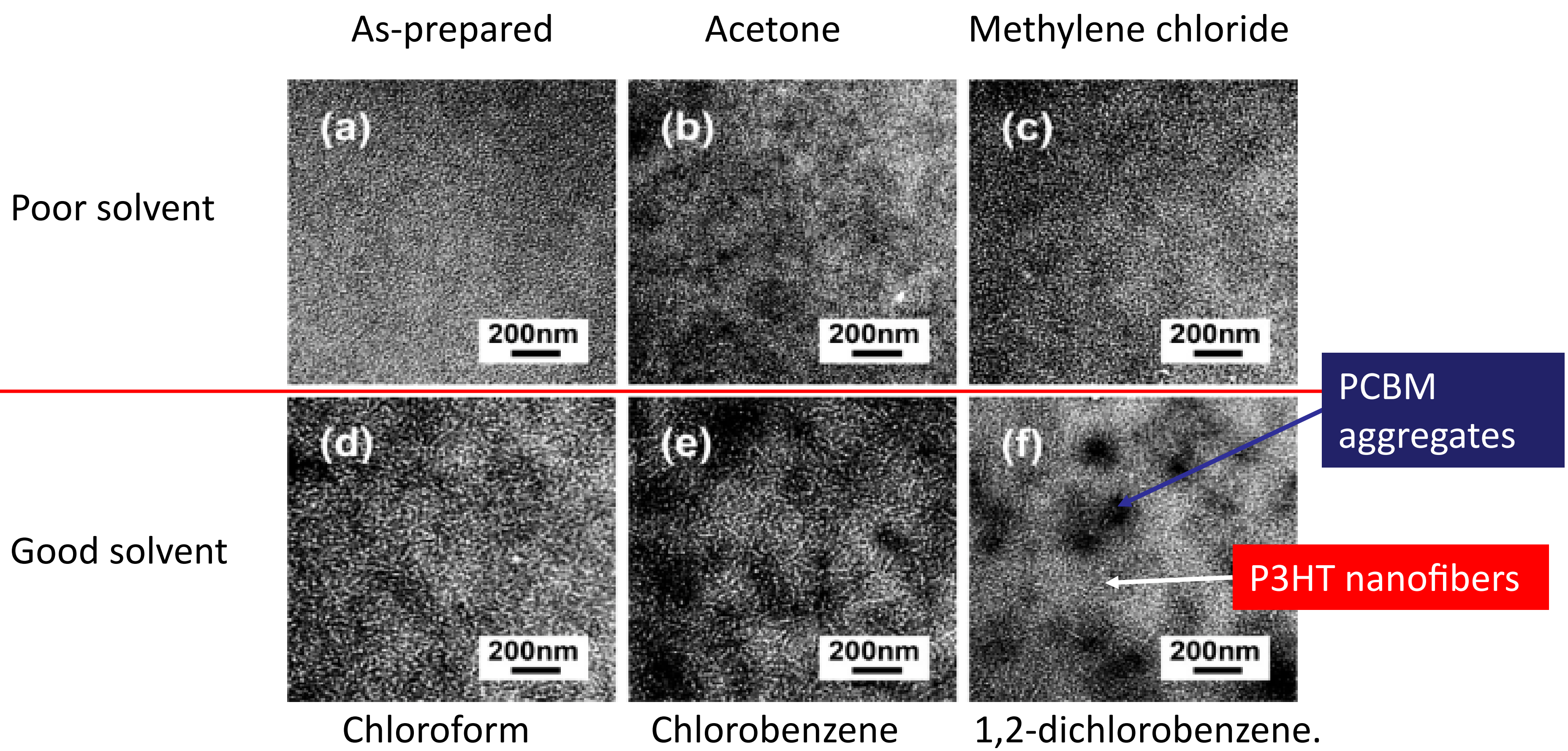

J. H. Park *et al.*, *J. Phys. Chem. C* **113**, 17579 (2009).

Morphology Controlled by Solvent Properties

(investigated by AFM)

Slow grown

↓

Rough surface (nanoscaled texture→internal light scattering and light absorption↑)

↓

Jsc ↑

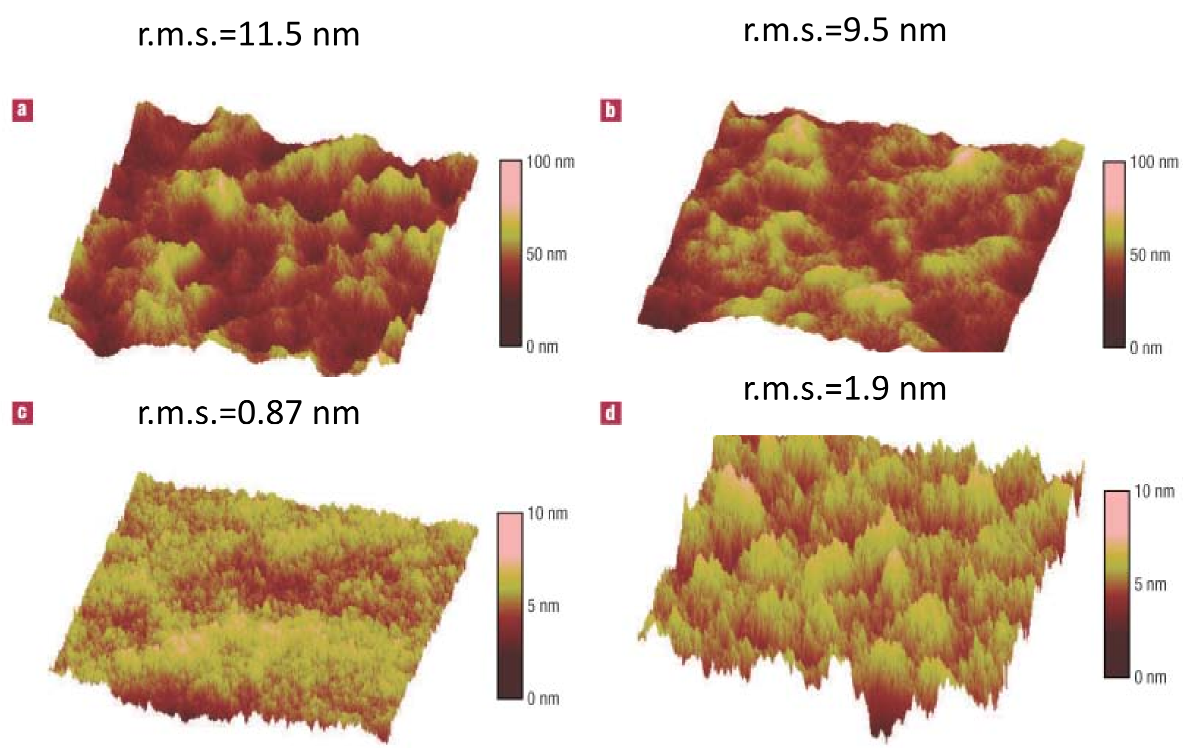

(a) Slow-grown film before thermal annealing. (b) Slow-grown film after thermal annealing at 110 °C for 10 min. (c) Fast-grown film before thermal annealing. (d) Fast-grown film after thermal annealing at 110 °C for 20 min.

G. Li *et al.*, *Nat. Mater.* **4** , 864 (2005).

The Concept of Solvent Additives

The addition of solvent additives provides the similar function of preserving P3HT crystallinity in P3HT:PCBM blend as achieved in the "solvent annealing" approach.

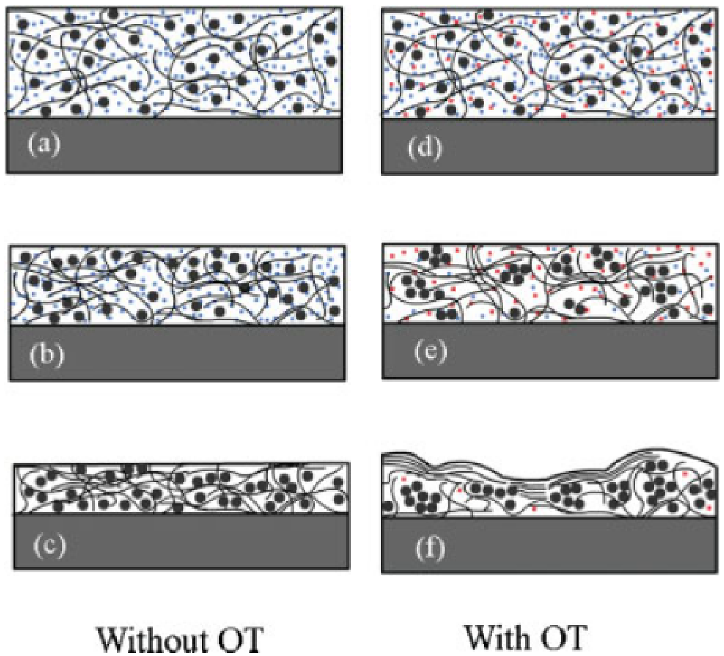

Figure 5. Proposed model during spin-coating process. Black wire: P3HT polymer chain; Big black dots: PCBM; blue dots: DCB molecules; and red dots: 1,8-octanedithiol molecules. (a–c) correspond to three stages in the spin-coating process when DCB is the sole solvent; (d–f) correspond to three stages in the spin-coating process when octanedithiol is added in DCB. Note the difference of PCBM distribution in the final stage of each case, (c) and (f). The total numbers of big black dots are same in all the images.

DCB evaporate much faster than OT during spin-coating, and gradually the concentration of OT increases in the mixture.

Due to the limited solubility of PCBM in OT, PCBM form clusters and precipitate.
With a smaller amount of PCBM contained in the solution, P3HT chains are able to self-organize in an easier fashion.

Pre-formed PCBM clusters not only provide a percolation pathway for better electron transport, but also enable better hole transport in the polymer phase.

Solvent	Boiling points [°C]	Vapor pressure at 30 °C [Pa]	PCBM solubility [mg ml^{-1}]
1,2-dichlorobenzene (DCB)	198	200	100
1,8-octanedithiol (OT)	270	1	19
di(ethylene glycol)diethyl ether	189	100	0.3
N-methyl-2-pyrrolidone	229	10	18

Y. Yao *et al.*, *Adv. Funct. Mater*. **18**, 1783 (2008).

Absorption

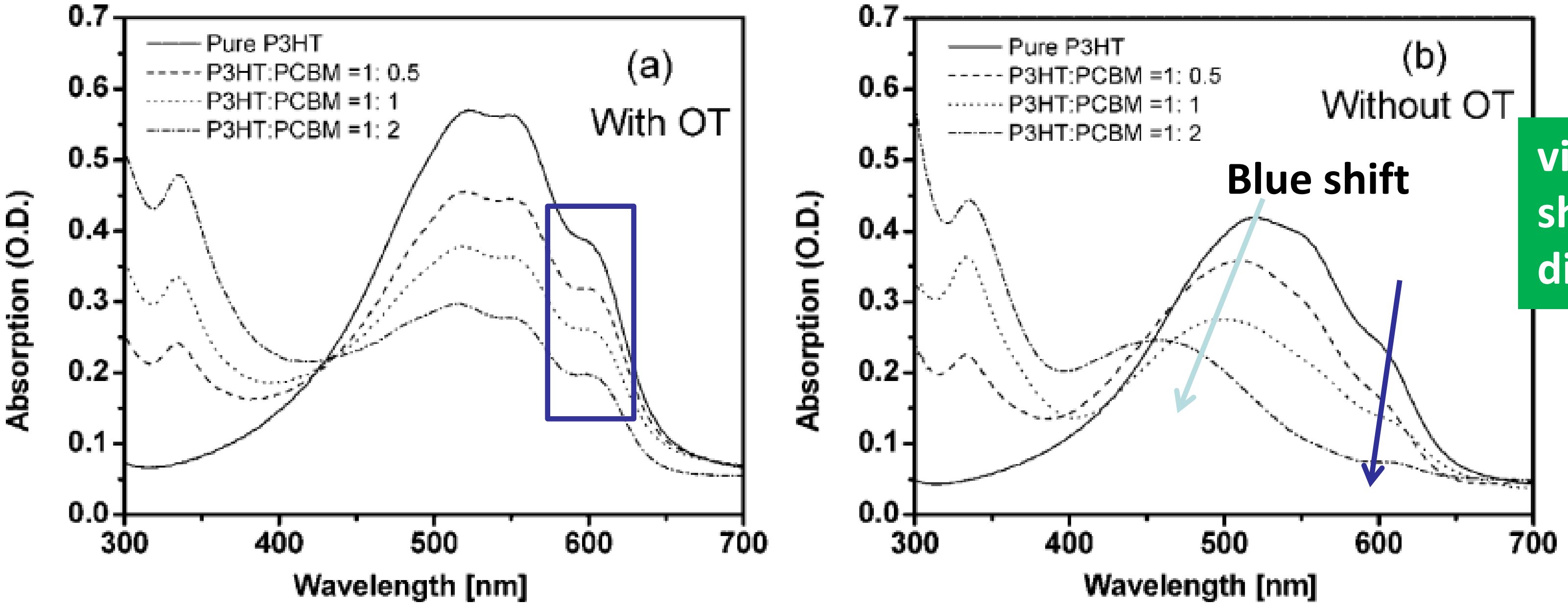

vibronic shoulders diminish

With additives
➡ obvious vibronic shoulder

w/o additives
➡ vibronic shoulder diminish

Y. Yao *et al.*, *Adv. Funct. Mater*. **18**, 1783 (2008).

Morphology

(investigated by TEM)

Pronounced fibrillar P3HT crystals (c) suggest the crystallinity has been improved compared to pristine film (d).

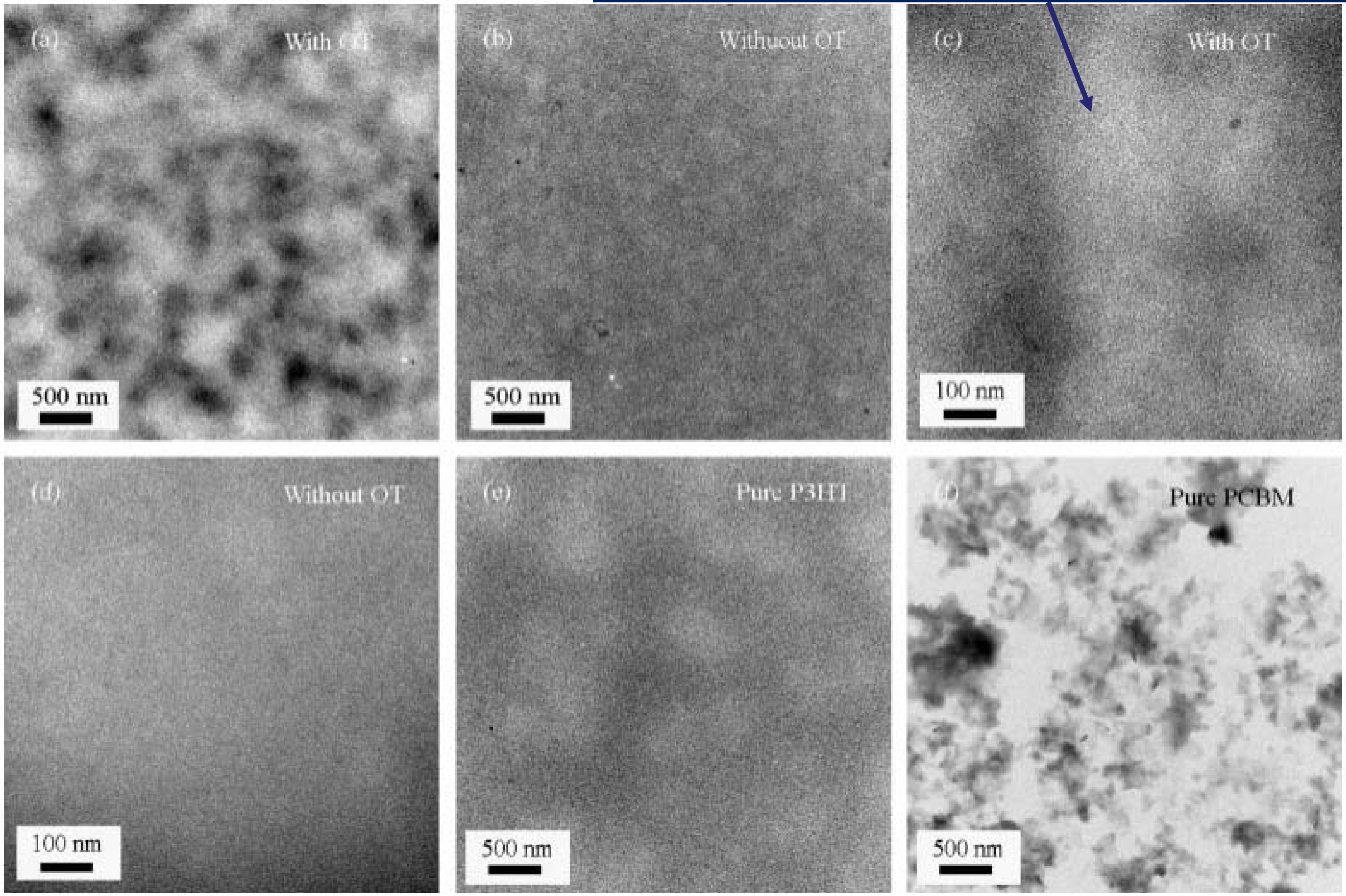

Y. Yao *et al.*, *Adv. Funct. Mater*. **18**, 1783 (2008).

Morphology

(investigated by AFM)

Height image

P3HT fibrillar crystalline domains

Phase images

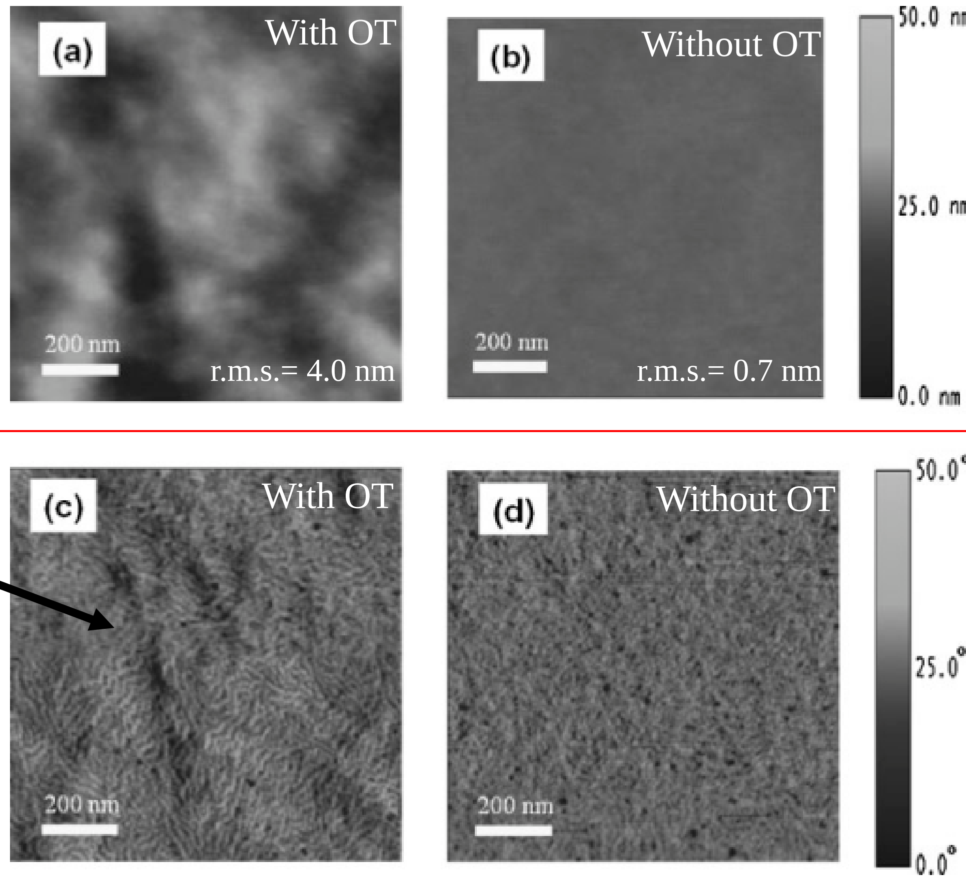

A rough surface is a "signature" of high efficiency solar cells both in "thermal annealing" and "solvent annealing".

Highly ordered P3HT chain alignment is achieved when OT is added in the mixture.

Y. Yao *et al.*, *Adv. Funct. Mater*. **18**, 1783 (2008).

For organic solar cell-

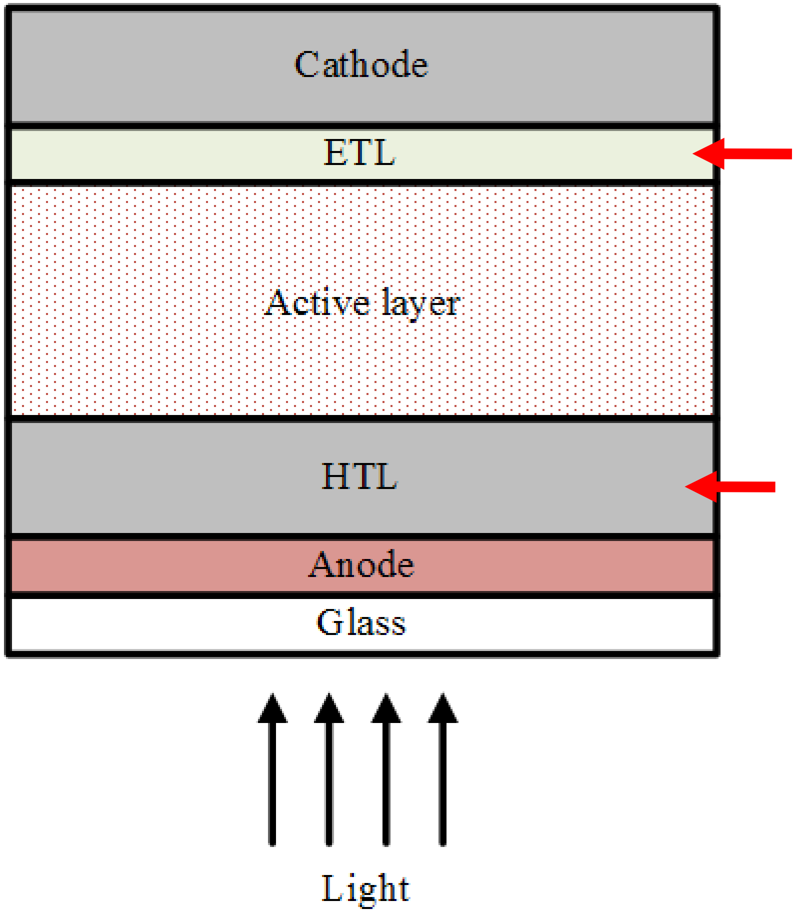

Functions-

1. To prohibit the electron transfer from metal to active layer
   → a desired built-in electric field
   → promote the free carrier collection
2. To prevent excitons/hole from recombining at cathode

1. To improve the hole transporting from active layer to anode
2. To prevent excitons/electron from recombining at anode

Cathode Buffer Layer - BCP

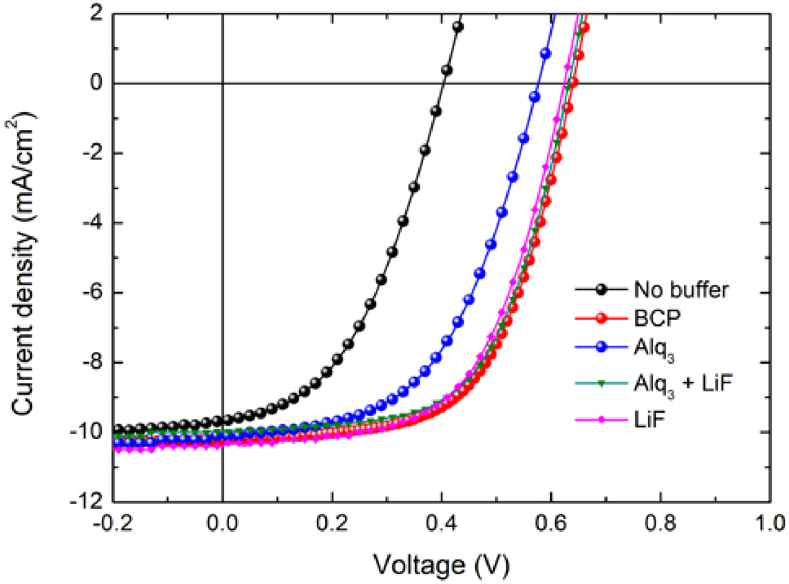

P. Peumans and S. R. Forrest, *Appl. Phys. Lett.* **79**, 126 (2001).

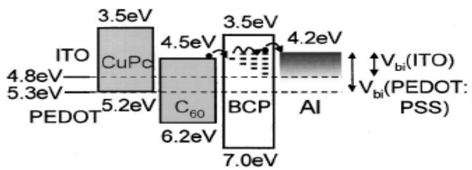

T. Mori, *Appl. Phys. Lett.* **73**, 2763 (1998).

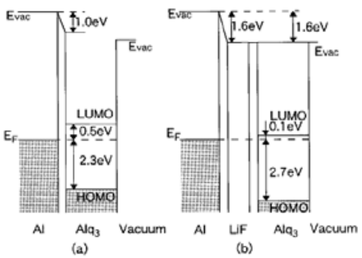

	Voc (V)	Jsc (mA)	FF (%)	eff (%)	Rsh (kΩ)	Rs (Ω)
w/o buffer	0.41	9.7	44	**1.77**	9.27	643
BCP (2 nm)	0.64	10.1	60	**3.89**	35.95	207
Alq3 (2 nm)	0.59	10.1	53	**3.18**	23.68	316
Alq3 (2 nm) + LiF (1.2 nm)	0.65	10.0	59	**3.83**	37.43	224
LiF (1.2 nm)	0.64	10.5	58	**3.89**	31.50	199

Appl. Phys. Lett. **96**, 263506 (2010).

Optimizing Polymer Solar Cells with BCP Buffer Layers

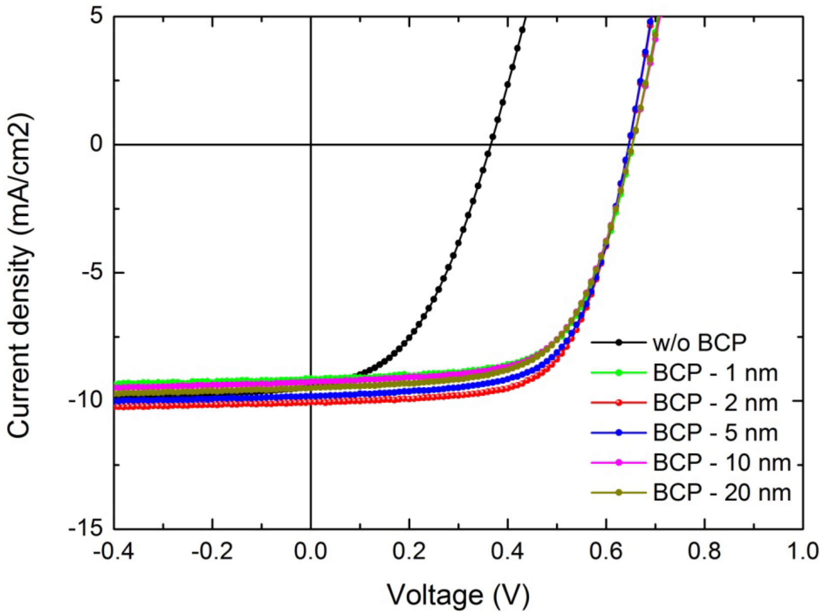

	Voc (V)	Jsc (mA/cm^2)	FF (%)	eff (%)	Rsh (kΩ)	Rs (Ω)
w/o BCP	0.38	9.54	44	1.63	8.59	449
BCP – 1 nm	0.65	9.85	62	3.91	37.34	174
BCP – 2 nm	0.65	9.96	63	4.11	41.68	173
BCP - 5 nm	0.65	9.89	63	4.03	33.26	154
BCP – 10 nm	0.65	9.29	62	3.74	30.36	191
B CP – 20 nm	0.65	9.38	59	3.59	31.19	219

Appl. Phys. Lett. **96**, 263506 (2010).

Cathode Buffer Layer – Cs_2CO_3

Cs_2CO_3 decomposed into metallic Cs during thermal evaporation.
This interfacial material tends to react with oxygen and moisture.
Cs_2CO_3 buffer layer works as an excellent shielding and scavenging protector.

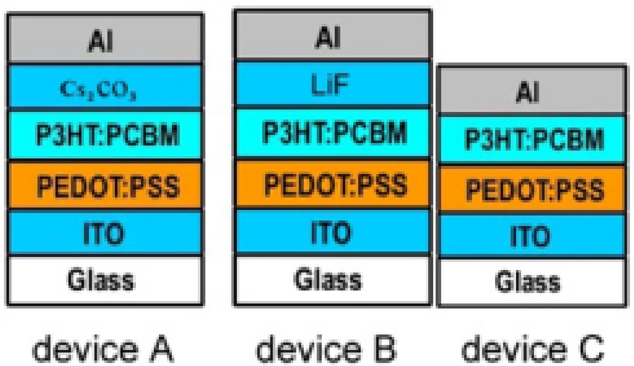

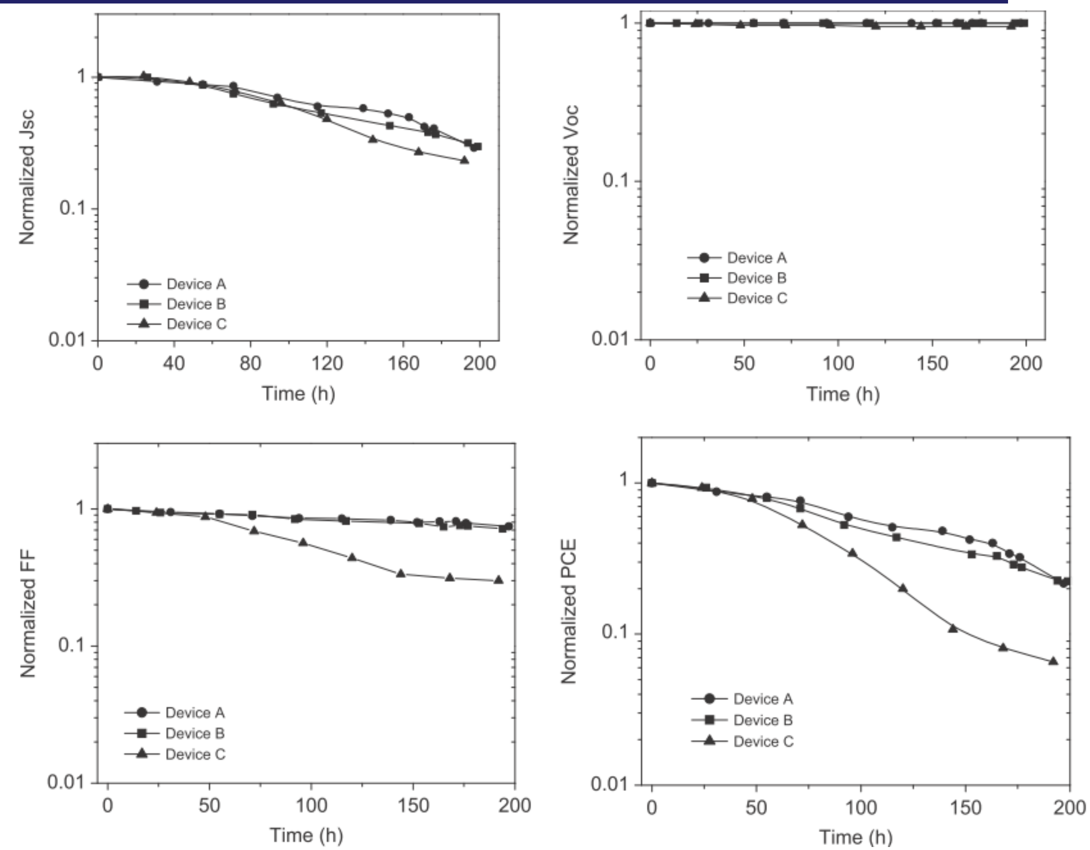

Device A with half-life of 130 h gets a 33% improvement compared with the control device B with half-life of 100 h.

L. Yang *et al.*, *Solar Energy Materials & Solar Cells* 94, 1831 (2010).

Other Kinds of OSC

- **Dye-sensitized solar cell**

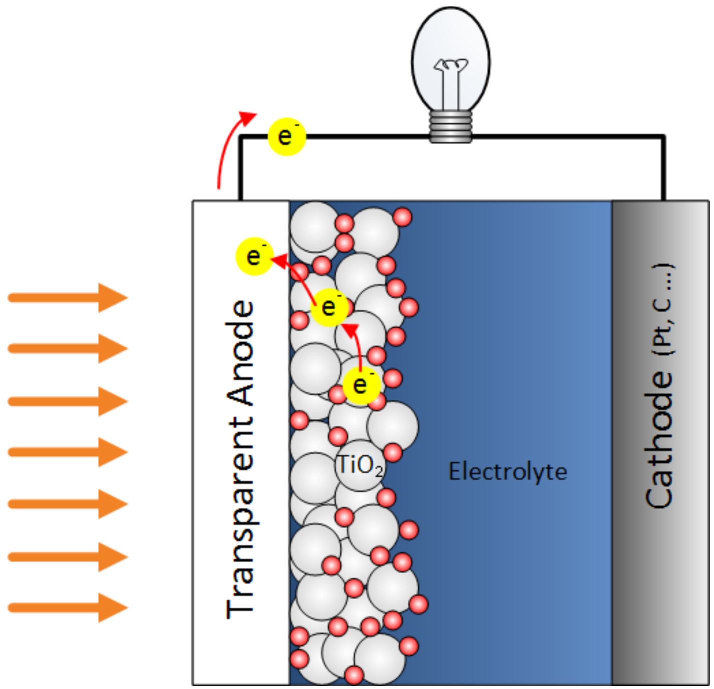

Advantages

-Most efficient 3rd generation solar technology

-Work in low-light conditions

-Flexible

Drawback

- Temperature stability problems
- Encapsulation issue

Why Nano?

To Improve Absorption

- Anti-reflection coating/layer

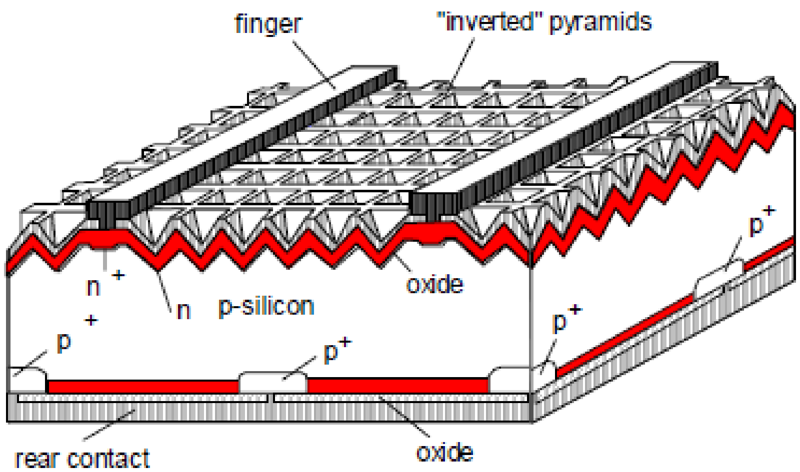

Si-based solar cell

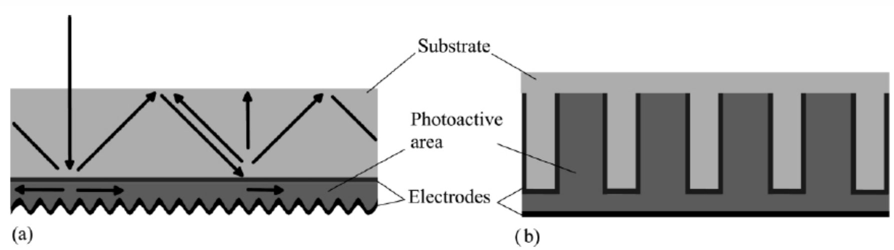

Cell-concepts of organic solar cells. (a) Light trapping with diffraction gratings; (b) buried nano-electrodes

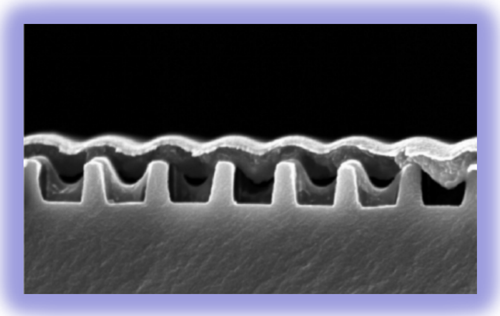

M. Niggemann *et al.*, *Thin Solid Films* **451-452**, 619 (2004).

To Improve Absorption

- Surface plasmon resonance (SPR)

giant near-field enhancement and the enhanced scattering cross section upon exciting localized plasmon polaritons

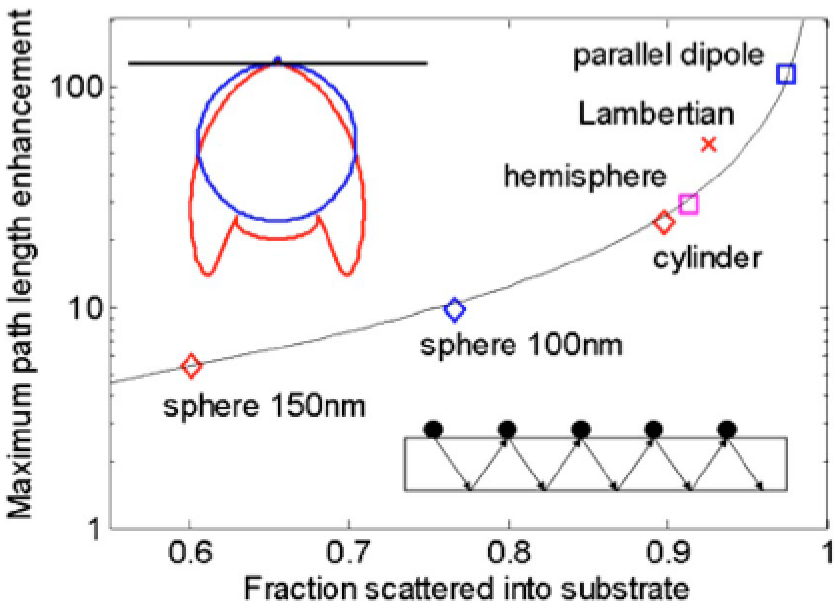

K. R. Catchpolea and A. Polmanb, *Appl. Phys. Lett.* **93**, 191113 (2008).

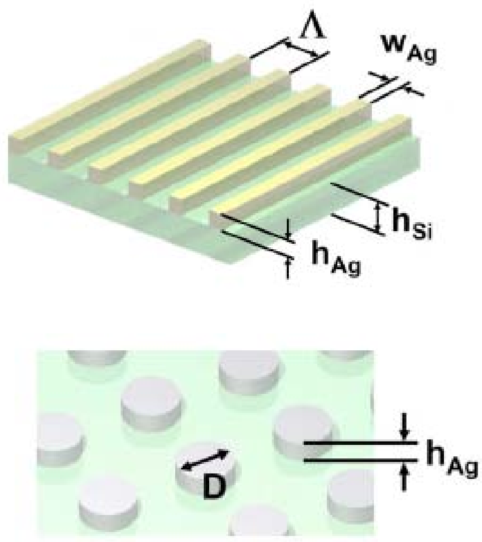

Grating

Nanostructure

C. Rockstuhl *et al.*, *J. Appl. Phys*. **104**, 123102 (2008).

To Improve Absorption

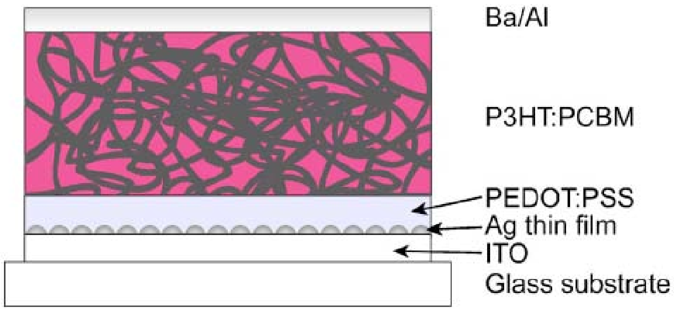

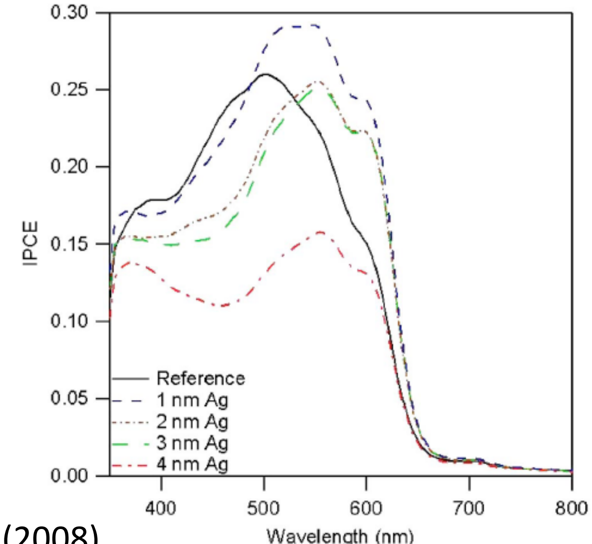

TABLE I. Average device parameters as a function of nominal silver film thickness. Errors reported as one standard deviation.

Ag height (nm)	J_{sc} (mA/cm^2)	η (%)	V_{oc} (mV)
0 (Ref)	4.6±0.4	1.3±0.2	566±5.6
1	6.9±0.2	2.2±0.1	590±5.8
2	7.3±0.3	2.1±0.1	581±8.8
3	6.5±0.1	1.8±0.2	564±30.9
4	2.6±0.4	0.9±0.1	599±6.2

A. J. Morfa *et al.*, *Appl. Phys. Lett*. **92**, 013504 (2008).

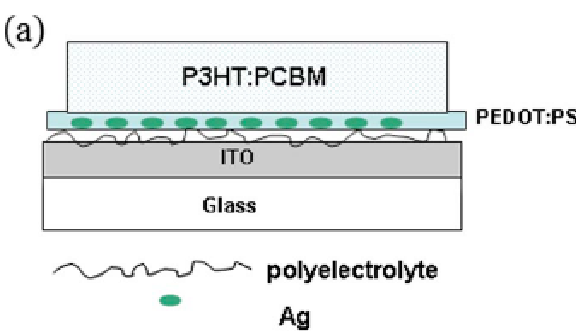

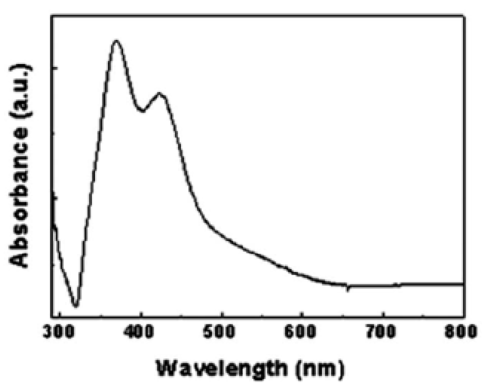

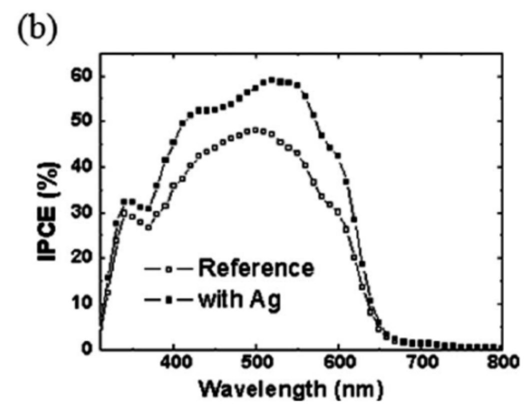

3.05% ➡ 3.69%

S. S. Kim *et al.*, *Appl. Phys. Lett*. **93**, 073303 (2008).

Exciton Diffusion Length

Typically, the diffusion length ~ 10 nm

<< absorption length of many of the materials employed in organic photovoltaic device

To solve this issue

➡ Bulk heterojunction

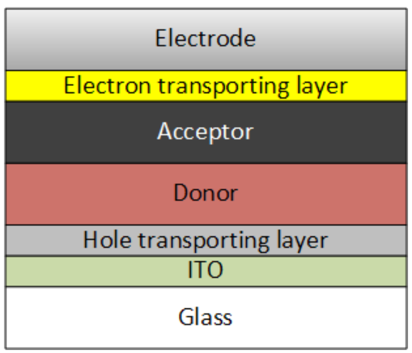

Bi-layer structure

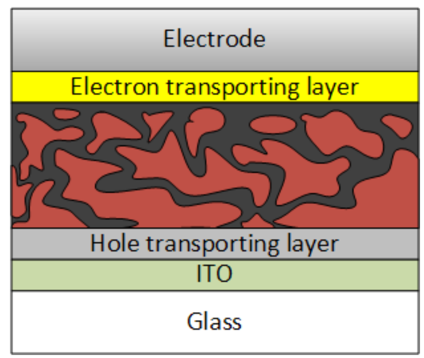

Bulk heterojunction structure

➡ Inter-digitated structure

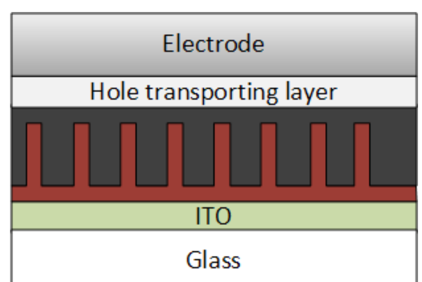

Exciton Diffusion Length

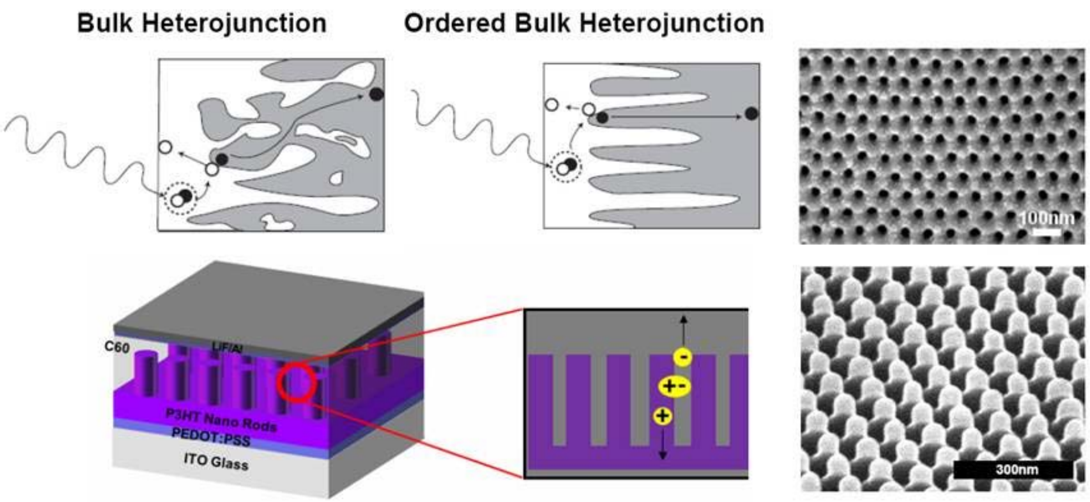

Interdigitated structures also benefit the charge transporting properties

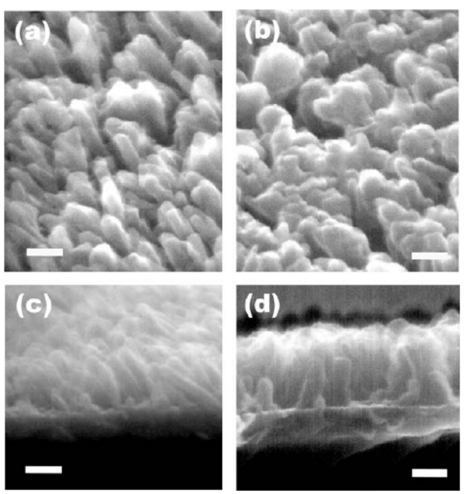

Topographic ((a) and (b)) and cross-sectional ((c) and (d)) scanning electron microscope (SEM) images of CuPc nanorods grown on a stationary ((a) and (c)) or rotational ((b) and (d)) substrate. The scale bar is 100 nm in all four images

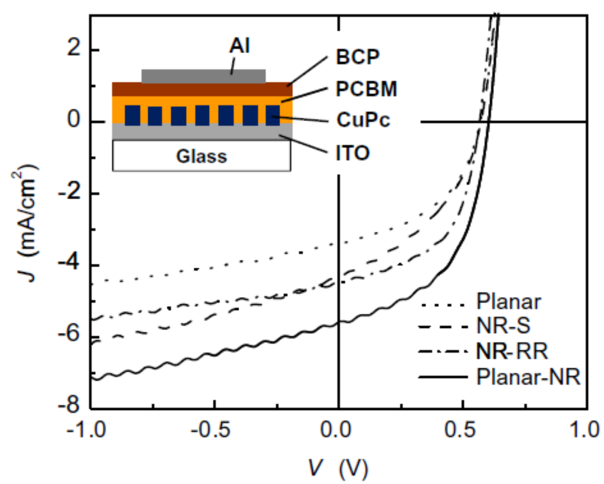

Y. Zheng *et al*., *Org. Electronics* **10**, 1621 (2009).

To Improve Charge Separation

To dissociate electron-hole pairs before recombination
➡Morphology control (BHJ/interdigitated structure)
➡Sieve layer

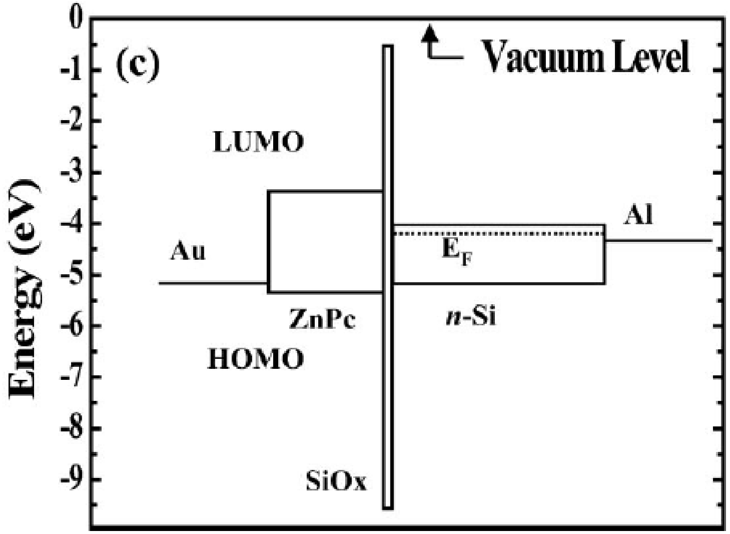

The energy levels of the individual components of the photovoltaic cell

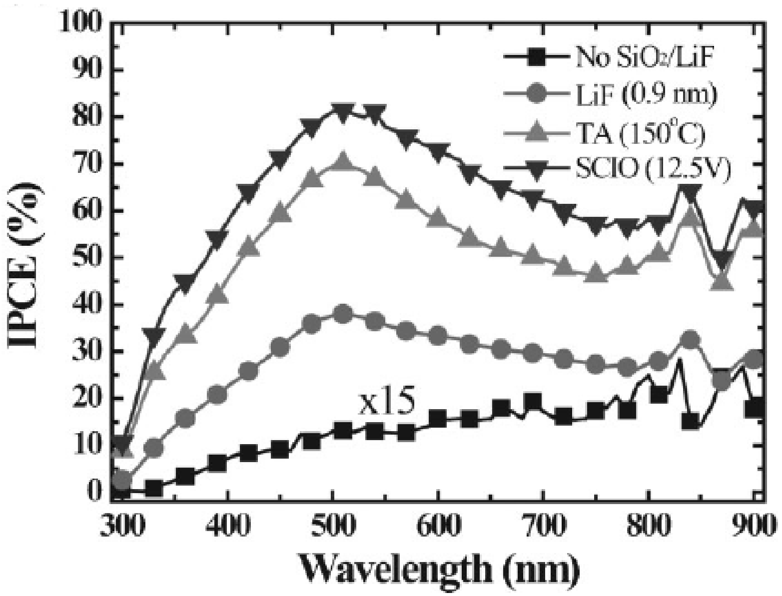

The incident photon-to-current collection efficiency (IPCE) of the device with and without the different electronic sieve layers

Adv. Mater. **21**, 759 (2009)

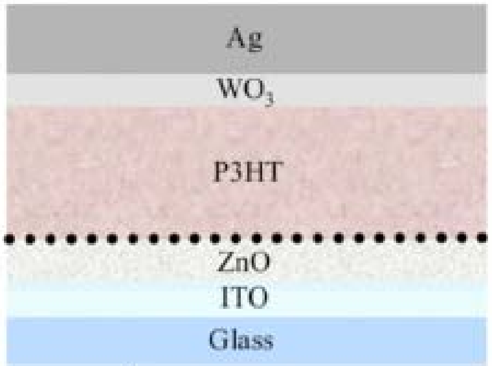

Structure of the inverted hybrid PV device and the chemical structure of the PCBA molecule

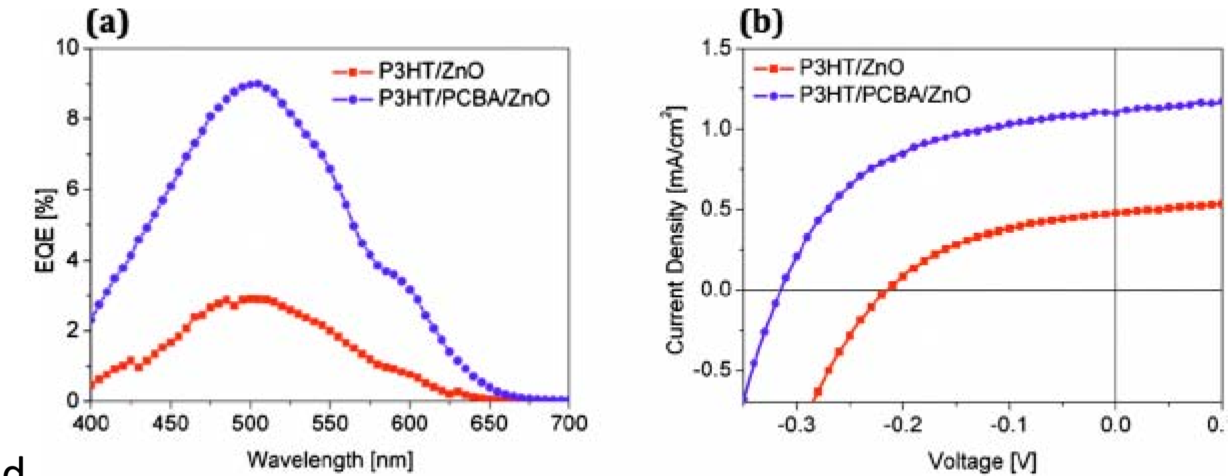

(a) EQE of inverted hybrid P3HT solar cells on bare ZnO and PCBA/ZnO. (b) I-V curves measured under a solar simulator.

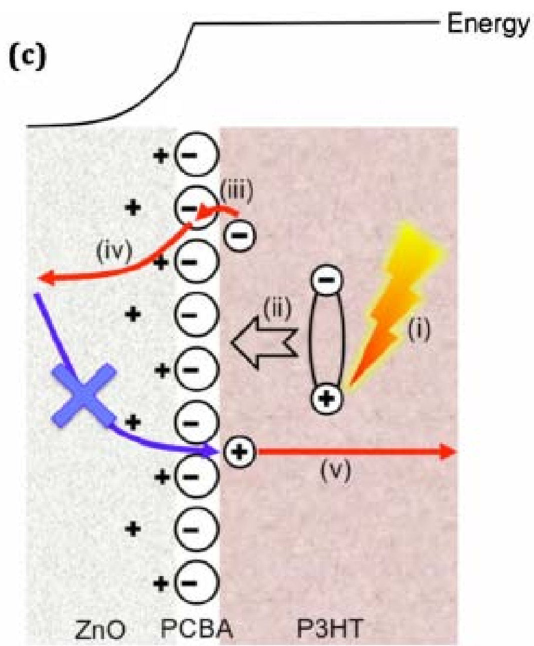

Mechanism of dipole assisted charge separation at the P3HT/PCBA/ZnO interface:

i excitation

ii exciton migration to the interface

iii rapid electron transfer to the PCBA monolayer

iv interfacial dipole assisted electron collection in the bulk of the ZnO

Y. Vaynzof *et al., Appl. Phys. Lett.* **97**, 033309 (2010).

Hybrid OSC

- **Organic/Inorganic hybrid solar with nanomaterial/nanostructure**

with 1-D nanostructure

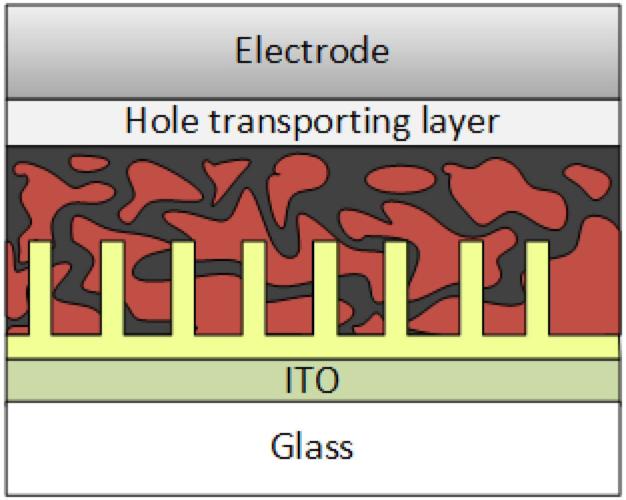

➡To increase the interfacial area
➡To enhance exciton dissociation and/or charge collection

with nanomaterial

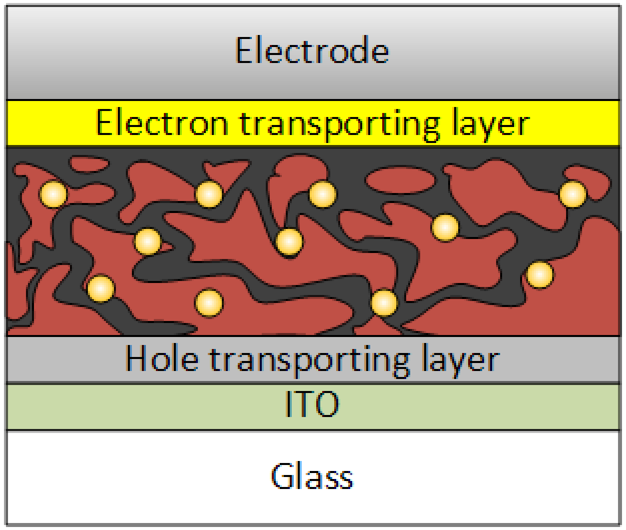

➡To enhance light harvesting

Interface Control is Critical in Hybrid Inorganic-Organic Solar Cells

Enhanced Charge Separation by Sieve-layer Mediation in High Efficiency Inorganic-organic Solar Cell

C. H. Lin, et al., Advanced Materials 21, 759-763 (2009) & US Patent 8,080,824, December 20 (2011)

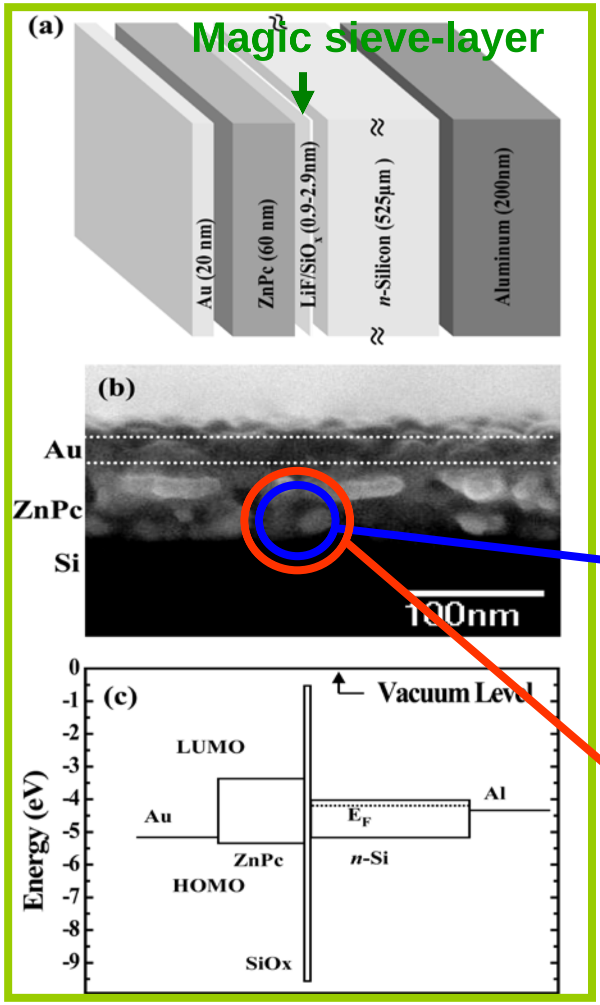

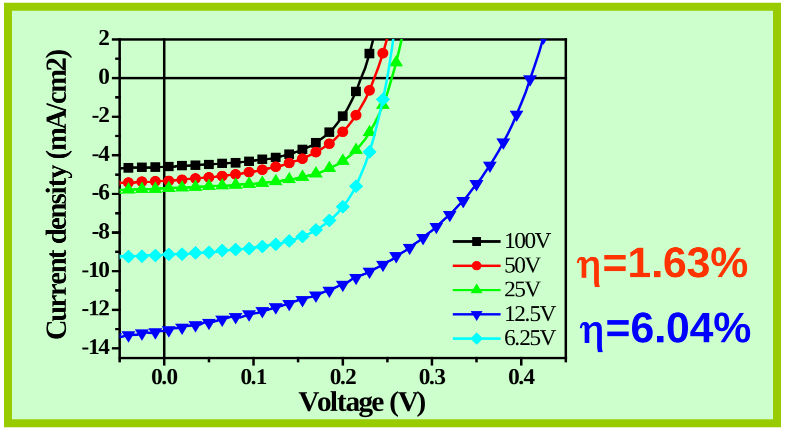

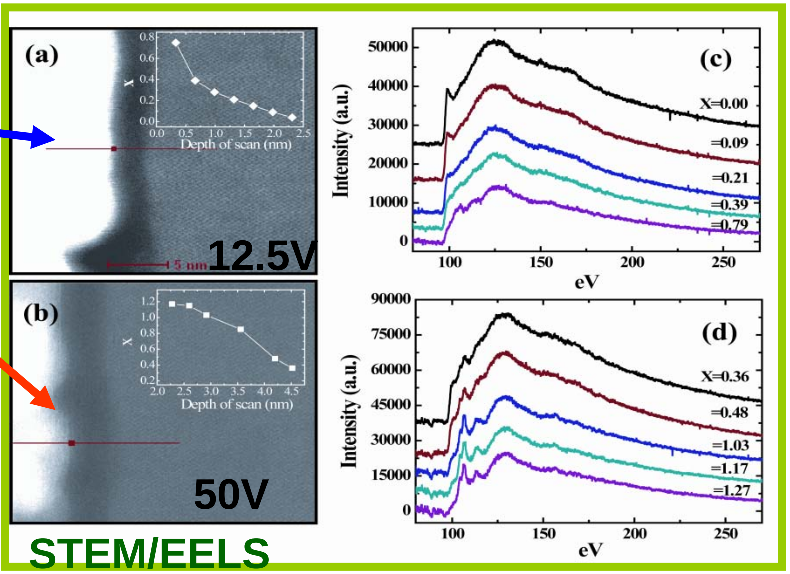

Nanomaterial - SPR effect

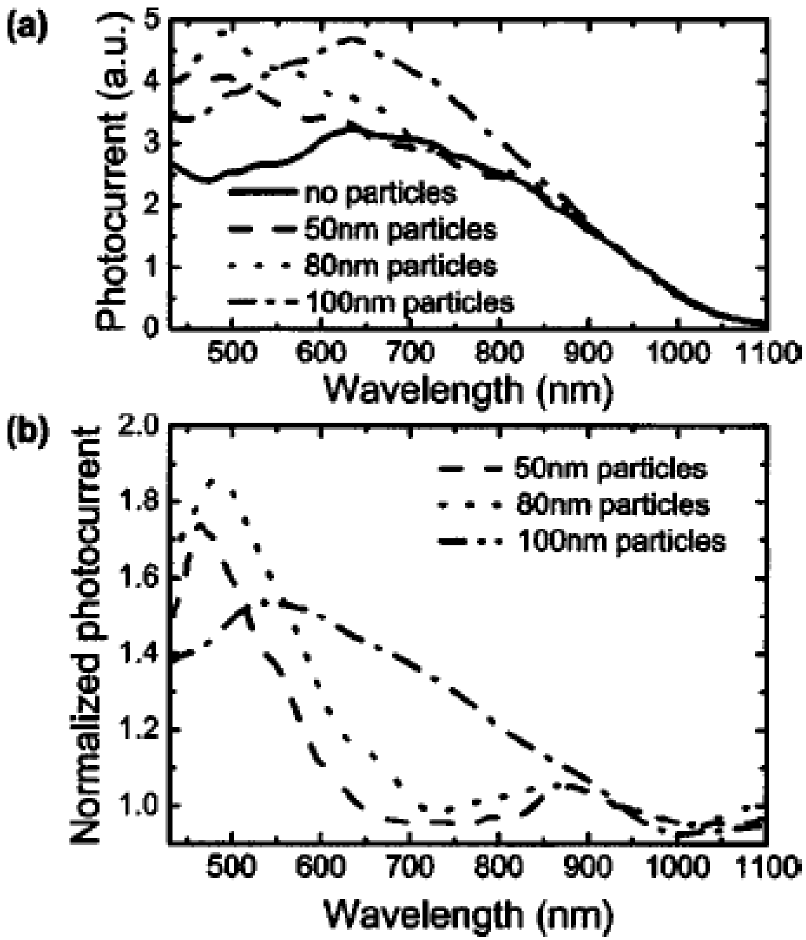

(a) Photocurrent response as a function of illumination wavelength for Si *pn* junction diodes in the absence of nanoparticles, and with Au nanoparticles 50, 80, and 100 nm in diameter.

(b) Photocurrent response spectra for diodes with Au nanoparticles 50, 80, and 100 nm in diameter from part (a), normalized to the photocurrent response measured in the absence of nanoparticles, revealing the increased response arising from the presence of the nanoparticles.

Surface plasmon-induced electromagnetic field

➡ increased field amplitude and increased interaction time between the field and the semiconductor

➡ to increase absorption of incident electromagnetic energy near the nanoparticle

Other Kinds of OSC

- **InGaN and InAlN solar cells**

For single III-V semiconductor solar cells
➡ large optical loss

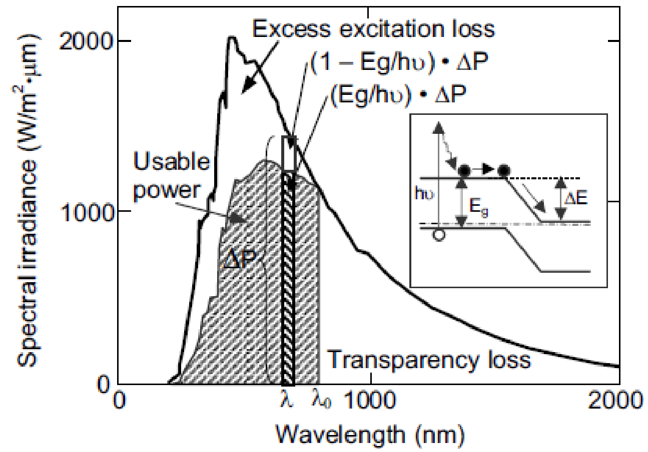

To solve this issue

To fabricate a multi-junction tandem solar cell, where sub-cells composed of a different band-gap material

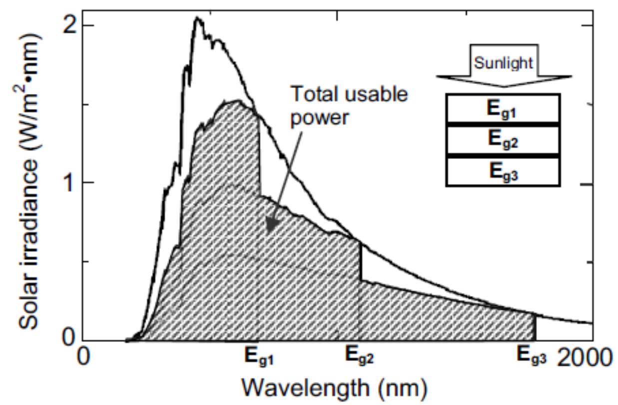

Current generated in each sub-cell should be matched (current matching) ➡ limit the efficiency

A. Yamamoto *et al.*, *Phys. Status Solidi C* **7**, 1309 (2010).

Potential and Status of InGaN and InAlN Solar Cells

- Band-gap of InGa(Al)N can be adjusted from 0.7 to 2.5 eV by changing only the composition .

➡Current matching will be easily achieved using InGa(Al)N system
(A current generated in each sub-cell is assumed to be the same)

➡ Multi-junction tandem cell (sub-cells > 4) is possible

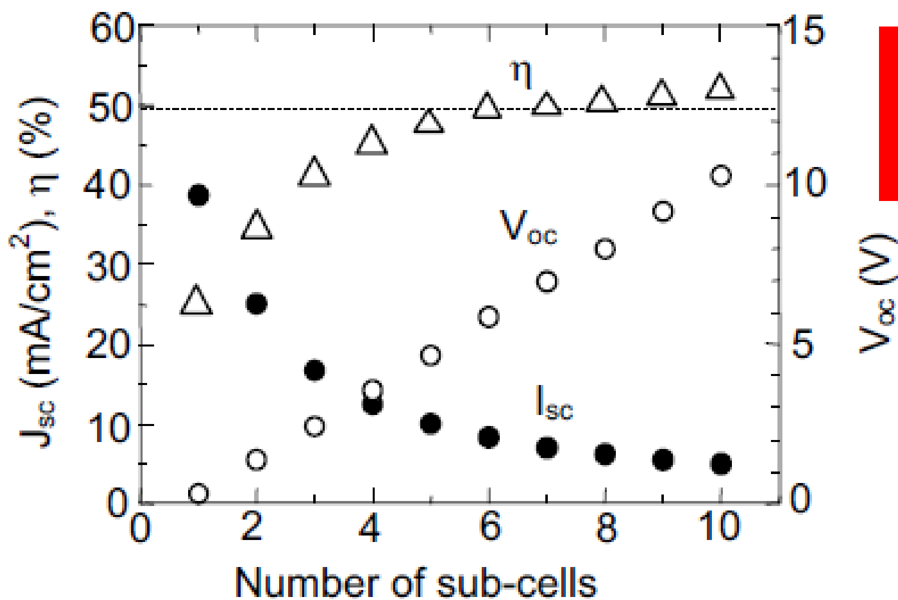

Efficiency > 50% !!!
(theoretically)

Expected output performance for multi-junction tandem cells with a different number of sub-cells

A. Yamamoto *et al.*, *Phys. Status Solidi C* **7**, 1309 (2010).

Applications of InGaN

Blue LEDs

Photodetector

Laser Diode

Solar Cell

Challenge for InGaN growth and applications

- Phase separation

➡reduces the V_{oc} of the solar cell

➡recombination ↑ → decreasing the photocurrent

Splendid Nitride Nanostructures

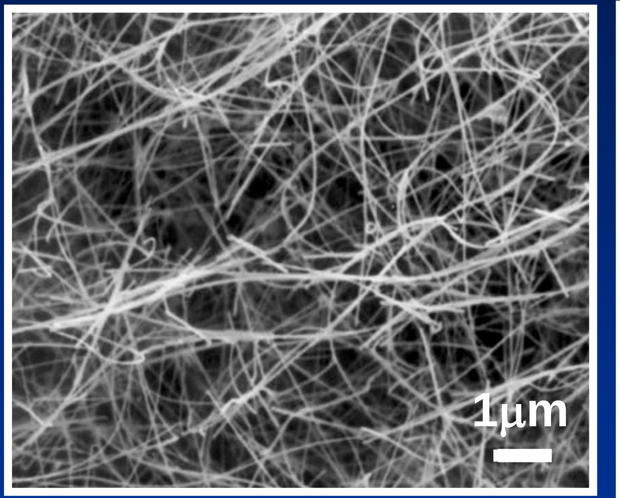

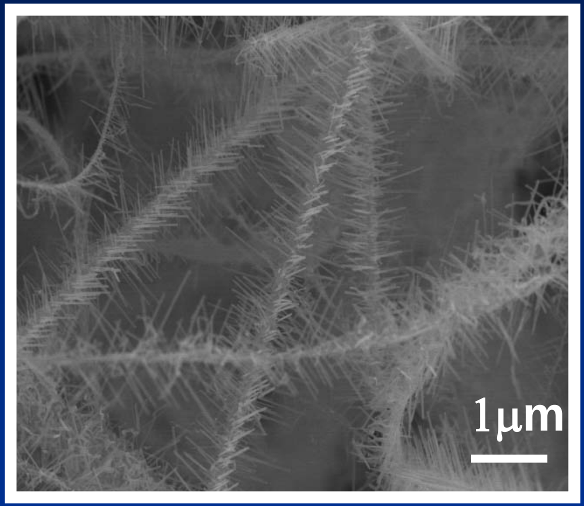

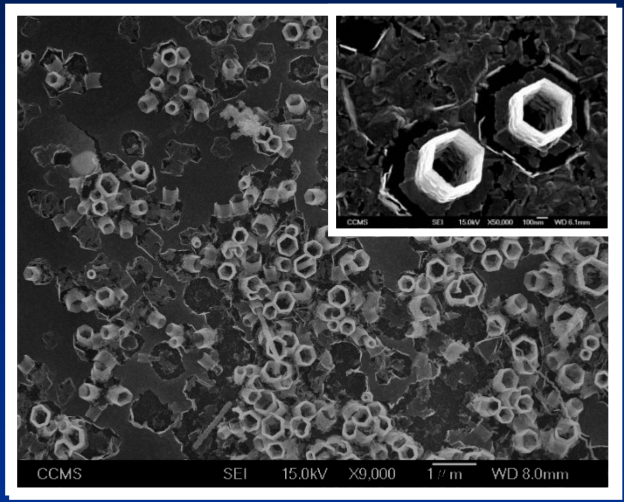

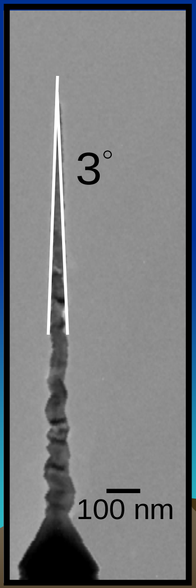

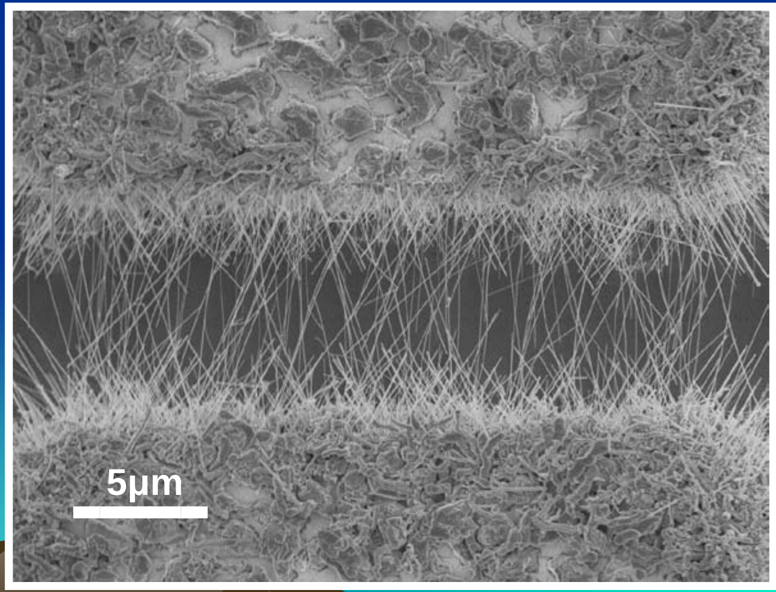

Motivation & Rational

III-N, a rapidly growing/maturing industry, mostly thin film based, but why 1D?

- The extended family of 1D nanostructures

  What makes them distinct from thin film or QD?

- Size-dependent optical & transport properties
- Control in size, site, shape & orientation (S^3O)

  How about S^3O-distribution tolerant devices?

- On-chip fabrication for integrated devices
- Applications beyond optoelectronics

  Bio-compatible & Corrosion-resistant

Single GaN Nanowire FET

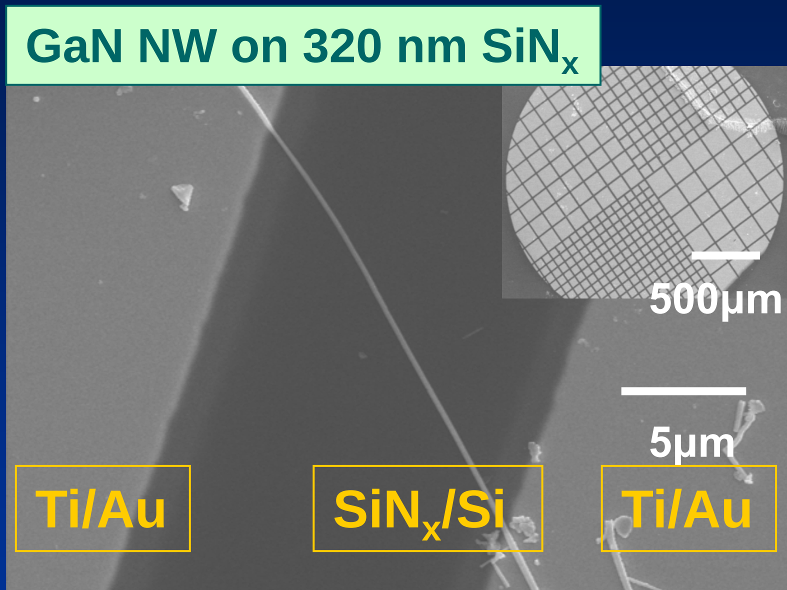

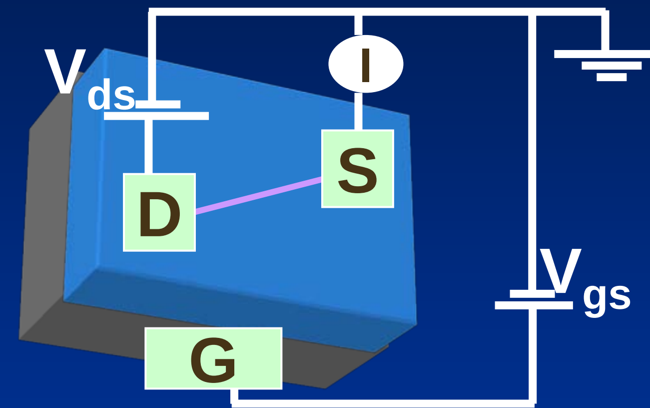

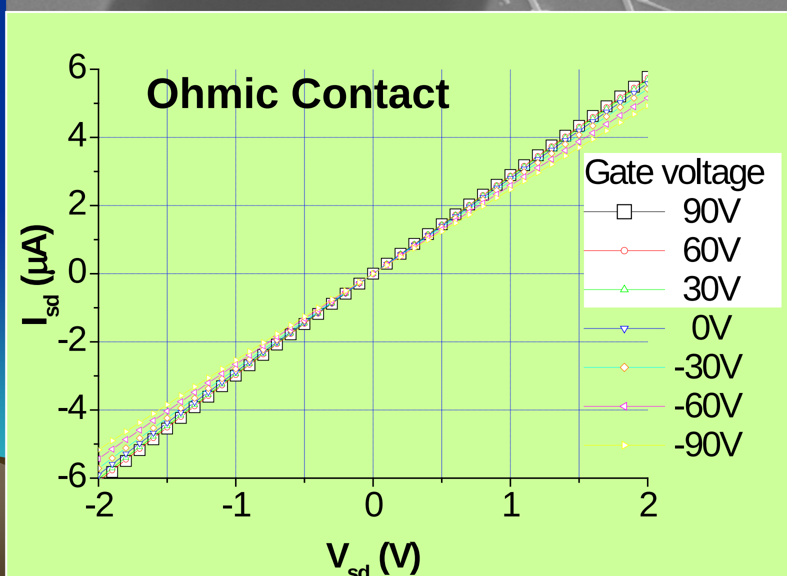

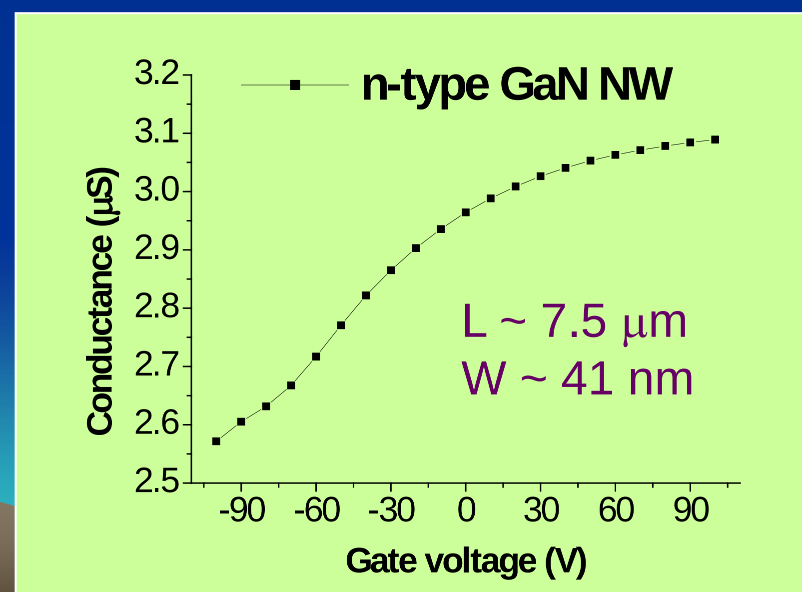

Toward Chip-process of Nanowire Devices

from

Single Nanowire

Size-, site-, shape- & orientation-controlled device

to

an Ensemble of Nanowires

S^3O-distribution tolerant devices

Fabrication of M-S-M Device

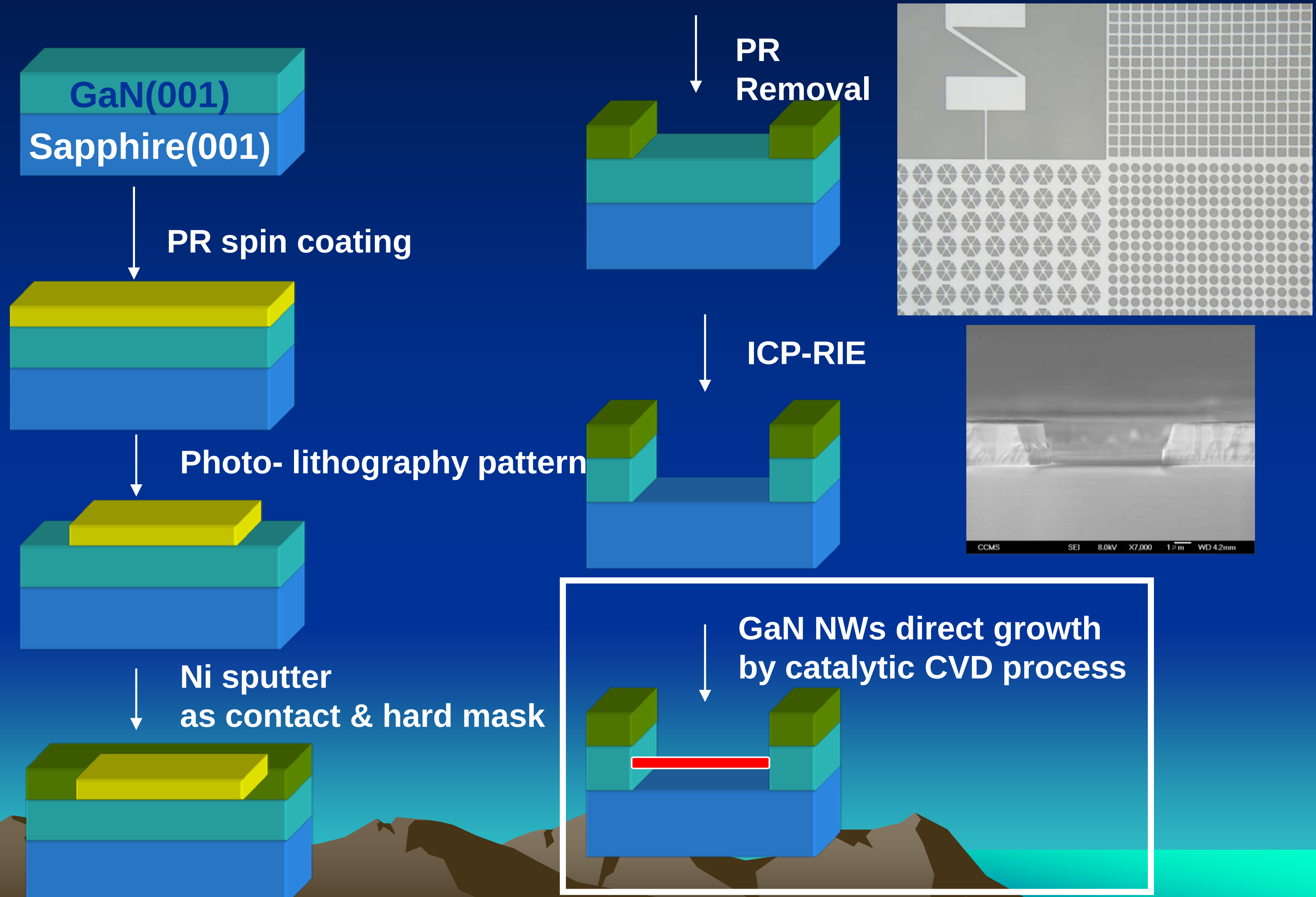

Epi-GaN NWs
M-S-M Structure

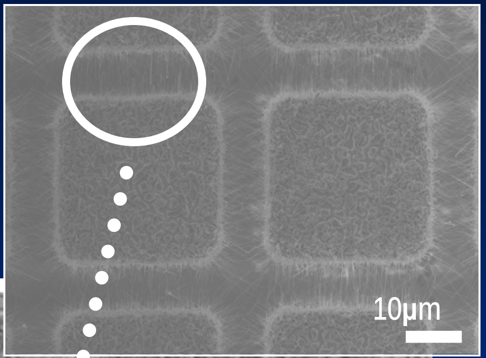

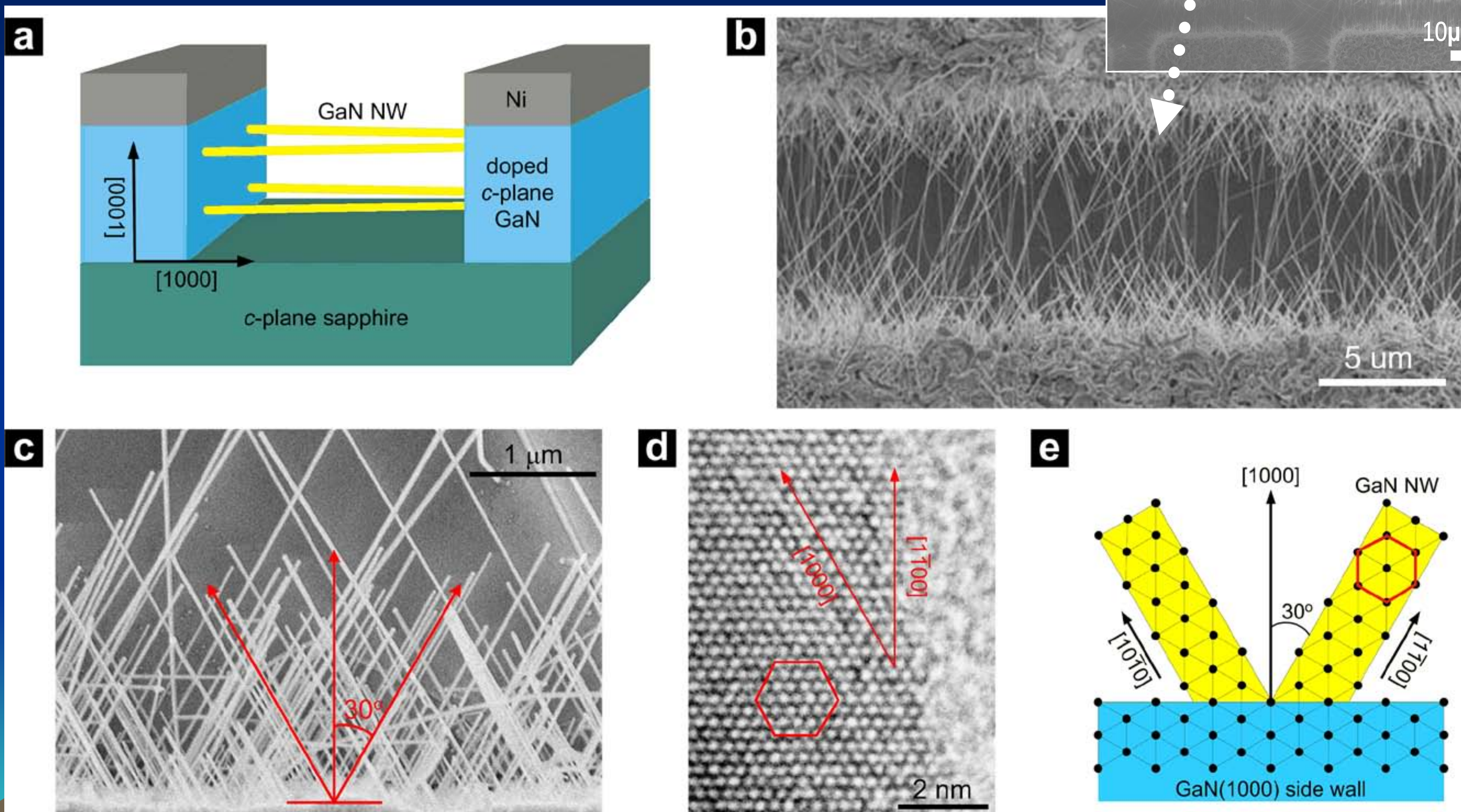

Small 4 (2008) 925

Photoconductivity (PC) Measurement of GaN Nanowires

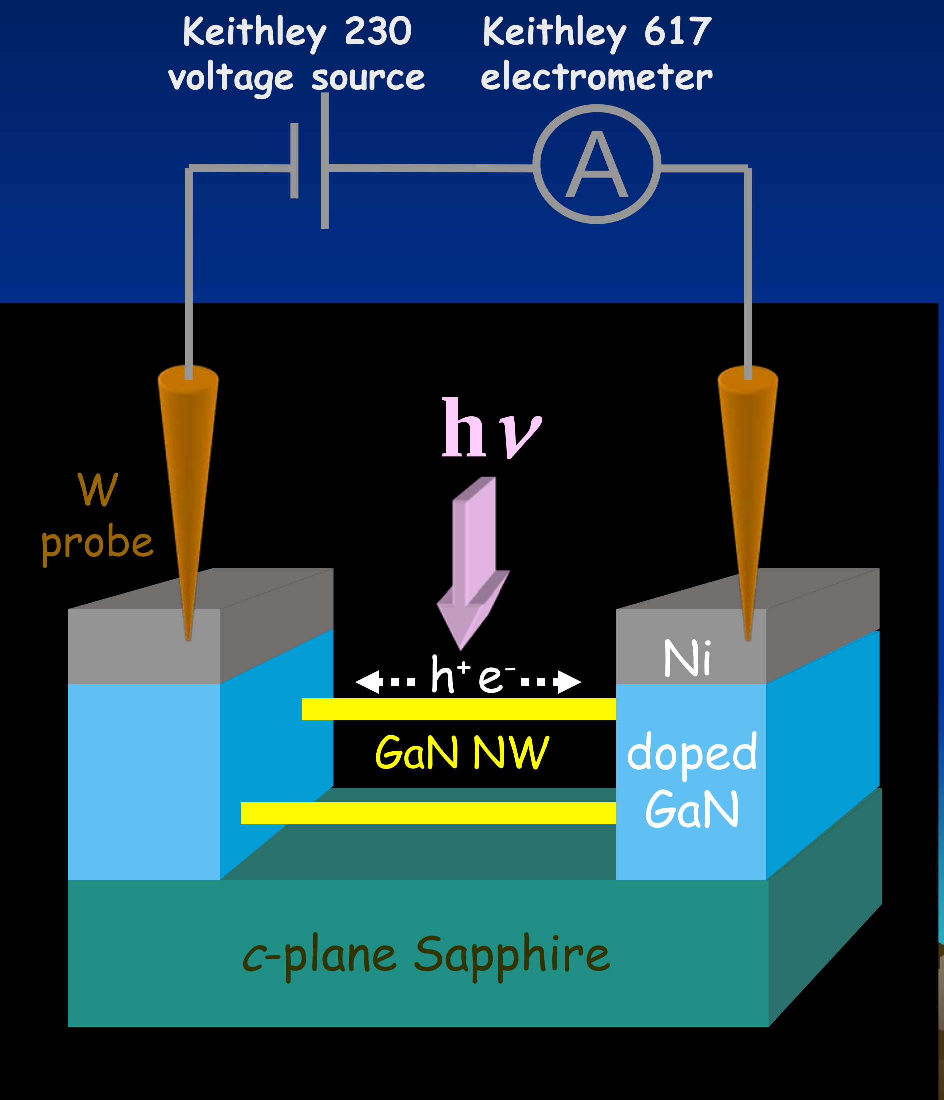

PC spectrum of GaN NWs

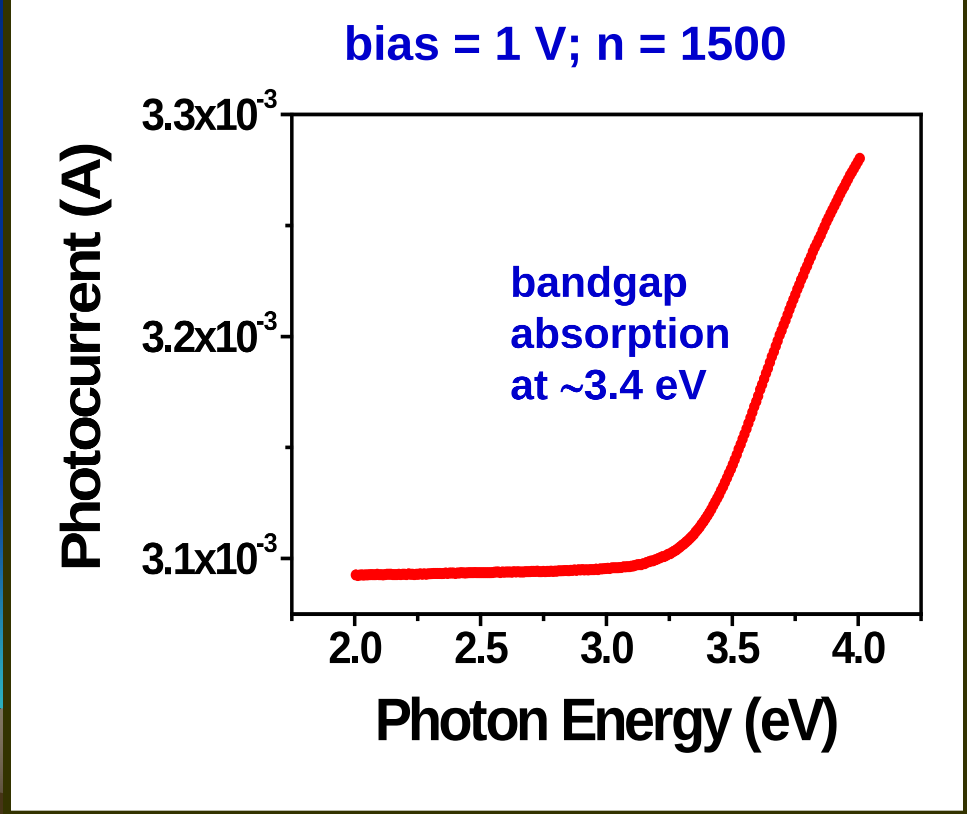

Size-dependent Photoconductivity of GaN NW-bundles and Single-wire

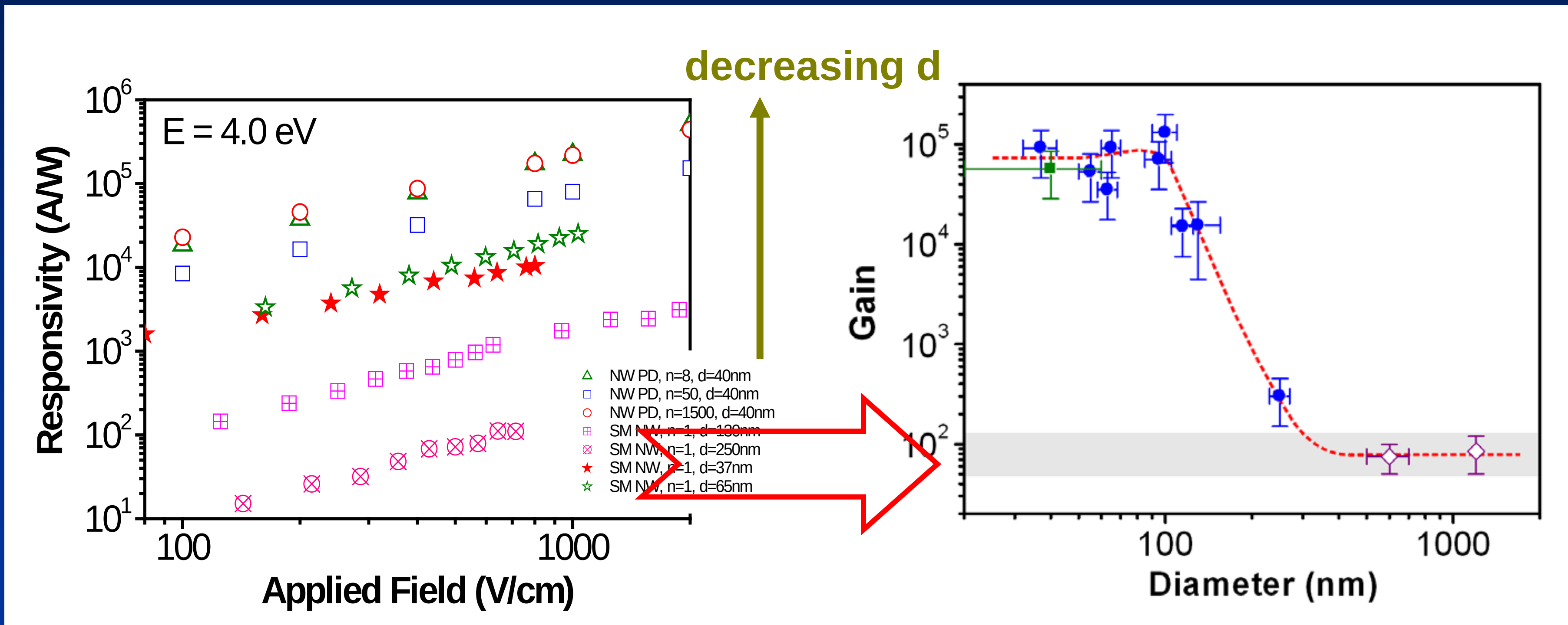

$$R = \frac{\Delta i}{P}$$

photon energy

gain $\Gamma = \dfrac{E}{e \times \eta} \times R$ responsivity

electron charge

quantum efficiency

Small 4 (2008) 925

APL 95 (2009) 143123

Comparison of Responsivity between the Nanowire and Thin Film Detector

Epi-GaN NWs

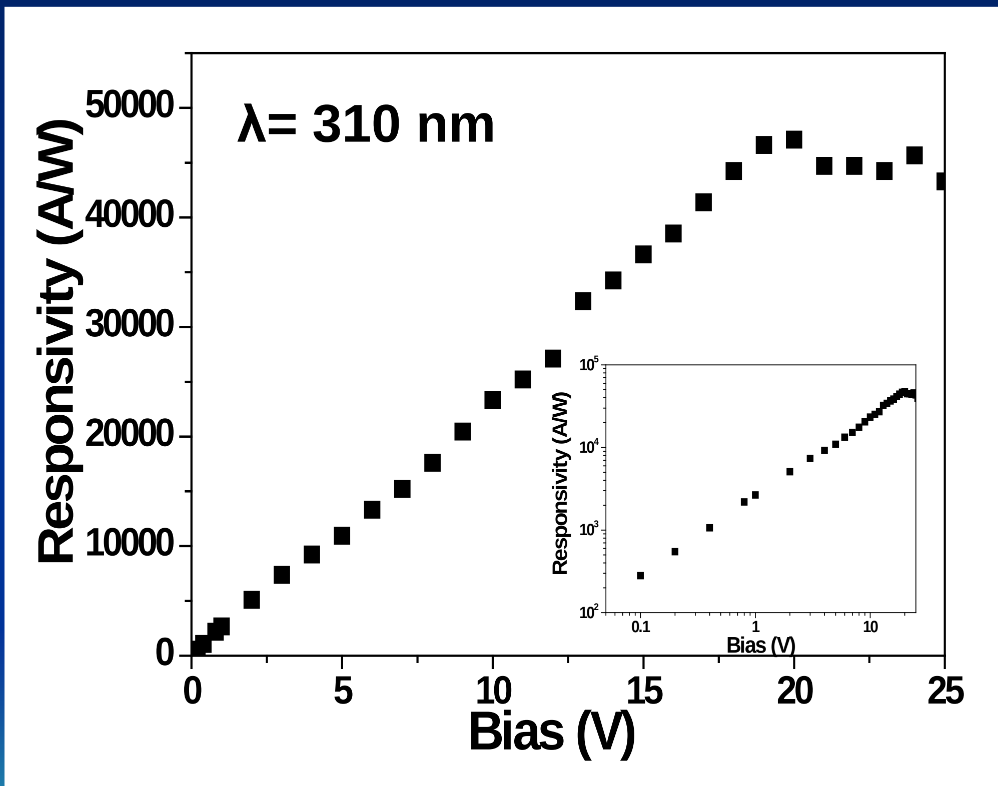

Maximum responsivity of ***50,000 A/W***
was obtained at 18V bias

GaN Thin film

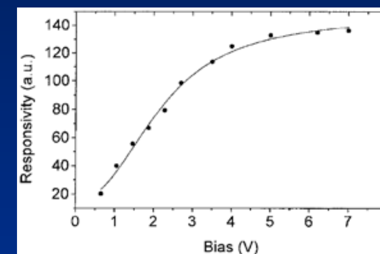

Jpn. J. Appl. Phys. Vol. 38 (1999) pp. 767–769
Max R= 133 A/W at 5V bias

App. Phys. Lett., Vol. 77, No. 3, 17 July (2000)
Max R= 6.9 A/W at 5V bias

Inter. J. Mod. Phy B, Vol. 16,Nos. 28&29(2002)
MaX R=2.53A/W at 7V bias

J. Vac. Sci. Technal. B 19(1), Jan/Feb(2001)
Max R= 6.9 A/W at 5V bias

What Happens to Band Structures as Nanowire Going Smaller and Smaller?

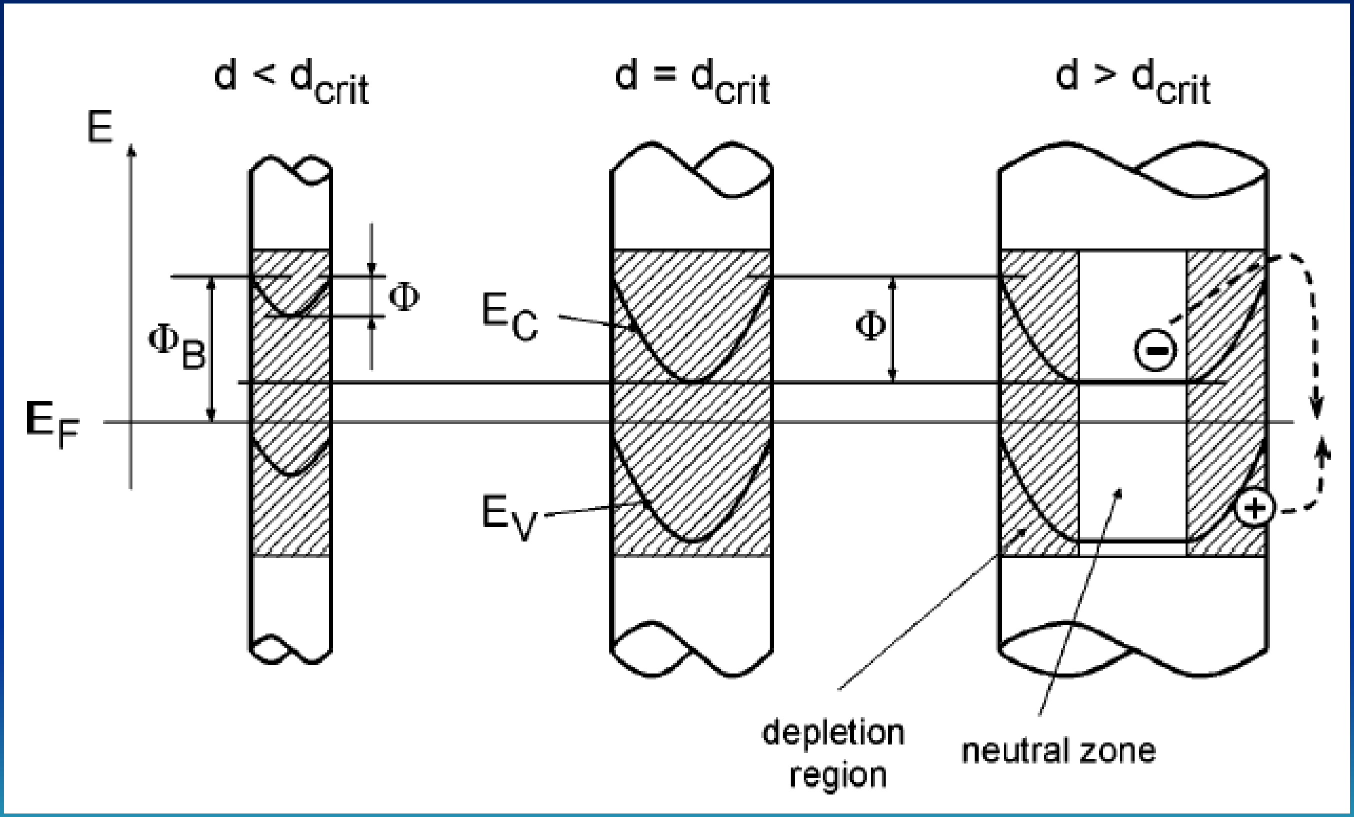

R. Calarco, *et al.*, ***Nano Letters*** *5 (2005) 981*

Surface-dominant Photoconductivity & Ultrahigh Gain in GaN Nanowires

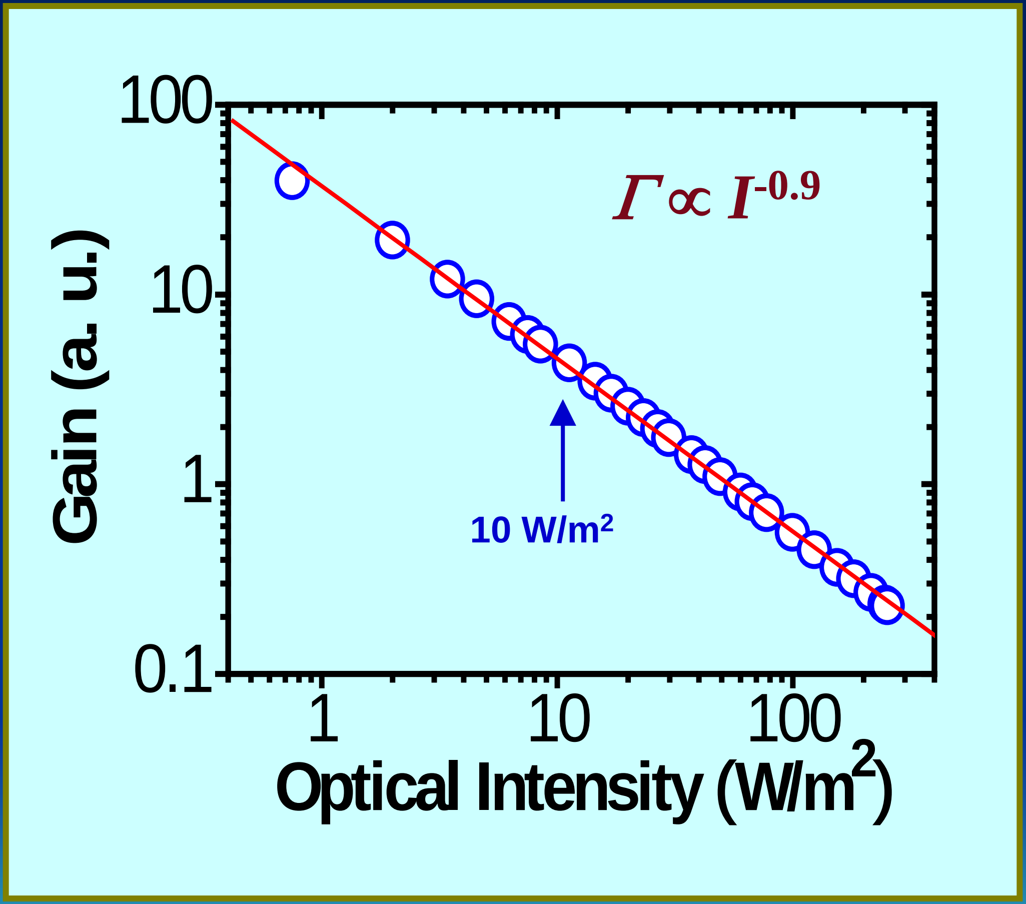

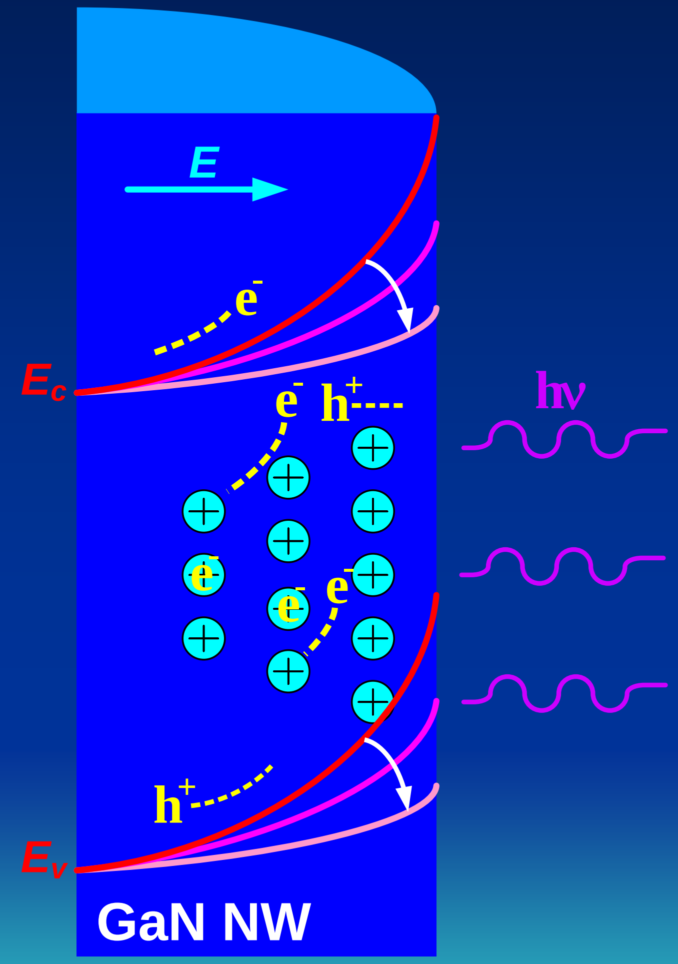

Appl. Phys. Lett. *91 (2007) 223106*

Environment-sensitive Surface Photoconductivity (under 325 nm UV Light)

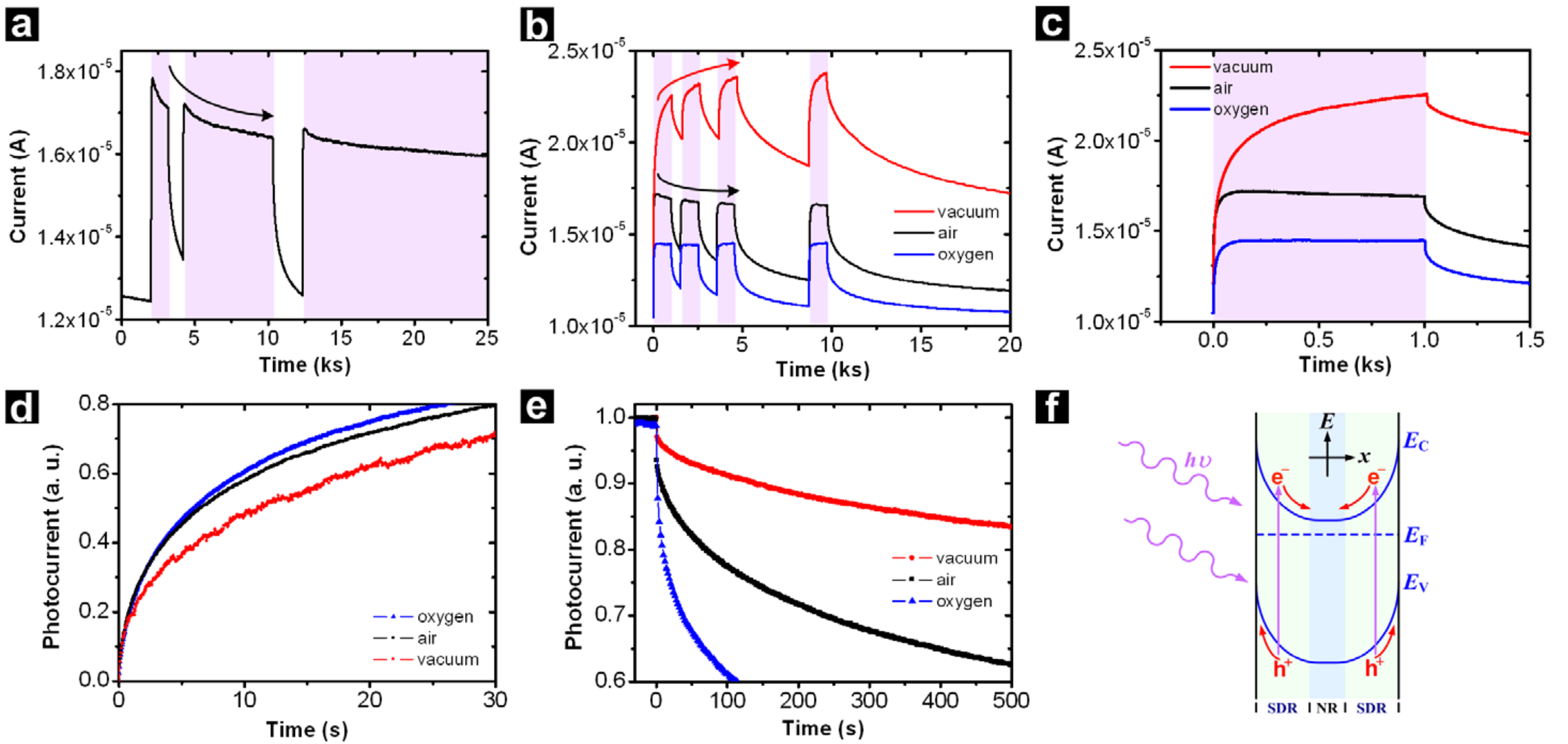

Appl. Phys. Lett. 95 (2009) 233119

Molecular Modulation at Surface

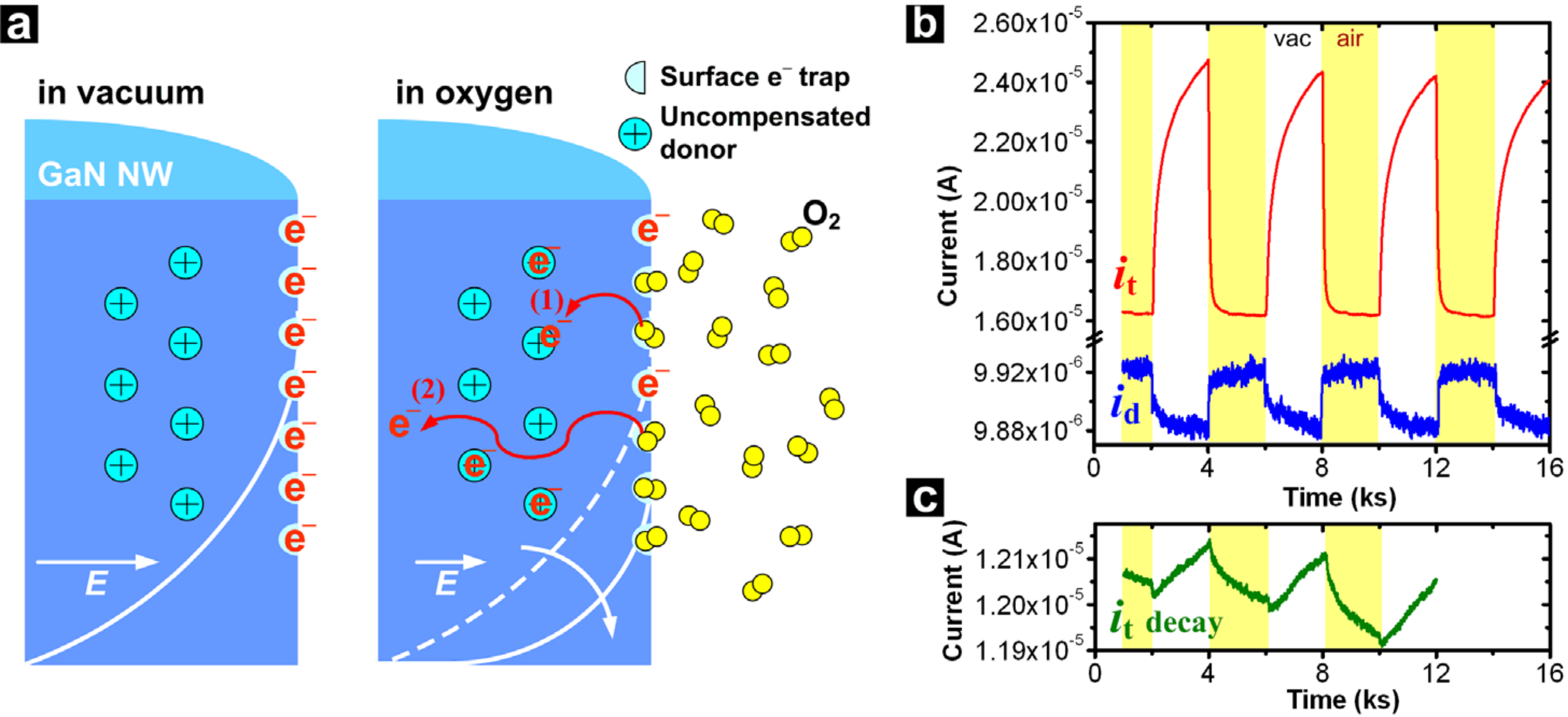

Appl. Phys. Lett. *95 (2009) 233119*

Case II: Photo-electrochemical Process

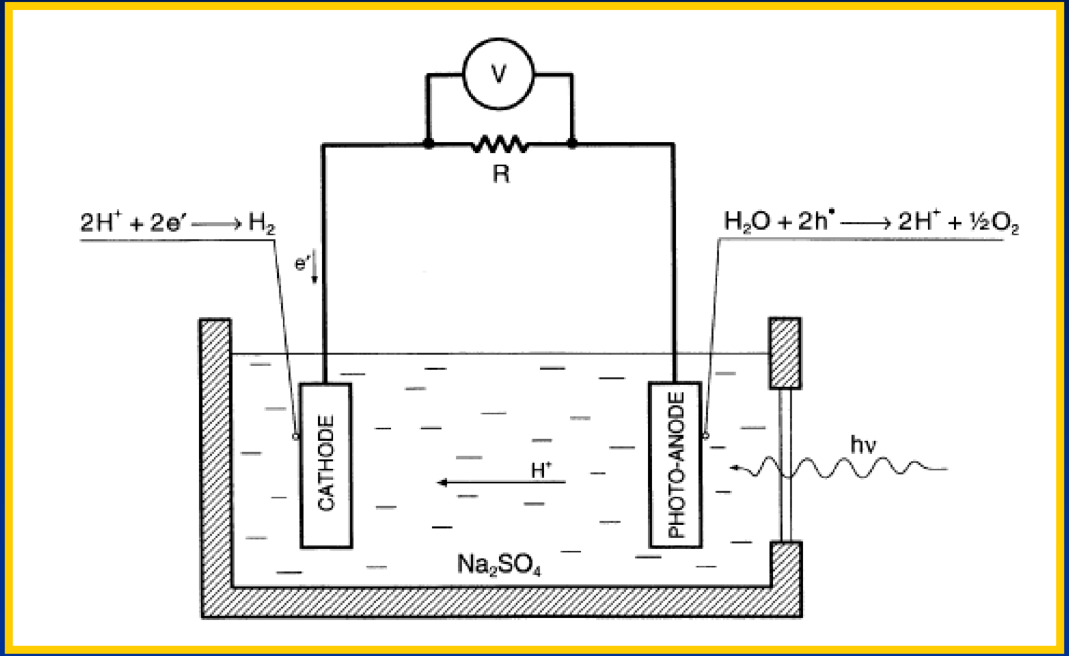

(1) Photo-generation of e-h pairs (in photo-anode)

(2) Charge separation and migration
(hole to anode-electrolyte interface &
electron to counter-electrode thru external circuit)

(3) Oxidation of water to H^+ and O_2 (at anode) &
Reduction of H^+ to H_2 (at cathode)

Criteria for Effective Water Splitting

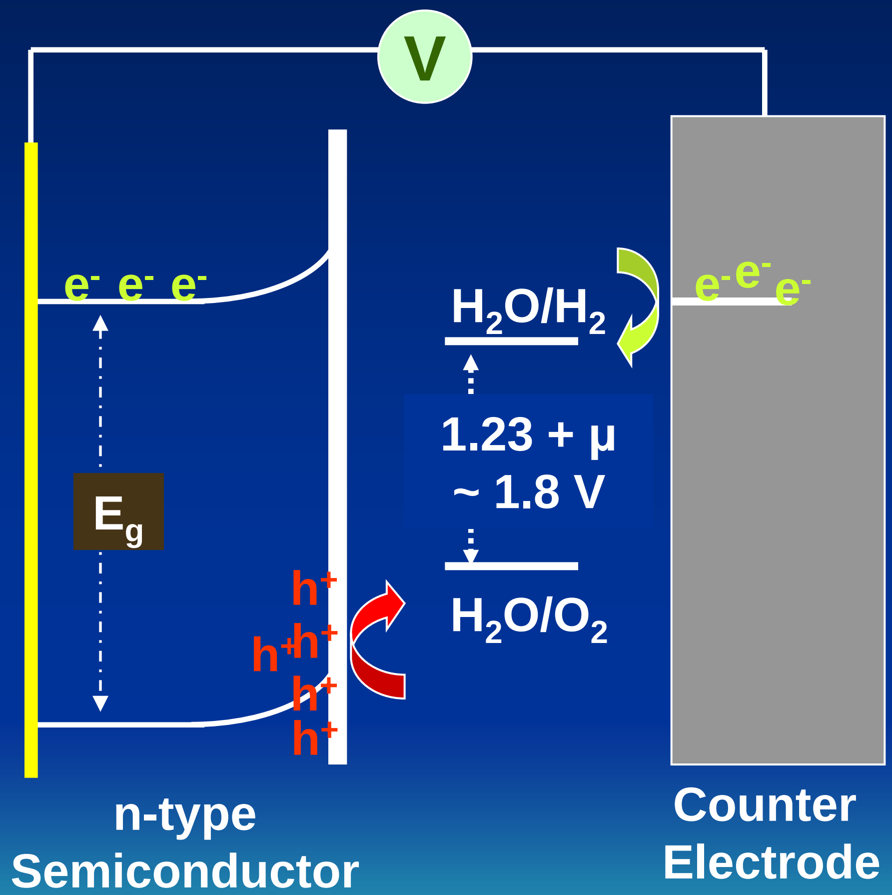

μ is overpotential

- **Photon-to-electron conversion efficiency**: $E_g > 1.8$ eV
- **Energetic:** Band edge potentials to straddle the hydrogen and oxygen redox potentials
- **Material durability:** Long-term stability in aqueous solution

All must be satisfied simultaneously!

Energy Levels of Semiconductors *versus* Water Splitting

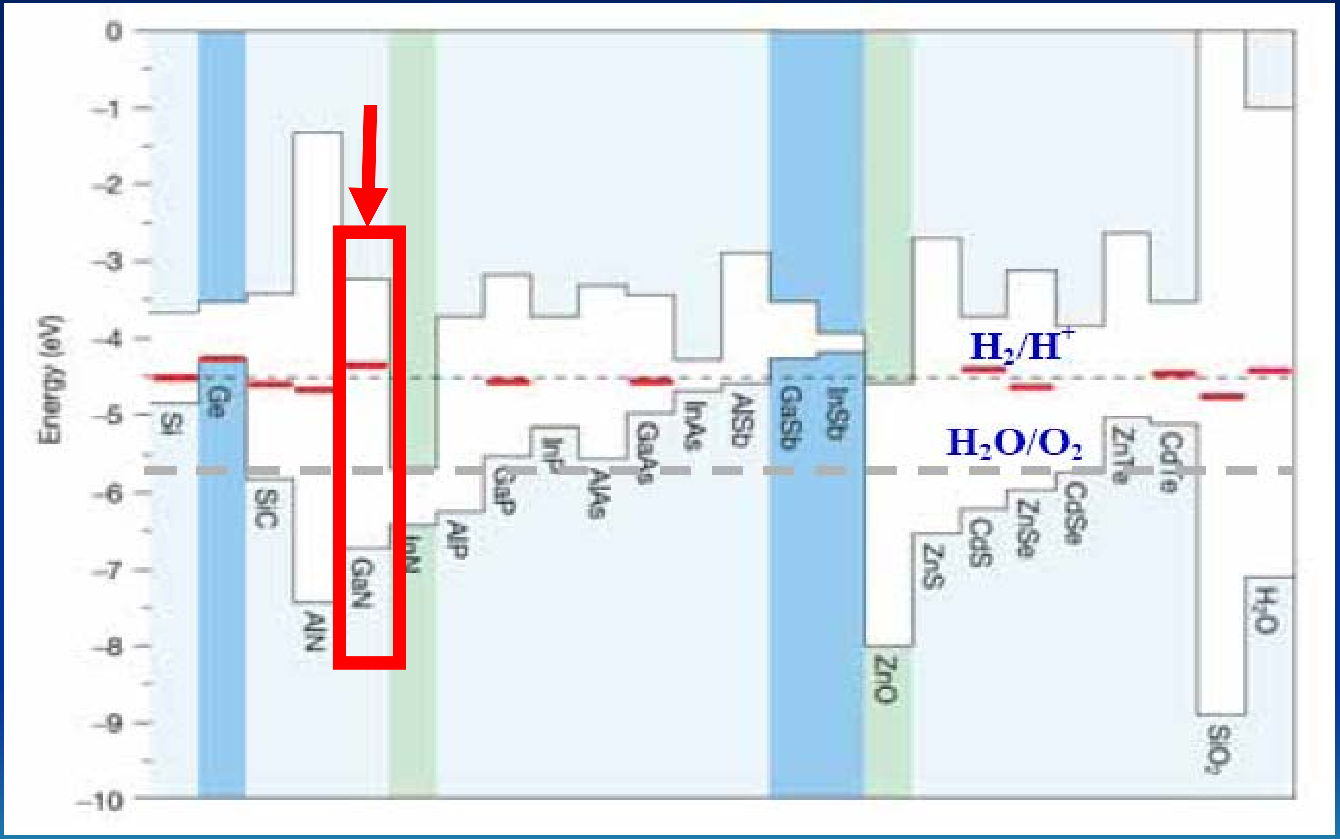

InGaN with tunable band gap

➢ **Optimize light harvesting & conversion efficiency**

Experimental Setup

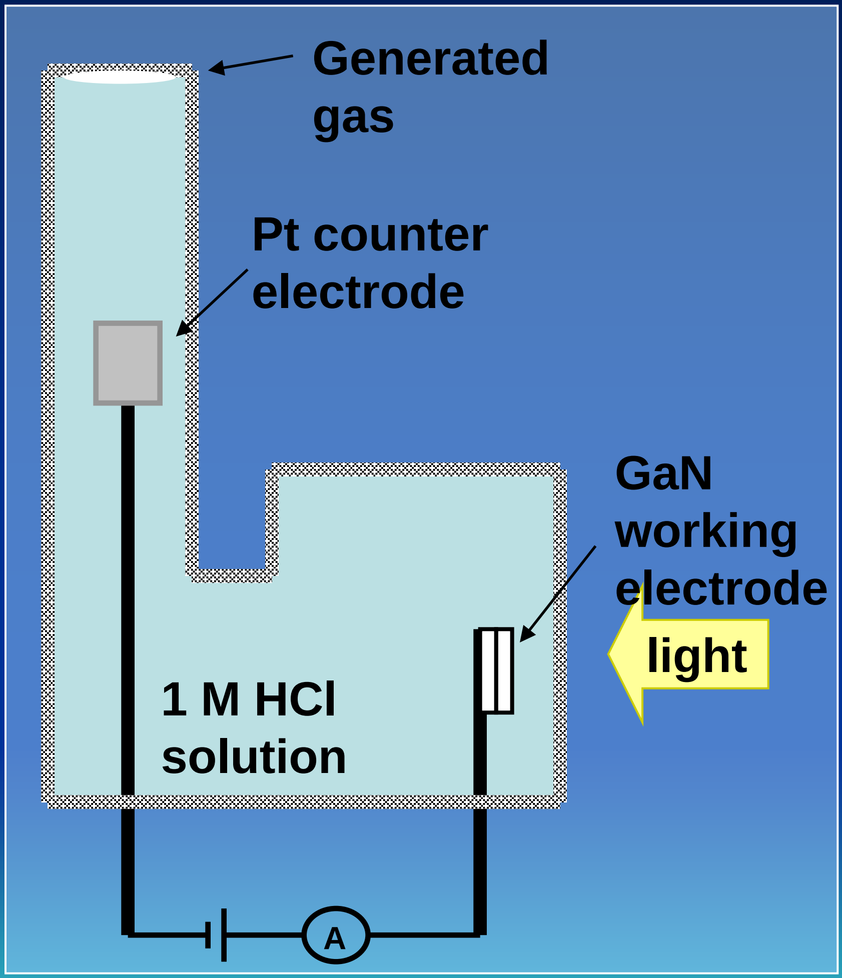

Reference electrode:
Ag/AgCl/NaCl (SSSE)

Photoresponse of N-type Photoanode

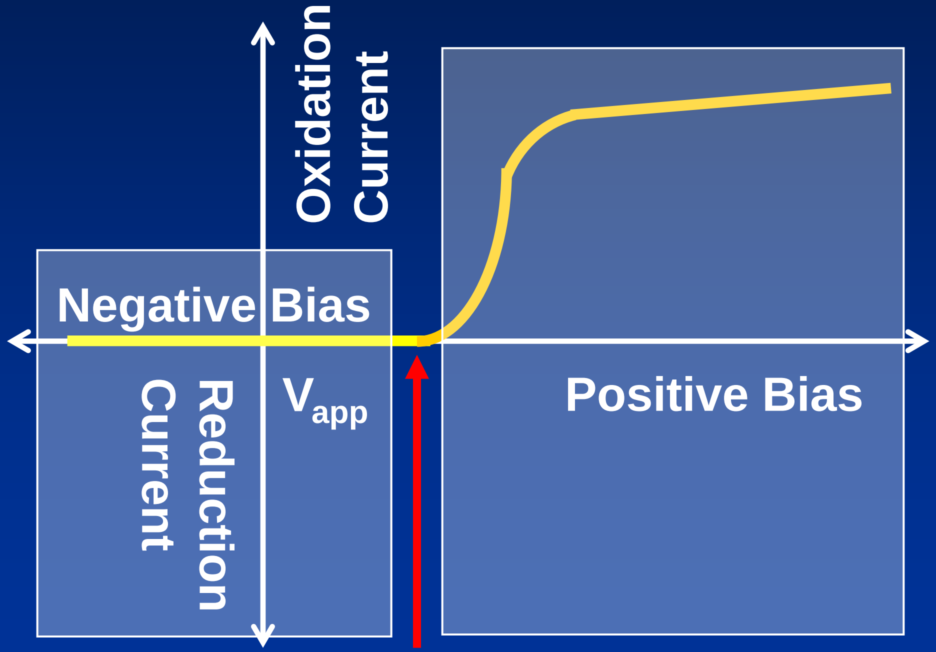

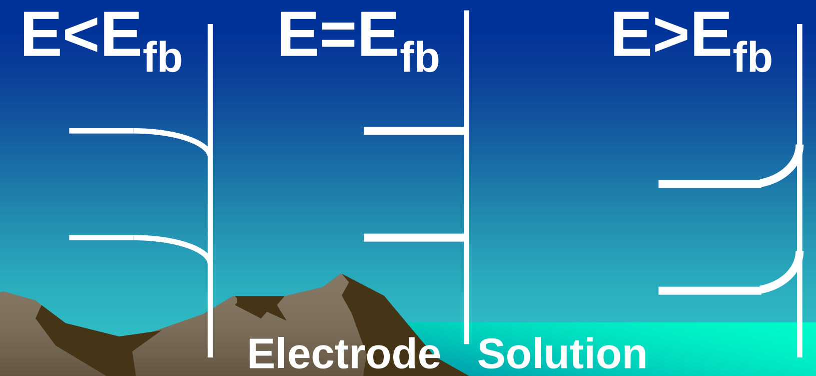

Factors Influencing Photo-electrolysis

- **Carrier Concentration**

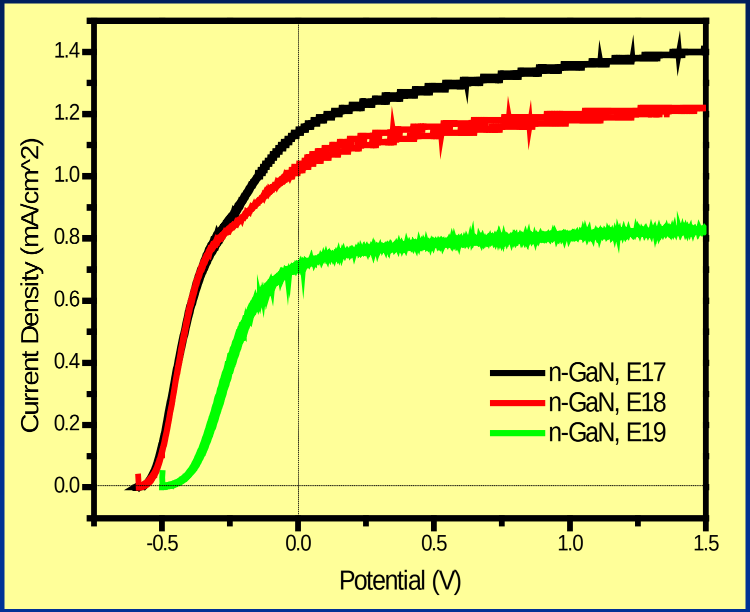

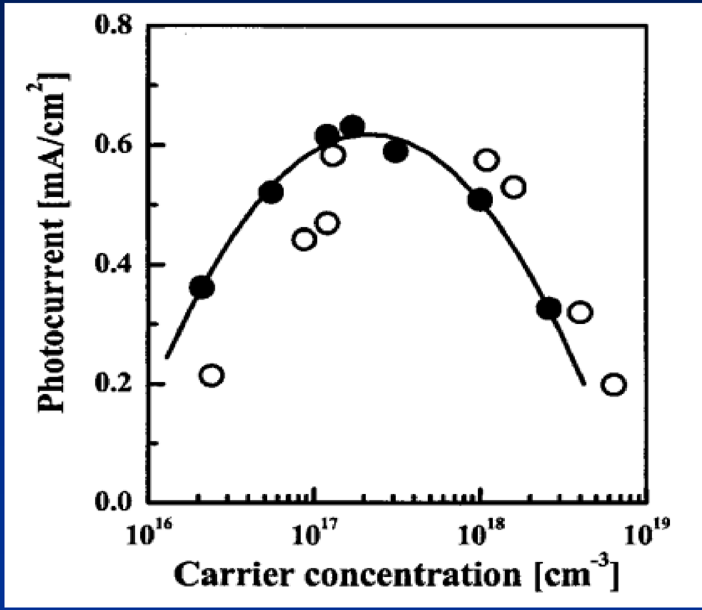

Resistivity ↑ **Recombination ↑**

M. Ono, et al., (Tokyo U. Sci. & Tohoku U.)
J. Chem. Phys. 126 (2007) 054708

- **Thin Film Orientation (Polar or semi-, non-polar)**
- **Surface Treatment of Film**
- **Type of Electrolyte**
- **pH value**

Potential of GaN and InGaN Nanowires in High-efficiency Photo-electrolysis Cells

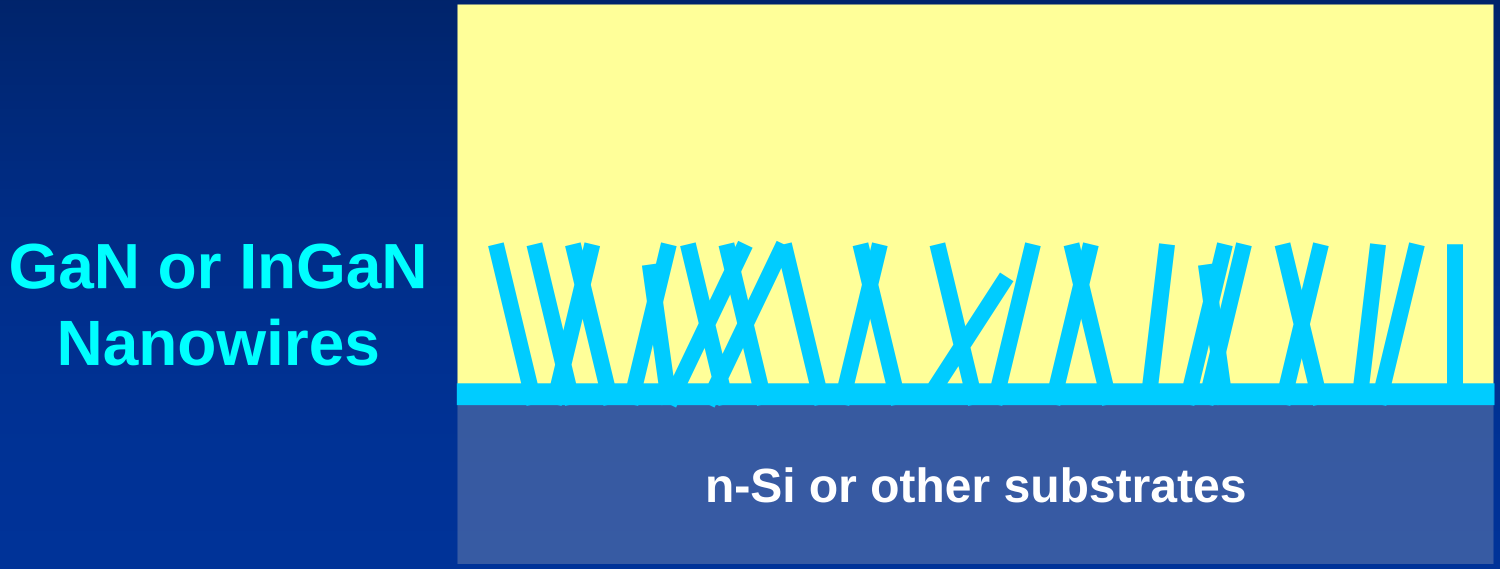

- Larger surface area
- More efficient charge separation

GaN Nanowires *versus* Thin Film

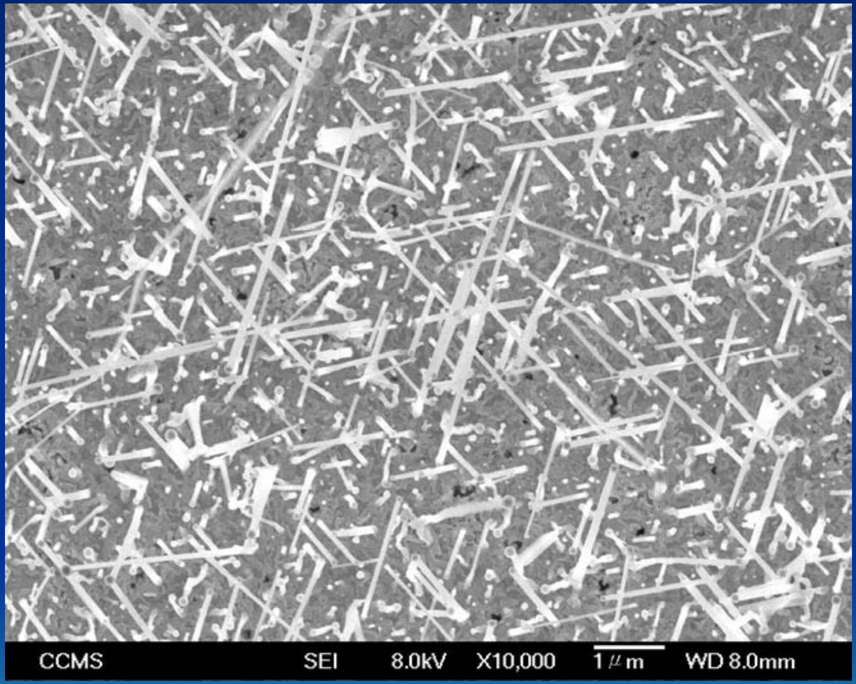

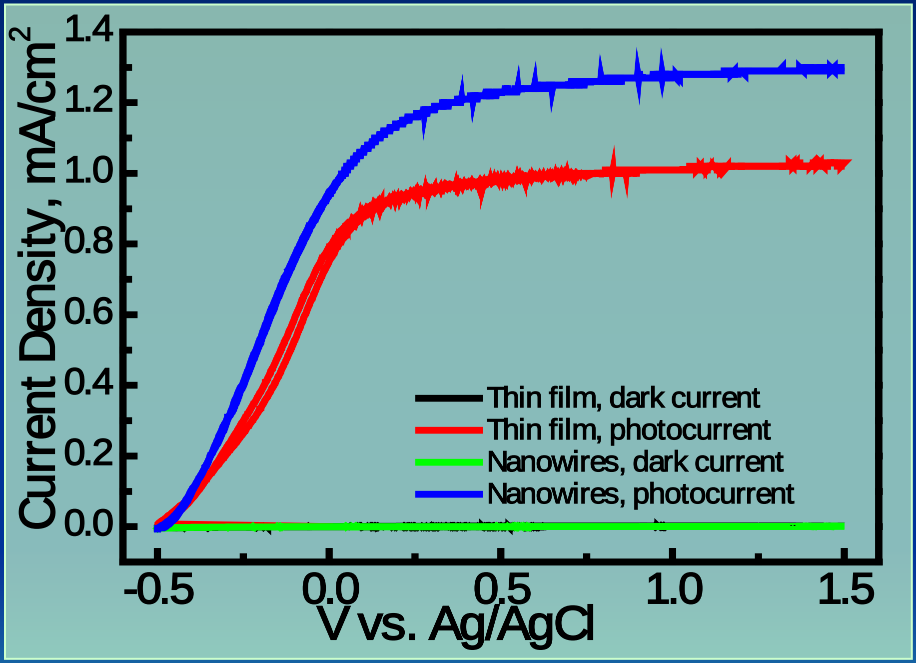

Outlook of Emerging Materials for Sustainability

Resource-Conscious R & D
Environment-Health-Safety Awareness

from Nano for the sake of Nano
to Nano for making an impact

- Hybrids, integrated device design
- Interface controlling/enabling
- IC-compatible, on-chip process
- Adding value to traditional/matured industry
- Next-generation electronic, optoelectronic, spintronic, energy devices operating at RT (or practical T) & lower power/cost

☆ Creativity is the only limit!